Okinawa Institute of Science and Technology
Graduate University

Thesis submitted for the degree

Doctor of Philosophy

The Role of Tails in Maintaining Balance: Neuronal and Behavioral Insights from the Mouse

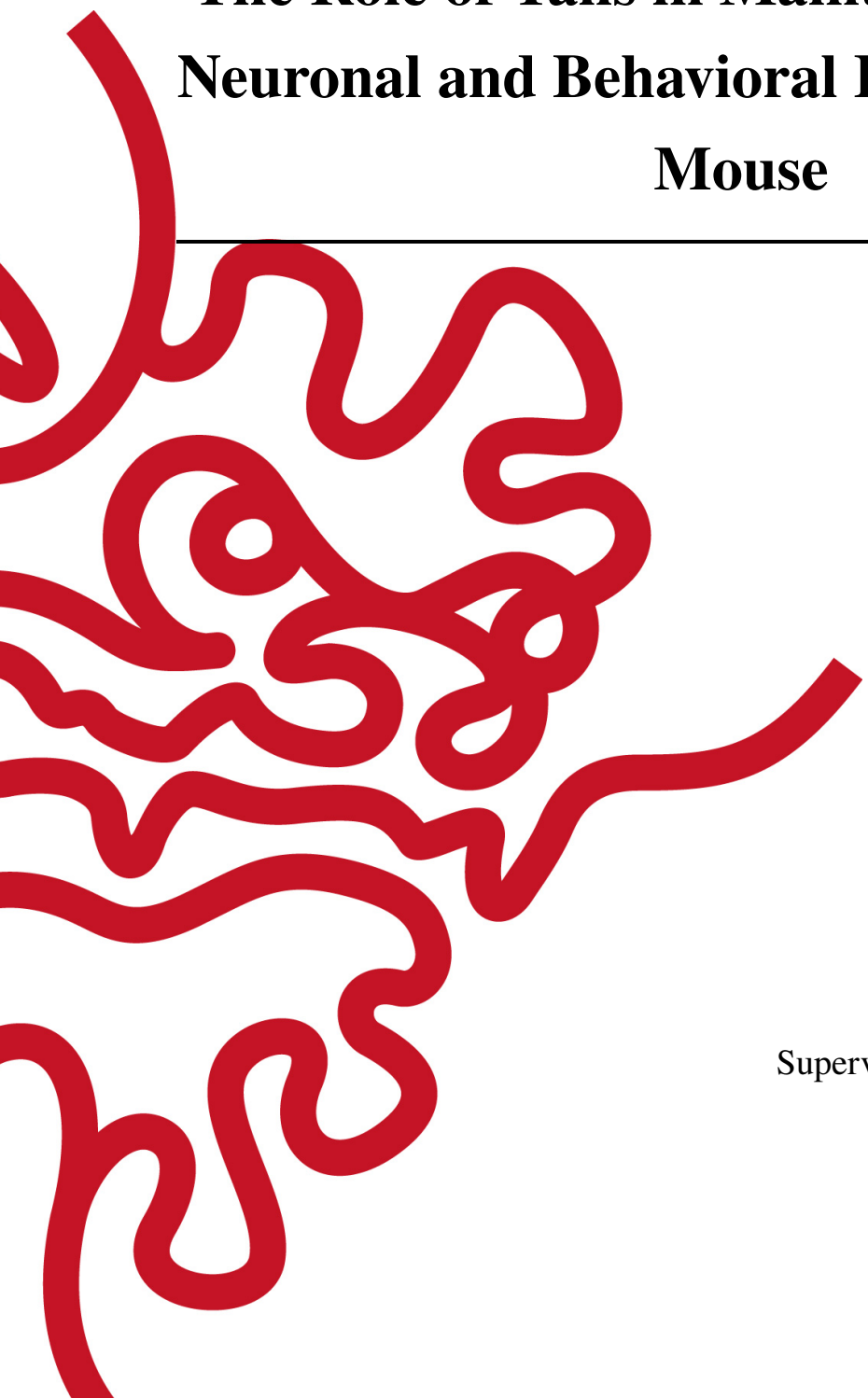

by

Salvatore Andrea Lacava

Supervisor: **Marylka Yoe Uusisaari**

September 2024

Declaration of Original and Sole Authorship

I, Salvatore Andrea Lacava, declare that this thesis entitled *The Role of Tails in Maintaining Balance: Neuronal and Behavioral Insights from the Mouse* and the data presented in it are original and my own work.

I confirm that:

- No part of this work has previously been submitted for a degree at this or any other university.
- References to the work of others have been clearly acknowledged. Quotations from the work of others have been clearly indicated, and attributed to them.
- In cases where others have contributed to part of this work, such contribution has been clearly acknowledged and distinguished from my own work.
- None of this work has been previously published elsewhere.

Date: September 2024

Signature:

Abstract

Tails are a distinguishing feature of animals and play a critical role in many aspects of their survival, such as maintaining balance. The present study aims to address the questions of whether and how laboratory mice (Mus musculus) use their tails to maintain balance and what are the neural mechanisms that control this behavior. To quantify how mice use their tails to maintain balance, I built a set-up (the ridge task) that simulates some of the challenges they may experience in nature. This task has led us to characterize a novel response from the tail in response to roll-plane perturbations and gave us insights onto how the tail is used during locomotion in challenging balancing conditions. In the anatomical part of the project, I will describe some of the neuronal circuits responsible for such behavior. Firstly, I characterized the morphology of tail motoneurons in the spinal cord and observed that these neurons (located in the sacral segment of the spinal cord) receive inputs from the vestibular system. Then I went on describing the subpopulation of vestibular neurons that project to the sacral spinal cord, revealing that they form a cluster mainly located in the Spinal Vestibular Nucleus. Finally, I used an optogenetic approach to stimulate either the entire vestibular nucleus, or selectively activate sacral-vestibulospinal neurons, to observe the effect of such manipulation on the tail. Intriguingly, given that the vestibular complex organization and functions are highly preserved across many taxa, the results from this project brings out exciting possibility for future studies on the organization of the neuronal control of tails in other chordates as well.

Acknowledgments

Firstly, I would like to thank my supervisor, Marylka Yoe Uusisaari, for hosting me as the first student in her unit. It was a gamble for both of us, but it paid off plenty (at least for me). Thank you for creating such a unique space to discuss ideas, not matter how out of the box, and for pushing me to pursue the big questions in science. You taught me the beauty of scientific discovery, and to savor that for the little time it may last, as most of science is about failure. In those low moments you taught me the beauty of rigor instead, which you helped me appreciate through the small things. I would like to thank also all of the members of the nRIM unit, the tough scientific discussions have instilled in me a critical perspective that I will bring in whatever future endeavour I will embark on. In particular I would like to thank Hugo and Isilak for their help with the optogenetic experiments and the anatomical processing respectively. I also would like to thank the Imaging Section at OIST and Julian Katzke for their help in obtaining the microCT scan of the tail and getting the muscle reconstruction respectively. I would like to thank the Mechanical workshop - especially Mouez Lassoued - for their help with 3D printing and all sorts of mechanical contributions that went into building the behavioral set-ups.
I would like to thank Laura and Carla from back home. Our friendship started off by our drive as teenagers to do what everyone else taught we could not. Thank you to Sarah and Lina for supporting me throughout my journey at OIST, I am looking forward to get back here together in the future to check our time-capsule. Thank you Yana, for introducing me to the rich music scene in Okinawa and our car rides to the orchestra practice, they were the lights of my Wednesdays.
I would like to thank Okinawa and Her people for hosting me in this place. I now have spent close to a fourth of my life in this precious island. Your serenity was a sweet companion when I felt overwhelmed by the mundane. You showed me the hardship you endured throughout the years, as well as the many possibilities you embrace. I hope the people that are here in passage will treat you with kindness and respect. You will be forever my second home.
A special thank you is to my partner, Seiji. It is your strength and heart that keeps me going. You gave me the space to feel safe.
Lastly, but most importantly, I would like to thank my Mum for having no doubts, while I had plenty, when I decided to move to a small island in the Pacific ocean to build an acrobatic playground for mice. You saw something that I could not see. Thank you also to the rest of my family, in particular my grandma Pina and my aunt Anna Lisa, who have shown me to lead with kindness and determination, the rest will follow.

List of Abbreviations

AAALAC	Association for Assessment and Accreditation of Laboratory Animal Care
AAV	Adeno-Associated Virus
AP	Anterior-Posterior
ASD	Autism Spectrum Disorder
BPPV	Benign Paroxysmal Positional Vertigo
CC	Central Canal
CNS	central nervous system
CL	Contralateral
CoM	center of mass
CnF	Cuneiform Nucleus
CPG	Central Pattern Generator
CTB	Cholera Toxin B-subunit
DCN	Deep Cerebellar Nuclei
DV	Dorso-Ventral
DS	Disynaptic
EPSP	Excitatory Postsynaptic Potential
EtOH	ethanol
FRA	Flexor Reflex Afferents
Gi	Gigantocellular Nucleus
GFP	Green Fluorescent Protein
GRN	gene regulatory network
Hox	homeobox genes
IL	Ipsilateral
Ia	Type Ia Sensory Afferents
I2KI	iodine potassium iodide
INs	Interneurons
LVN	Lateral Vestibular Nucleus
LVST	Lateral Vestibulospinal Tract
MIA	Maternal immune activation
ML	Medio-Lateral
MLF	Medial Longitudinal Fasciculus
MMB	Medetomidine HCL, Midazolam, and Butorphanol tartrate
MLR	Mesencephalic Locomotor Region
MNs	Motoneurons
MS	Monosynaptic
MVN	Medial Vestibular Nucleus

PBS	Phosphate-Buffered Saline
PFA	Paraformaldehyde
PPI	Prepulse Inhibition
PPN	Pedunculopontine Nucleus
QC	Quality Check
RF	Reticular Formation
ROI	Region of Interest
S tilt	Short tilt (10 degrees)
SVN	Superior Vestibular Nucleus
TS	Trisynaptic
TRT	Tilting Ridge Traverse
VCR	Vestibulocollic Reflex
VN	Vestibular Nuclei
VO	Vestibular-Only
VS	Vestibulospinal
VOR	Vestibulo-Ocular Reflex
coFRA	Contralateral Flexor Reflex Afferents
coVS	Contralateral Vestibulospinal
coVS	Contralateral Vestibulospinal
µCT	micro-computed tomography

“For a large number of problems there will be some
animal of choice, or a few such animals,
on which it can be most conveniently studied.”
Krogh’s principle

Contents

List of Figures

List of Tables

Introduction

The study of balance and motor control spans various species, behavioral contexts, and neuronal substrates. Mice (Mus musculus), as small mammals with remarkable adaptability, present an intriguing model for exploring these principles due to their dynamic and versatile movement strategies. This prologue introduces two chapters that delve into the intricate roles of the mouse tail in maintaining balance, offering new perspectives on vestibular and proprioceptive contributions to locomotion.

The first chapter describes the adaptive tail movements of mice in the ridge set-up, a behavioral task I built during the PhD where mice have to contend with external and self-generated balance perturbations. This research highlights the tail's ability to generate substantial angular momentum to counteract roll perturbations. Additionally, it explores the adjustments of hind-body and tail position during locomotion, suggesting that the tail acts to fine tune the mouse's balance strategy based on vestibular and proprioceptive cues.

In the second chapter I describe results from the anatomical investigation of the neuronal substrates responsible for tail movement in balancing conditions. Furthermore, I present the results from the vestibular activation (using optogenetics) on tail and overall body posture in mice. This research reveals context-dependent responses that underscore the adaptability of the vestibulospinal pathways. While on the ridge task the stimulation leads to direction-dependent tail movements, the same stimulation on a flat surface leads to an increase in the base of support (without the direction-dependent tail response). Further, selective stimulation of the sacral-vestibulospinal pathway (sac-VS, i.e. the direct projection of the vestibular system onto the sacral portion of the spinal cord), increases the likelihood of a tail swing motion, without clear effects on the rest of the body. This selective modulation suggests that sacVS neurons provide vestibular context to the downstream effectors in the spinal cord responsible for tail movement.

Together, these two chapters showcase the insights I have learnt in the past years addressing the questions of how mice use their tails to maintain balance as well as revealing some of the neuronal circuits involved in this process. While this is not an exhaustive description of all mechanisms and pathways involved in tail control, I hope the findings in this thesis will convince the reader that the tail plays a significant role in balance control and deserves a deeper appreciation in neuroscience research.

Chapter 1

Why does the tail matter (for balancing)?

1.1 Background

In the first chapter of this thesis I will introduce the mechanisms behind balance control, and what it means to lose balance. Then I will be defining the tail as an important evolutionary innovation, with focus on mammalian tails. Finally, I will describe what is known up to this point on mouse (Mus musculus) tail musculature organization, before moving to the results from the microCT scan data and finally the analysis from the kinematic data obtained in the ridge.

1.1.1 What is balance

Before going ahead with this document, I think it is important to clarify what is the definition of balance adopted in this thesis. The reason for wanting to dedicate an entire section to a definition might seem trivial, however I believe it is important as the term is used in a variety of different contexts without clarity on what it is. Work from early neurophysiology to characterize simple reflexes in the last century led us to believe that balance consisted of a set of reflexes that triggered motor programs based on visual, vestibular, or somatosensory triggers. This simplistic view contributed to our limited ability to assess the risk of falling ([1]). In fact, assuming that there is a singular balance system implies that a single test can measure overall balance performance. If balance control were solely controlled by one neural system, such as the vestibulospinal system, it might be plausible to focus on evaluating and treating this specific system to prevent falls. However, given that safe daily activities rely on a multifaceted interplay of physiological mechanisms, it becomes crucial to assess multiple systems to fully describe the balance constraints on an individual ([1]). In the following sections I will define different aspects that helps us to characterize balance as well as highlighting what it means to lose balance.

Biomechanical constraints

The primary biomechanical constraint affecting balance in terrestrial animals is their base of support and how this changes across different environments. Any limitation in the size, strength, range, or control of their points of contact with the ground (limbs in the case of most tetrapods) can influence balance. A fundamental aspect of balance control, which extends beyond living organisms, involves maintaining the center of mass (CoM) projection within the base of support. Balance, in this context, isn't a fixed position but rather a range of stability of possible movements

determined by the grounds contact-points and constraints on joint mobility, muscle strength, and sensory input.

The central nervous system (CNS) maintains an internal representation of this region of stability, directing movements and small adjustments to maintain balance. In animals with balance issues the region of stability may shrink, or the neural representation may become distorted, affecting their range of possible movements. An accurate CNS representation of the body's stability limits is critical, and conditions like Parkinson's disease can lead to abnormal representations, resulting in postural instability ([2]).

Movement strategies

Maintaining balance is a complex skill requiring enactement of context-dependent motor strategies that account for both passive and active self-movements [3]. For instance, "change-in-support" strategies (changing position of a limb) often serve as the most efficient mean to restore balance in healthy humans. However, when freedom of foot placement is constrained, "hips-and-ankles" strategies (torque-based shifts of the body's center of mass) become the primary balancing mechanism [4]. Under the most precarious balancing scenarios such as walking on narrow beams, humans additionally employ upper-body strategies involving arm movements [5–7]. Other strategies for regaining balance involve reaching, hip or trunk movements, anticipatory postural adjustments and so on ([8]). While animals can quickly employ postural movement strategies in response to disturbances, their strategy selection and response intensity can be influenced by intention, past experiences, and expectations ([9]). Anticipatory postural strategies prior to voluntary movements relies on forward models of how such movements affect the body and the external environment ([10]). When such models fail (for example, due to unexpected change in the environment), this may lead to instability during self-initiated movements.

Sensory strategies

To make sense of complex sensory environments, most animals combine information from their proprioceptive, vestibular, and visual systems. As the sensory landscape shifts (due to lesions, or simply aging), there's the need to switch the relative importance placed on each sense. In well-lit and stable environments, healthy humans primarily rely on proprioceptive cues (70 percent), followed by vision (10 percent), and vestibular input (20 percent) ([1]). However, when faced with unstable surfaces, they rely more on vestibular and visual inputs and less on proprioceptive cues for maintaining balance. The ability to adjust sensory reliance according to the situation is vital for stability when transitioning between sensory contexts. Additionally, certain central nervous system disorders, such as Alzheimer's disease, may compromise the ability to readily adjust sensory reliance even when the peripheral sensory systems remain intact ([11]). This challenge in adapting to different sensory contexts highlights the critical role of sensory integration in upholding stability and preventing falls.

Orientation in space

The capacity to orient the body in relation to the gravity vector, the support surface, visual surroundings, and internal references is a pivotal aspect of maintaining balance. The nervous system adapts body orientation based on the context and task at hand. For example, animals may

position their bodies perpendicular to their support surface until it tilts, at which point they adjust their posture to counteract the gravitational force ([12]). The perception of postural verticality entails aligning the body in space without visual cues, relying on proprioceptive and vestibular information. Consequently, individuals with unilateral vestibular loss display a skewed internal representation of verticality ([13]).

Cognitive skills

Maintaining posture requires considerable cognitive resources, even during apparently simple activities like standing upright. The cognitive load escalates with the complexity of the postural task, resulting in decreased reaction times and performance in concurrent cognitive activities, since cognitive resources are distributed between postural control and other cognitive functions, participating in a secondary cognitive task can hinder performance in postural tasks ([14]).In fact, inadequate cognitive resources available during engagement in a secondary cognitive task can lead to falls due to compromised postural control ([15]).

What does it mean to lose balance?

Considering that animals possess unique constraints and resources for postural control, their ability to maintain balance and orientation varies depending on the specific environment that surrounds them. As a result, animals may encounter falls in various situations, depending on the systems required for successful task completion. Identifying the risk factors for falling in animals requires understanding their morphological constraints, as well as identifying physiological risks for balance disorders. To predict the risks of falling and develop effective interventions for animals with balance impairments, it's essential to evaluate the integrity of underlying physiological systems and available compensatory strategies. Simple measures of balance are not adequate to predict the situations that lead to lose balance, as such measures cannot identify the specific constraints on the sensorimotor processes contributing to postural control.

As discussed up to this point, balancing is a complex ability that necessitates the integration of multiple sensory inputs. When evaluating balance, several confounding factors may restrict a comprehensive description of this ability. The approach to simplify the problem, adopted in this thesis, is to examine how the tail is used to maintain balance. Unlike limbs, the tail is not essential for locomotion in mice, making it an intriguing subject of study for those of us interested in dissecting balance strategies from other confounding motor programs (such as locomotion).

1.1.2 Tail as an evolutionary innovation

Tails represent a distinctive feature among chordates, exhibiting considerable variation in both function and form ([16]). Despite their shared evolutionary and genetic developmental origins, tails show remarkable variety in both their physical characteristics and roles. They can vary significantly in length, thickness, and texture as shown in the drawing in 1.1.

Tails have been defined classically based on anatomy as "the post-anal appendage". However such definition would be inaccurate in fish, as it would include parts of the dorsal, caudal and anal fin. Particularly in teleosts it was proposed that tails evolved by gradually growing larger and changing shape. However, Sallan (2016, [17]) looked at ontogenetic data from Aetheretmon

(a 350-million-year-old teleost) and found that they actually had two separate parts to their tails: one lower part with fins and one upper part with vertebrae, similar to what we see in animals with backbones like mammals. This means that instead of the tail just getting bigger over time, it started out with these two parts from the beginning. In some modern fish the upper part of the tail stopped growing while the lower part expanded, eventually becoming the dominant part of the tail. This change may have helped these fish swim more efficiently. So, rather than tails evolving by simply getting bigger, this new theory suggests that they evolved by changing the growth of different parts across tetrapods ([17]).

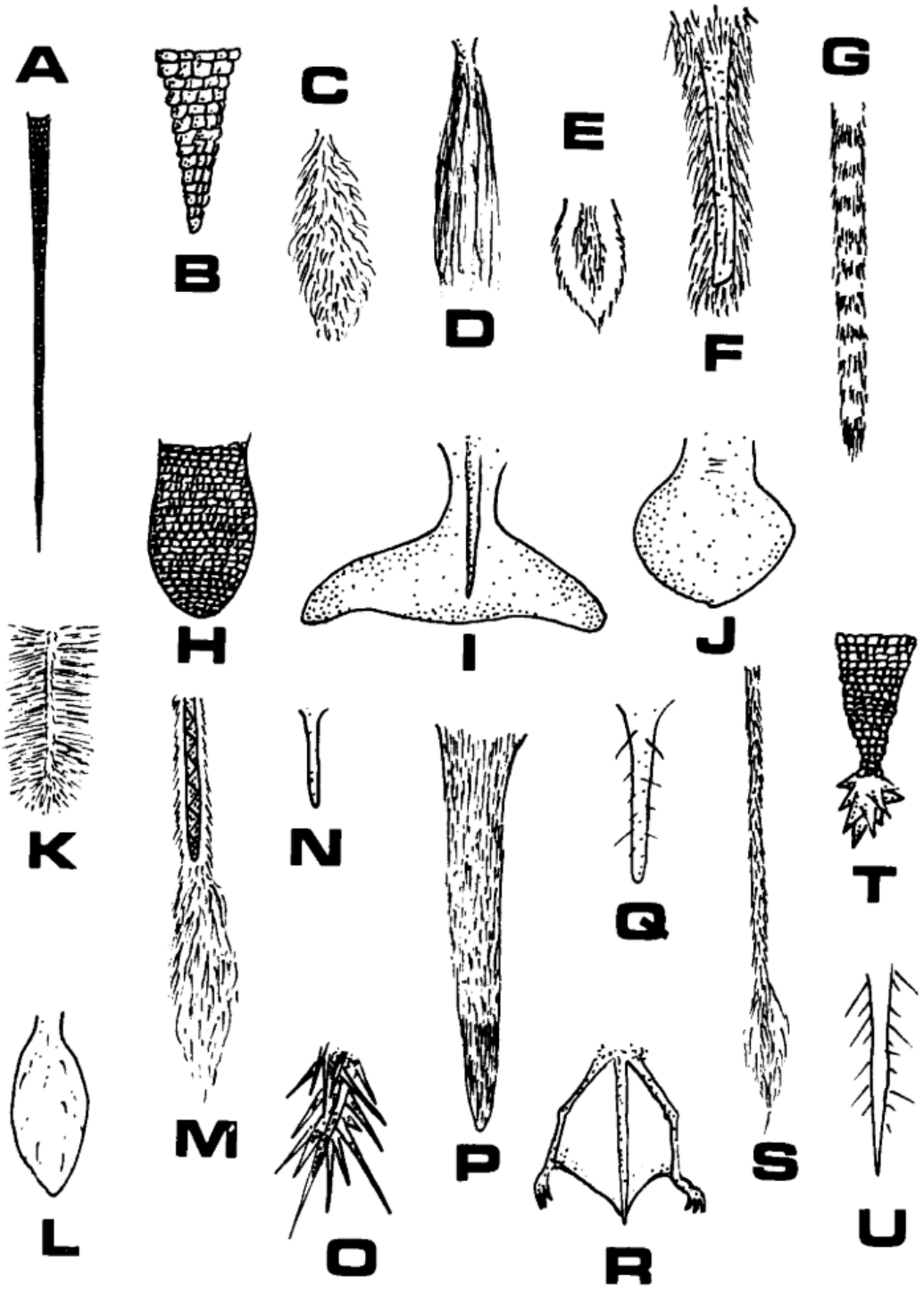

Figure 1.1: Tails of different mammals. Various tails of mammals shown from the dorsal side. The illustrations were not drawn to scale. A - *Rattus rattus* (Black Rat), B - *Dasypus novemcinctus* (Nine-banded Armadillo), C - *Sciurus carolinensis* (Grey Squirrel), D - *Equus caballus* (Horse), E - *Dama dama* (Fallow Deer), F - *Brachyteles arachnoides* (Wooly Spider Monkey, ventral aspect), G - *Nasua nasua* (Coatimundi), H - *Castor canadensis* (Beaver), I - *Hyperoodon ampullatus* (Bottle-nosed Whale), J - *Trichechus manatus* (Manatee), K - *Glaucomys volans* (Flying Squirrel), L - *Pachyuromys duprasi* (Fat-tailed Gerbil), M - *Anomalurus pelii* (Scaly-tailed Squirrel, ventral aspect), N - *Geomys bursarius* (Plains Pocket Gopher), O - *Hystrix brachyura* (Porcupine), P - *Macropus giganteus* (Great Grey Kangaroo), Q - *Heterocephalus glaber* (Naked Mole-rat), R - *Eptesicus fuscus* (Big Brown Bat), S - *Dipodomys merriami* (Merriam's Kangaroo Rat), T - Glyptodont (extinct), U - *Pseudopodus ceylonus* (Ceylon Shrew). Drawing from Hickman, 1979 [18].

More recently, advances in sequencing technology has allowed us to look at the role of genes in the development of the tail. Such approach could likely be useful to determine homology across chordates' tail structures, and therefore help us defining what the tail is across chordates. Three main gene regulatory networks (GRNs) are known to be involved in tail development: Hox (not too surprising given its role in the development of anterior-posterior body plan), T-box transcription factors, and Hedgehog signaling genes. As an example, six genomic regions have been identified as contributing to differences in tail length in deer mice (Peromyscus maniculatus), with three affecting caudal vertebra length, three affecting vertebra number, and two of these regions showing allele-specific decreased Hoxd13 expression linked to vertebra number variation ([19]). Another recent study that looked at the genetic mechanisms behind tail loss in humans found that simply an individual insertion of an Alu element in the genome of the hominoid ancestor may have contributed to tail-loss evolution ([20]). These studies combined may suggest that even though several genetic mechanisms are involved in tail development, only a few may have contributed to tail loss. Hinting at the speculation that if enough environmental pressure is applied tail gain or loss of function can be implemented through even just a few simple point mutations.

1.1.3 Mammalian tail use

Given that all mammals have caudal vertebrae, all mammals have a tail (even if not visible). Throughout evolution, mammalians' tails have diversified for various purposes, such as swimming, hopping, climbing and so forth. As previously discussed, although humans (along with other animals) have experienced tail reduction or loss, a significant portion of vertebrates have retained, lengthened, enriched, or re-purposed their tails. This supports its possible evolutionary significance in adapting to different ecological environments.

Many terrestrial animals, such as felines, have long tails that helps maintaining balance and flexibility at high speeds. Some primates use the tail while walking on two legs to balance, and many animals use tails when balancing in trees. As mentioned above, the tail of deer mice is much longer for the arboreal ecotype than the terrestrial ones [18]. In line with this, a recent review study from Mincer et al.(2020, [21]) explores the factors influencing the evolution of mammalian tail length. The research reveals that substrate use, particularly arboreal substrates, plays a significant role in tail length across all mammals, with arboreal environments favoring longer tails. Non-arboreal substrate use leads to diversification, resulting in varying tail lengths. Moreover, tail loss is more common in non-arboreal species, but certain arboreal species may lose their tails, potentially due to factors like increased body size or specific locomotor modes.

Finally, one of the most impressive examples of tail usage in mammals comes from the rodents family, the kangaroo rat. When reaching for objects overhead, the tail is used as a prop. Also, during very high leaps the tail is swung over the back. This dynamic use of the tail is thought to counteract sudden changes in the angular momentum of the body, preventing the animal to flip. Kangaroo rats also use their tails to keep balance while hopping 1.2 [22], and in escaping predators ([23]). Another example of tail usage in rodents includes the deer mouse, whose tail usage was described as early as the 1950s ([24]). More recently, its evolutionary and genetic makeup has been described by the lab of Professor Hoekstra ([19, 25]).

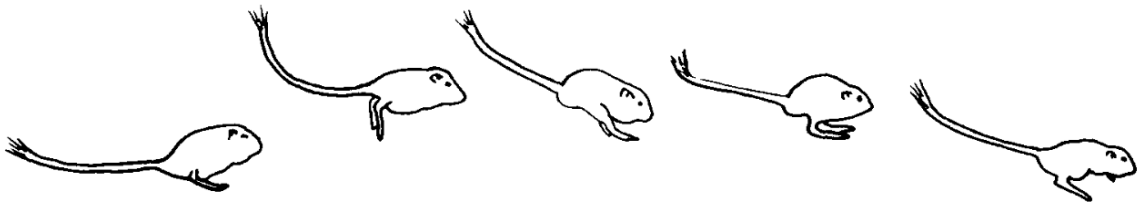

Figure 1.2: Kangaroo rat tail. The tail is used for balance in the bipedal locomotion of a kangaroo rat (drawing by Bartholomew and Caswell, 1951 [18]).

1.1.4 Anatomy and function of mouse tail (Mus musculus)

The organization of the mouse tail musculature is based on repetitive fusions between the extrinsic and intrinsic muscles, that is muscles that lie at the surface and in the deep layers respectively, at each vertebra. This design is also known as the metameric arrangement. Surprisingly, the organization, arrangement and function of muscles in the tail have features in common with those muscles in the digits of the human extremities [26]. The mouse tail is supported by 29 coccygeal vertebrae (Co1 – Co29). Each coccygeal vertebra consists of a body, cranial and caudal processes. The tail is defined as the coccygeal region that extends from the lumbo-sacro-coxal region. Its body consists of 10 longitudinal elements: 4 fasciculi of tendons and 6 stripes of short muscles that span 1 or 2 vertebrae. Shinohara [26] reveals that the tail muscular system has 3 main features.

1. Tail muscles are classified as ventral, lateral, and dorsal, and each has rostral and caudal heads. The extrinsic and intrinsic muscles are fused and terminate on the same coccygeal processes.

2. The tendons of the muscle that starts from the coxal bone are perforated by the tendon of bicipital muscle. This is also a feature preserved in human hands.

3. There is a pattern of insertions and origins of bicipital muscles (also known as metameric pattern) along the tail main axis.

These features define mouse tail motility and its mechanical constrains.

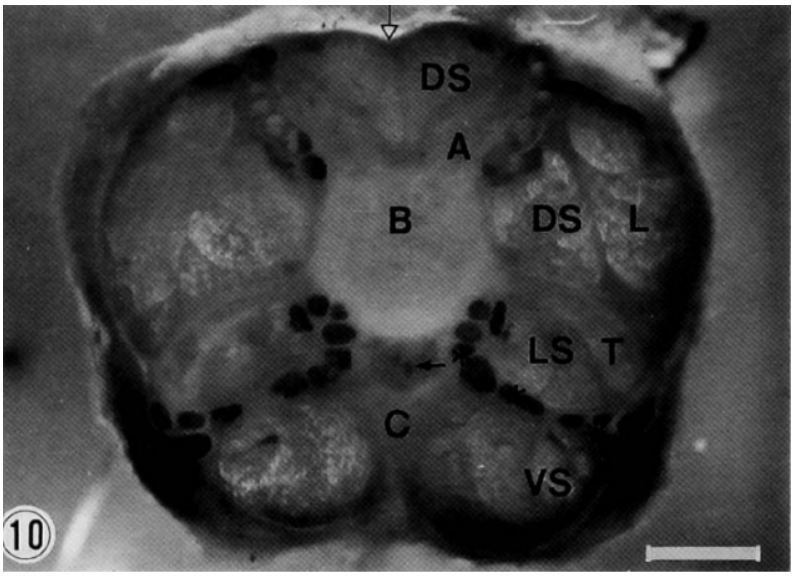

Figure 1.3: Cross section of the tail at Coccygeal vertebra 4. In the picture, you can observe: The dorsal short muscle (DS), the lateral short muscle (LS), and ventral short muscle (VS), ventral and lateral tendons (solid circles), the lateral portion (L; dorsal side). A: articular process. Solid arrow: artery of the tail. From Shinohara (1999) [26].

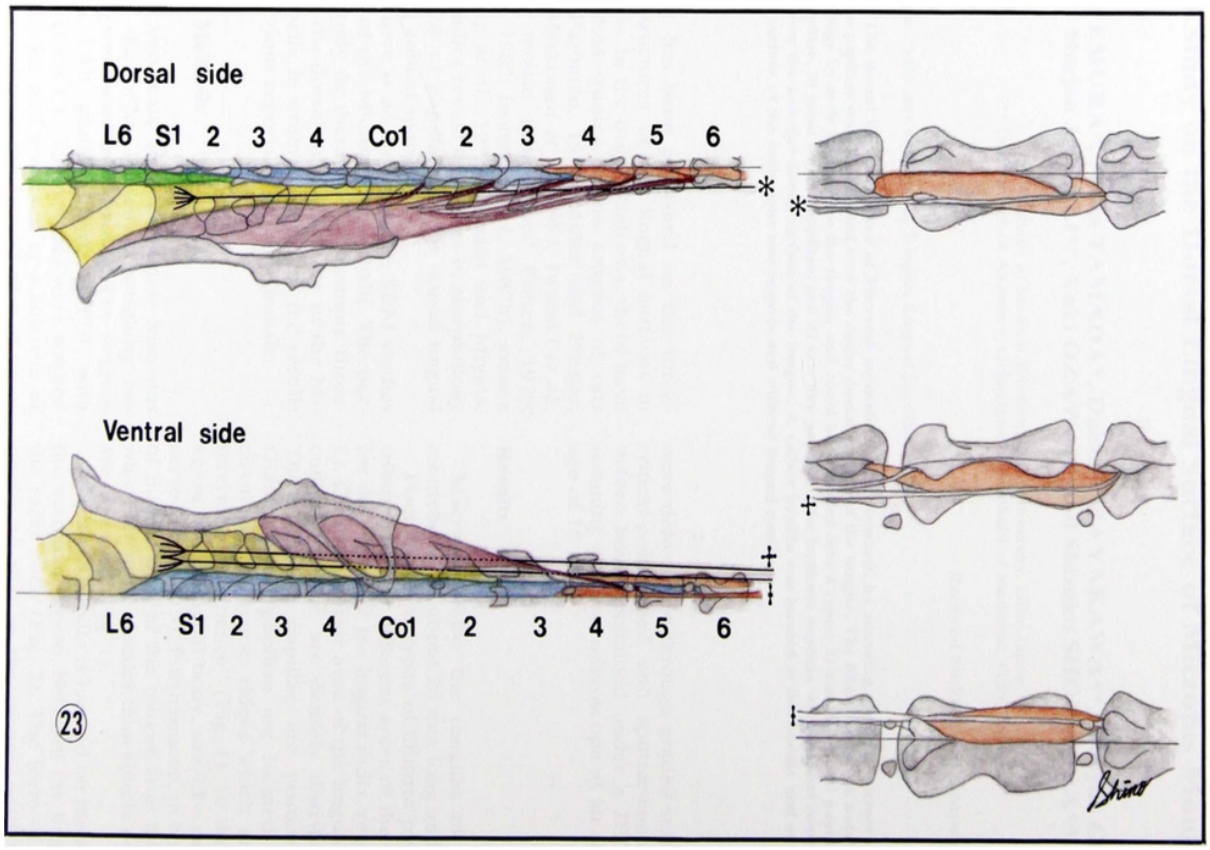

Figure 1.4: Drawing of the dorsal, lateral, and ventral bicipital muscles. The dorsal bicipital muscles originate from the intermediate portion (yellow) of the dorsal lumbo-sacro-coxal region. The dorsal tendon (asterisk) is continuous to the dorsal short muscle (red in the right drawings) to form a bicipital muscle and terminates at the cranial articular process. Green, multifidus muscles; Blue, muscles of the medial portion that function dorsiflexion of the tail base; Violet, muscles of the lateral portion that function in ipsilateral flexion of the tail base and prevent the dorsal tendons from going off track. On the ventral side, the lateral and medial bicipital muscles that are inserted at Co5—Co9 originate from the medial portion (blue). From Shinohara (1999) [26].

The number of studies on Mus musculus's tail function have been few in numbers and have found little evidence of a clear function for it. For example, tail contribution in thermoregulation is just modest (contrary to other rodents such as rats, [27]). Anecdotally, researchers routinely working with mice have observed them shaking their tails when they are exposed to anxiety-indusive environments, although a conclusive analysis of this is lacking ([28]). Common house mice which have had their tails cut were shown to be impaired in climbing [29], which suggests that tails could be used for balancing. On the other hand, a recent study from Machado [30] suggested that mice oscillates their tails passively during locomotion. Most studies looking at balance in mouse have mostly focused on forelimbs and hindlimbs, and no study to our knowledge have described the function of mouse tail in balancing with high spatial and temporal resolution. In the next section I will describe the tail musculature architecture I obtained from microCT scan data (which largely confirmed the description by Shinohara (1999) [26], as well as the behavioral recording in the ridge, a set-up I built to probe the tail to respond to balance perturbation, as well as during locomotion in an increasingly challenging environments.

1.2 Methodology and Results

1.2.1 Aim 1: Mouse tail muscle reconstruction via microCT scan

In this section I describe the tissue preparation, acquisition and image processing from the microCT scan to reconstruct the basic organization of tail muscles in the mouse (Mus musculus). These results were collected in collaboration with the imaging facility at OIST (for microCT scanning), and Julian Katzke from the Biodiversity and Biocomplexity Unit (for the muscle reconstruction using Amira).

Specimen preparation and iodine incubation

The tail of one mouse (male mouse 12 weeks old), was collected after perfusion for perfusion-fixing, the animal was deeply anesthetized with MMB overdose (containing Medetomidine HCL, 1 mg/ml; Midazolam, 5 mg/ml; and Butorphanol tartrate, 5 mg/ml; dosage 0.05 ml/g) and after he was unconscious (verified with an absence to the toe pinch reflex), the heart was exposed and the animal was transcardially perfused, first with sucrose solution to clear the blood and then with fixative solution (4 percent paraformaldehyde), and finally the tail was extracted for anatomical examination. The tail dissection was done from 1 cm from the tail base rostrally, the fat and skin was carefully removed from the muscle. The tail was placed in a straight position along a 15 ml falcon tube. It was immersed in PFA 4 percent for 24 hours, and then other 24 hours in EtOH, before moving it to Iodine for staining. While formalin fixation can influence the density and volume of isolated muscle tissue, this was not accounted for in this study as the muscles were still connected to the bones in their natural position (keeping the tail as straight as possible within the falcon tube). The specimen was then removed from the solution and immersed in ethanol for one day.

Computed tomography and image segmentation

The I2KI-stained tail was scanned using a BIR ACTIS 225/300 high-resolution microCT system, operating at 130 kV and 0.1 mA with a 0.5 mm brass filter. The resulting TIFF images were reconstructed in 16-bit format, with an isometric voxel size of 4.5 um × 4.5 um × 4.5 um. The tail muscles were segmented and visualised using Amira software (Peeters et al. 2020). The µCT dataset was then cropped to contain the basal portion of the tail muscles only (including the coccygeal bones) and exported as a new image stack for further processing. As shown in 1.5 the microCT scan provided a comprehensive overview for the reconstruction of mouse tail musculature. Panel A offered dorsal and lateral perspectives of the tail reconstruction, top and down sub-panels respectively. Coronal sections (B) and (C) depicted the distribution of extrinsic and intrinsic muscles around the coccygeal vertebrae. The color scheme distinguished between different muscle types: red represented lateral extrinsic muscles, blue denoted dorsal extrinsic muscles, green indicated ventral extrinsic muscles, and orange highlighted intrinsic muscles. Coccygeal vertebra number 4 was marked in white for reference. Such reconstruction confirms that the tail has a metameric arrangement (similar to the forelimbs) as described above, according to Shinohara's reconstruction ([26]).

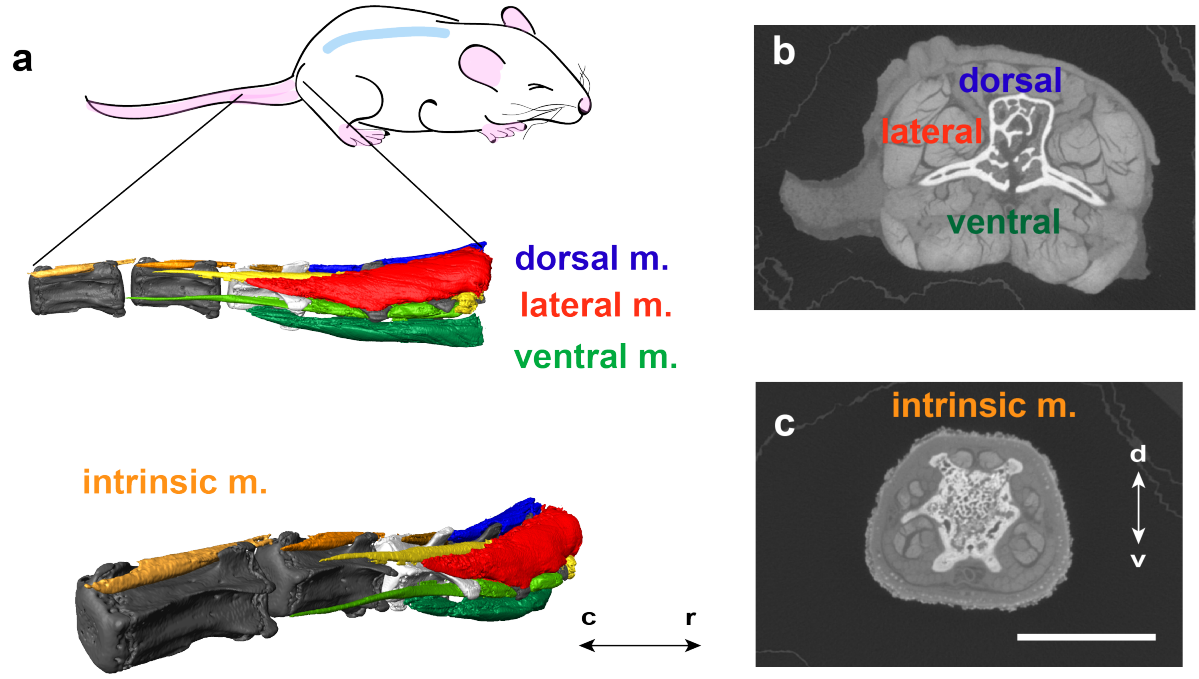

Figure 1.5: Tail muscle reconstruction overview from microCT scan. Dorsal and lateral overview of the tail reconstruction after microCT scan acquisition (panel A top and down respectively). Coronal sections showing extrinsic muscle (B), and intrinsic muscles (C) distribution around the respective coccygeal vertebrae. Red: lateral extrinsic muscle, Blue: dorsal extrinsic muscle, Green: ventral extrinsic muscle, Orange: intrinsic muscles. White vertebra is Coccygeal 4. Scale bar = 0.5mm.

1.2.2 Aim 2: Description of the tail kinematics in the context of balance

In this section I will provide an overview of the key results from the kinematic analysis of the tail in response to an external roll perturbation and locomotion in a challenging balancing task (the ridge). I developed this task following the observation that mice swing their tails while their body rotates in the roll plane, but not in the yaw or pitch. I then built a mechanical swing to test whether this tail motion can be systematically elicited in response to body roll movements. Finally, I showed that the tail swings not only during external roll perturbation, but oscillatory movements are produced as well during self-generated body rotations (i.e. during locomotion). A biomechanical model is provided as well to quantify the contribution of the tail to overall stability. These results are described in more details in my preprint available in bioRxiv at ([31]).

Rotational tail movement generates significant angular momentum

In order to describe how mice use their tails to maintain balance, I developed a novel experimental task ("Tilting ridge traverse", TRT; 1.6B). In the task, the ridge is tilted randomly left or right to produce balancing responses that are recorded with two high-speed video cameras positioned

above and posterior to the mouse.

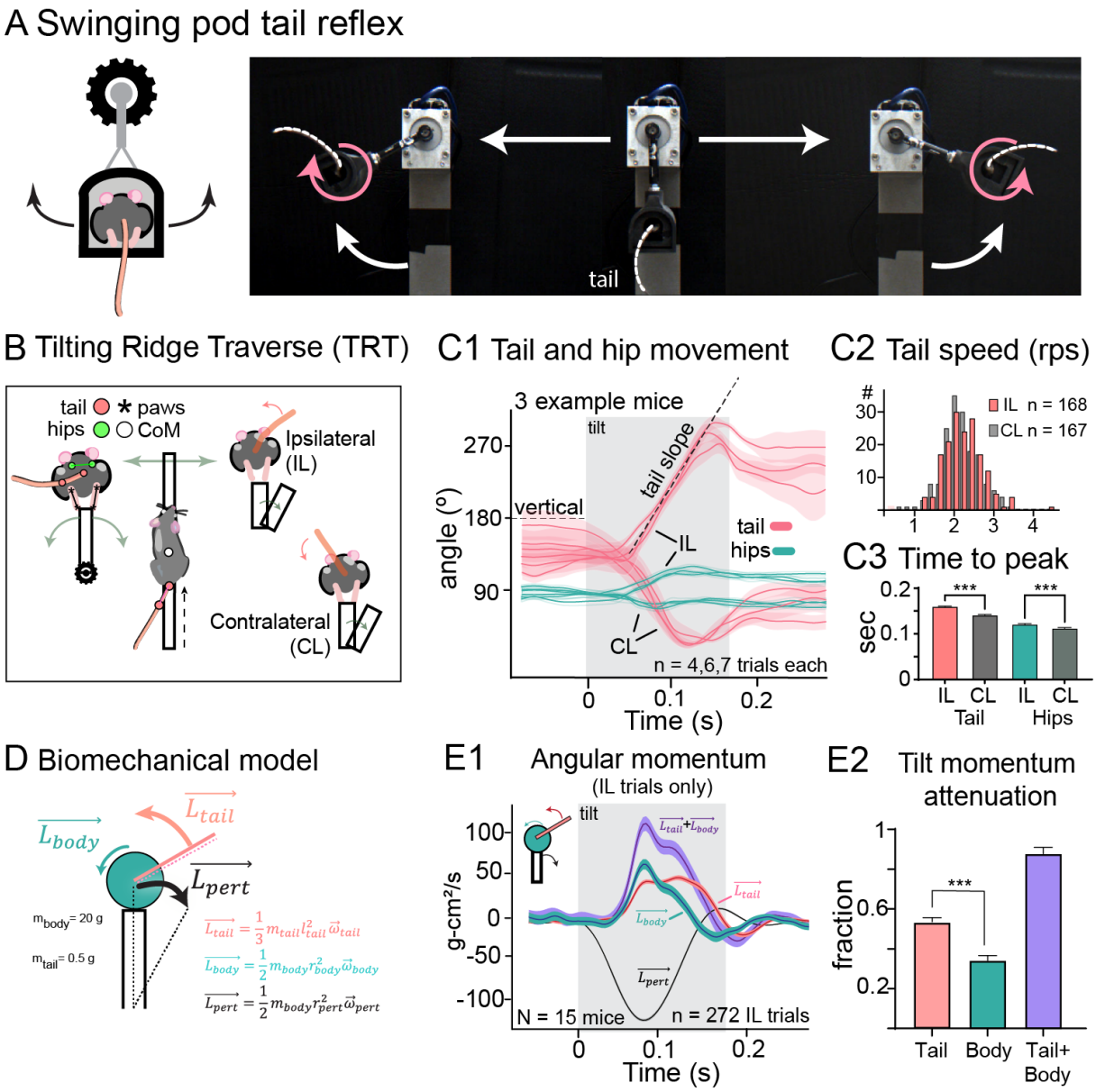

Figure 1.6: Roll-plane tilting evokes counteracting tail responses. A: mice experiencing lateral rolls in a custom-made swing rotate their tails in the countering direction. Schematic illustration (left) and screenshots (right). B, schematic illustration of the Tilting Ridge Traverse (TRT) task. Left: location of tracked body parts as seen from rear and top cameras. Right: depiction of "ipsilateral" and "contralateral" trials, defined by whether the tilt occurred in the same or opposite direction of the tail position, respectively. C, tail and hips angle changes in response to tilts. C1, tail and hip angle trajectories (pink and green data, respectively) from 3 example mice experiencing either ipsilateral (IL) or contralateral (CL) tilts. Traces show mean ± SEM for n = 4, 6 and 7 trials. Gray area indicates ridge movement. C2, comparison of mean tail acceleration (defined as the slope as indicated in C1) in IL and CL trials. C3, comparison of tail and hip movement duration (to the maximal displacement) in IL and CL trials. D, schematic illustration of the biomechanical model used to estimate angular momenta experienced by the mouse as well as the compensation generated by body and tail rotation based on tracked movements. For details, see Appendix A. E, comparison of angular momenta generated by the tilt perturbations and tail and body rotations elicited by IL tilts. E1, instantaneous momenta estimated using the model. Traces show mean ± SEM for n = 272 trials N = 15 mice for tail, body and the sum of tail and body, as well as the estimated rotational momentum generated by the perturbation. Downwards direction corresponds to the direction of the tilt. E2, total angular momentum generated by tail, hips and their sum, shown as a proportion of the perturbation-generated momentum. All data shown as mean ± SEM and groups were compared using t-test (d) or one-way ANOVA (e) followed by Bonferroni's post-test (*** $p < 0.001$). Figure from preprint [31].

While crossing the ridge, mice typically keep their tails to one side of their body. Initially, I analyzed trials where the tilt happened in the direction of the tail ("Ipsilateral (IL) tilt"; 1.6B), anticipating a body posture adjustment that would shift the CoM in the opposite direction. As expected, the tilt not only caused a moderate back-and-forth motion of the hips (1.6C1, green data) but also prompted a tail swing to the opposite side with remarkably consistent kinematics (1.6C, red data).

Surprisingly, tilts directed away from the tail ("Contralateral (CL) tilt"; 1.6B) also triggered tail responses with mirrored kinematics and nearly identical speed profiles (IL, 2.20 ± 0.037 rotations per second (rps); CL, 2.12 ± 0.038 rps; p = 0.15), despite the movement being restricted by the tail contacting the ridge (1.6C1-C3). Since the tail cannot provide additional counterweight during CL tilt trials, the primary mechanism by which the tail aids in balancing may be related to rotational momentum rather than simply shifting the mouse weight.

To determine whether the angular momentum generated by the tail's swing could make a sufficient compensation, I developed a simple mechanical model. This model approximated the mouse body as a cylinder and the tail as a rigid rod attached to the cylinder's base (1.6D; see appendix A for model details). Using body part weights from carcasses and angular velocities from live experimental animals, I estimated the angular momenta that the ridge-tilt conditions would induce in the body and the theoretical compensation provided by the tail and body rotation. Given that contralateral tail movements were restricted due to ridge contact (evidenced by the limited movement range in 1.6C) and the compensatory momentum largely depends on the tail's position at the onset of the tilt, I primarily focused on ipsilateral trials for the analysis.

Despite making up for only a small fraction of the body mass (2.56 ± 0.12 percent of the body without the tail), the mouse tail's movement generates compensatory momentum with a peak magnitude comparable to that produced by the rest of the body (1.6E1). Additionally, the total momentum generated by the tail exceeded that of the body during the tilt (1.6E2). This is due to the tail's high speed (up to 6 full rotations per second) and its continuous rotation nearly throughout the 190 ms tilting motion, whereas the hip movement stops earlier (time to peak position for tail and hips during IL tilts: 0.16 ± 0.0014 s and 0.12 ± 0.0016 s, unpaired two-sample t-test $p < 0.001$). Ultimately, the combined compensatory momentum from the body and tail accounted for over 80 percent of the total estimated rotational momentum experienced by the body in response to the ridge tilt (1.6E2, blue).

Adjustments of the tail to decrease in platform width

Furthermore, I tested if the the tail and body were affected by changes in the magnitude of perturbation (tilt angle), increasing it to 30° ('L' tilt) or decreasing it to 10° ('S' tilt) (1.7A1). To assess the relative difficulty of different tilts, I measured their impact on the mouse's forward movement (1.7A2-4). The performance of mice under 10 or 20-degree tilts was similar, but the largest tilt (30 degrees) posed a greater challenge, leading them to stop completely (defined as forward speed less than 1 mm/s, previously defined as the immobility threshold in [32]) and significantly reducing the distance traveled in the 0.5-second window following the tilt (1.7A3-4). Therefore, mice could not fully compensate for the largest tilt perturbation and had difficulty maintaining forward movement.

When analyzing the time courses and magnitudes of compensatory momentum originating from the tail and body, I showed that the tail swing duration increased slightly with medium tilts compared to short tilts (1.7B1, red). However, with long tilts, the tail movement was restricted

by contact with the opposite side of the ridge. As a result, the total compensatory momentum could not increase further (1.7B2). Without additional modulation of the hip movements, this led to incomplete compensation for the perturbation during long tilts (1.7B3).

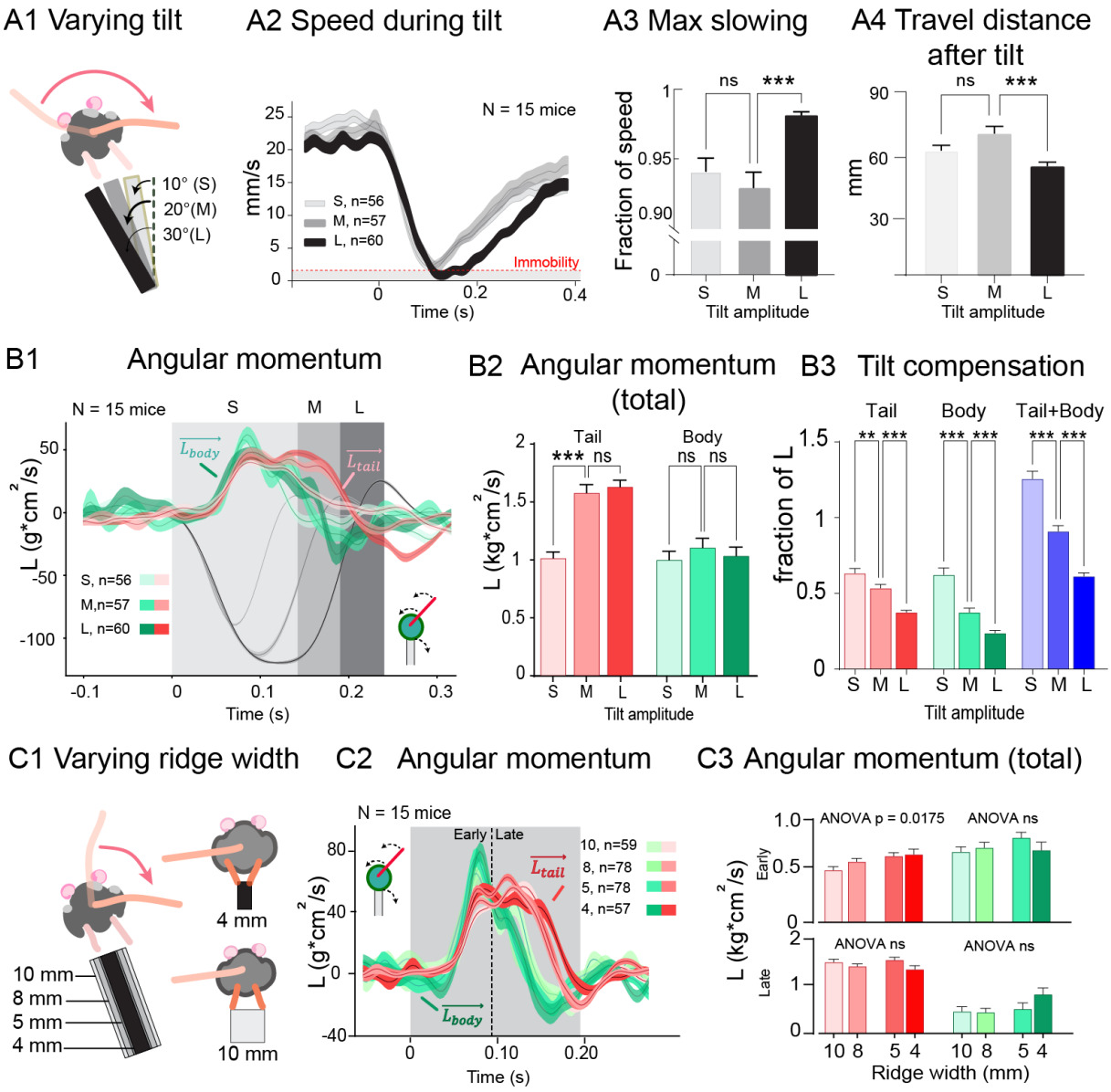

Figure 1.7: Tilt duration and ridge width effect on tail response to external perturbations. A, effect of tilt amplitude on balancing performance. A1, three tilt angles used: short (S), medium (M), long (L). A2, decrease in forward velocity of the mice during perturbations. Dashed line indicates threshold value for immobility (1 mm/s). A3, effect of larger tilt on task performance quantified as extent of slowing from pre-tilt-velocity. A4, distance travelled during the 0.5 sec following a tilt. Data from 15 mice; number of trials on each tilt amplitude indicated in panel A2. B, effect of tilt amplitudes on tail and body responses. B1, time course of the tail (red traces) and body-generated (green traces) angular momenta opposing the tilt-induced momenta (gray traces). Shading denotes tilt durations and the time windows from which total momenta are calculated in B2-B3. B2, total angular momenta generated by the tail and body during tilts. B3, total momenta for the tail, body, and their sum as a fraction of the total tilt-induced momentum. C, narrowing stance on ridge leads to slight changes in tail swing response. C1, schematic depicting different alignment of hind paws on narrow and wide ridges. C2, time course of tail and body angular momenta in response to medium-duration tilts on ridges of different widths. Shaded area indicates tilt duration; dashed line denotes division into early and late halves used in C3. C3, total momentum of the tail response increase on narrower ridges during early phase of the response (top panels) but not late phase (bottom panels). Data are presented as the mean ± SEM, and statistical comparisons were conducted using one-way ANOVA followed by Bonferroni's post-test (*$p<0.05$, **$p<0.01$, and ***$p<0.001$). Figure from preprint [31].

The kinematic invariance (i.e., consistent speed profile) of the tail responses to both ipsilateral and contralateral tilts (1.6C) suggests it may be a previously overlooked balancing reflex, similar to other corrective motor programs related to balance [33, 34]. To determine if tail swing and body rotation responses are influenced by proprioceptive context, I repeated the experiments using ridges of different widths (4, 5, 8, and 10 mm), which caused the mice to adopt slightly but significantly different postures (1.7c1). Focusing on the early phase of compensatory responses, which are most likely to be affected by different body configurations, I observed a slight trend towards higher tail-generated compensatory momentum on narrow ridges (ANOVA $p < 0.5$; 1.7C3) during the first half of the response, while no effects were seen in momentum generated by body rotation. No differences were found in either body- or tail-originating momenta in the late phase of the response.

Balance performance in different degrees of challenging conditions

The variations in tail kinematics on the narrowest ridges likely indicate increased balancing challenges, as shown by the gradual and significant rise in slips during traversal and a reduction in traversing speed in trials without tilt perturbation (1.8A1-2). To better understand how mice use their tails for such precarious locomotion, I needed to develop more precise metrics of balancing performance, since simply counting paw slips might not provide enough information. Therefore, I complemented the paw slip counts with additional metrics based on the center of mass (CoM) position relative to the lateral extent of the base of support.

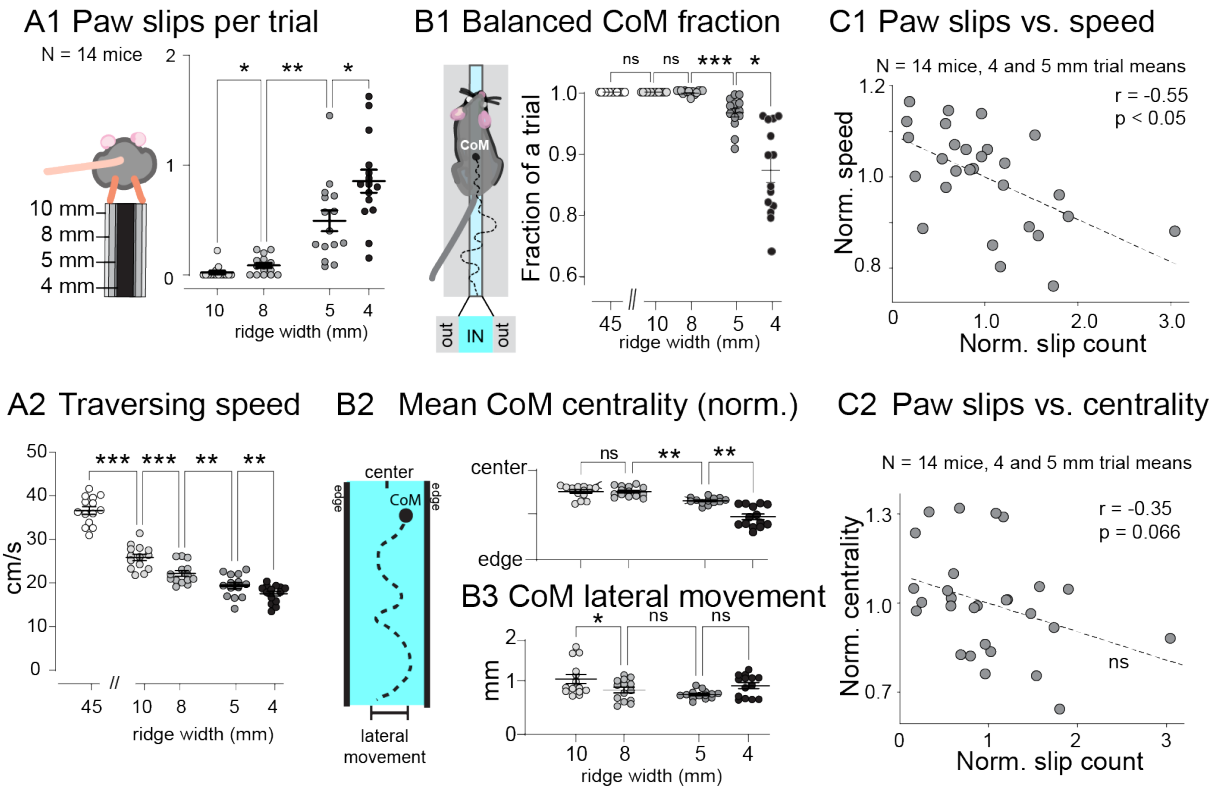

Figure 1.8: Effect of ridge width on body posture and task performance. A, quantification of ridge traverse performance by number of paw slips (A1) and traversing speed (A2). B, TRT performance based on Center of Mass position. B1, percentage of frames in which the Center of Mass (CoM) was within the Base of Support (BoS), as determined by the ridge edges (schematic on the left). B2, left: depiction of CoM centrality measure that ranges from 1 (at center of the ridge) to 0 (at or beyond the edge). Right, top panel: CoM position is less central on narrow ridges. Bottom panel: amplitude of lateral CoM movement does not differ on narrowest ridges. C, comparison of balancing performance metrics. C1, paw slip counts versus traversing speed; C2, paw slip counts versus CoM centrality. As very few paw slips occur on 8 and 10 mm ridges, only 5 and 4 mm trials are shown. Figure from preprint [31].

As shown in 1.8B2, the animals managed to keep their CoM above the ridge (serving as the base of support, BoS) in almost all trials, except on the narrowest (4 mm) ridge. On the 5 mm ridge, the CoM only rarely deviated outside the support base, and even on the 4 mm ridge, the animals maintained balance for most of the trial ($89 \pm 0.16\%$ of the frames). A complementary and analogue (instead of binary) measure, "Relative centrality" (1.8B2), is based on the idea that for the most energy-efficient locomotion, the mouse should aim to keep its CoM as close to the center of the BoS as possible. I found that mice had no trouble keeping their bodies near the midline on ridges wider than 5 mm. However, the centrality measure indicates that on the 5- and 4-mm ridges, the CoM position becomes significantly more precarious, as the lateral oscillation of the CoM related to locomotion cannot be reduced further (1.8B3).

Importantly, the narrower footholds (see schematic in 1.9C) on the 4- and 5-mm ridges required an adjustment in hind paw posture. Additionally, although mice kept the head and front body aligned with the platform on all trials (1.9A1, green), on the 5- and 4-mm ridges, their caudal body posture became angled (1.9A1, red), likely due to the difficulty of placing paws on the narrow support. However, the angles of both the front and hind body were not linked to

slower movement, despite a slight and expected correlation with CoM centrality (1.9A2-3).

In addition to adjusting their hind-body posture, mice also held their tails at larger angles relative to the hind body when traversing 4-5 mm ridges (1.9B1). Since the capacity to generate rotational momentum increases with the angle of the rotating mass [35], such adjustments could be part of a motor strategy for mice to compensate for the increasing challenge of locomotion on narrower ridges. Indeed, mice traversed the ridges more quickly during trials in which they held their tails at higher angles (normalized to ridge-group means; Figure 1.9B2). However, as there was no effect of tail angle on the centrality of the center of mass (1.9B3), the typical tail position might contribute to the biomechanical efficacy of locomotion rather than solely maintaining balance.

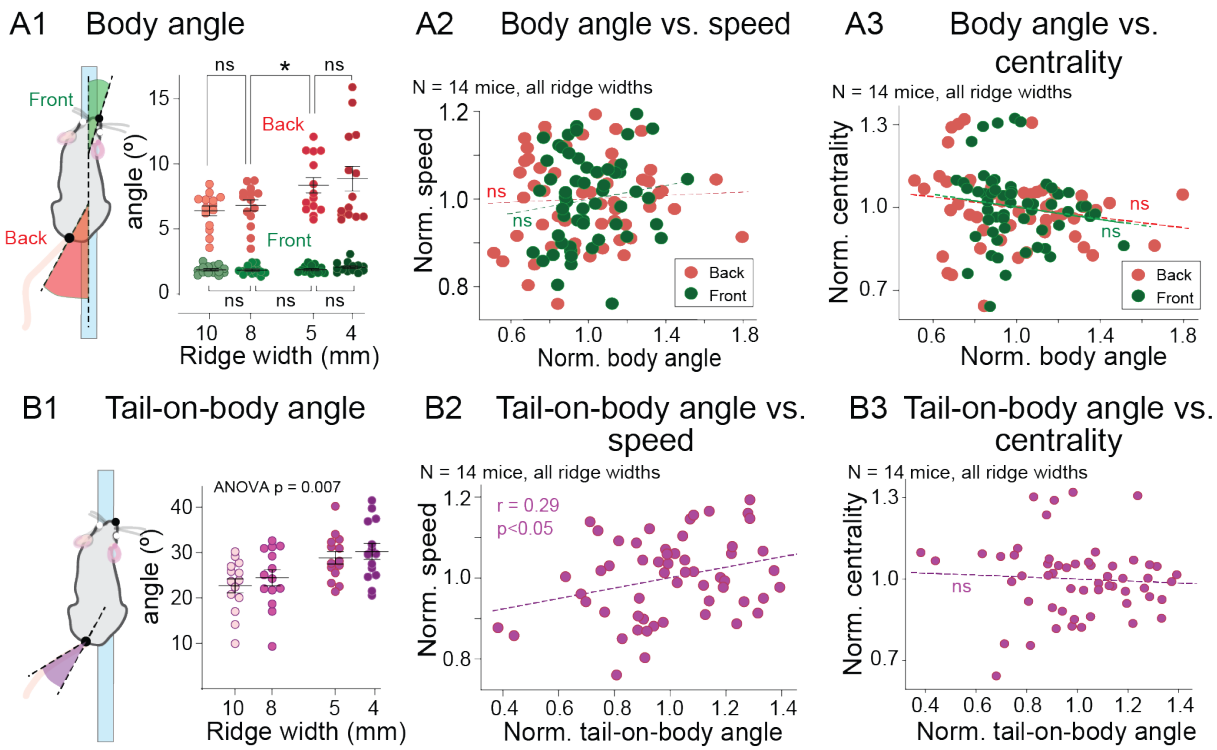

Figure 1.9: Effect of ridge width on body posture and task performance. A1: schematic (left) and summary of mean alignment angles of front and hind-body with respect to the ridge. A2: posture adjustment angle does not correlate with traversing speed. A3, increasing body angles (red, back; green, front) correlates with slightly less central CoM position. B, tail-on-body alignment on different ridge widths. B1, schematic (left) and summary of mean tail angles with respect to the hind-body angle. B2, larger tail-on-body angles were correlated with better performance in terms of traversing speed. B3, tail-on-body angles do not correlate with CoM centrality. In A and B the values are normalized to ridge width-group means.

Motor strategies of tail control in narrow-substrate locomotion

When mice move on surfaces narrower than their hips, it is expected that their bodies will exhibit significant roll-plane oscillations, potentially requiring compensation to prevent falling. Therefore, I proposed that the progressively lateral positioning of the tail on narrower ridges (1.8E2) might serve as a strategy to generate counteracting momentum to stabilize the hips. To explore this hypothesis, I monitored the roll-plane movement of mouse tails (1.10A1, top)

and hips (1.10A1, bottom) from a rear camera view as they traversed unperturbed across the ridges. Similar to the tail's increasingly lateral positioning when viewed from above, the tails, which were held nearly vertical on wider ridges, angled towards horizontal alignment on the most challenging ridges, while the hips maintained a horizontal orientation.

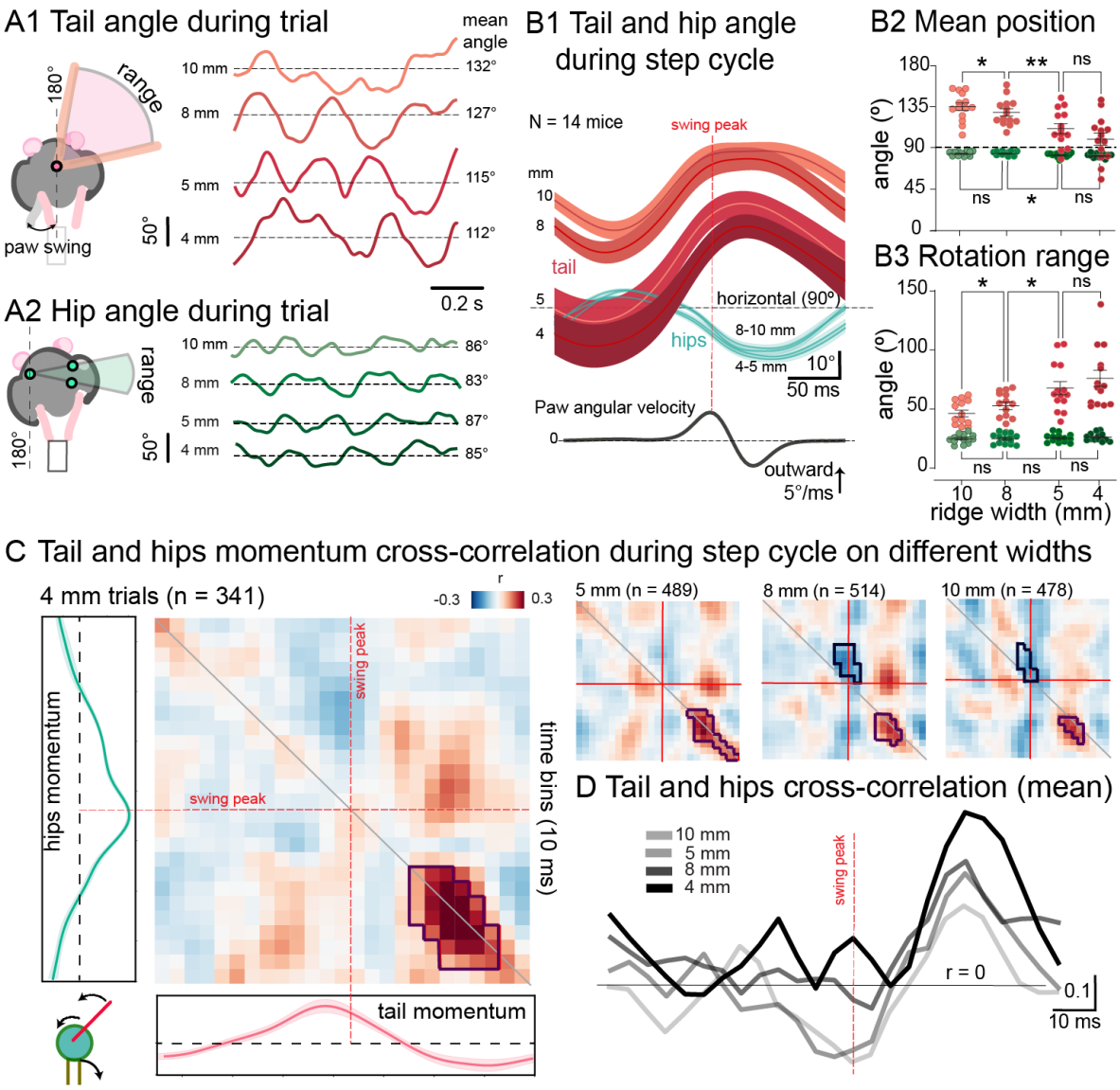

Figure 1.10: Tail and hip movements during unperturbed ridge traverse. A1 and A2, rear-view angle trajectories of tail (A1) and hip (A2) angles of an example mouse traversing ridges of different widths. One second of the trials is shown starting from the beginning of ridge traverse. Dashed lines indicate the mean position for the tail in a given trial. Schematics on the left depict the measurements. B, Tail and hip movements temporally aligned on the contralateral paw swing. B1, mean ± SEM angle trajectories of tails (red) and hips (green) of 14 mice. Bottom panel shows average of contralateral paw angular velocity, aligned on the outward peak. B2, mean position of the hips and tail. Data are shown as averages of single animals over all trials of a given width. B3, range of tail and hips motion through step cycles. C, cross-correlation between the tail and hip momenta through the step cycles centered on swing peak. Left, cross-correlogram for the 4mm ridge condition. Cross-correlation values are displayed in a normalized intensity range between 0.3 (red) and -0.3 (blue). Cross-correlograms for 5mm, 8mm, and 10mm ridges are shown as smaller panels to the right. "Hotspots" and "coldspots" (see appendix A) are depicted with dark contours. Dashed red lines indicate swing peak times. D, Mean correlation values along the diagonal for each ridge width. Darker lines correspond to narrower ridges trials. Red dashed line indicates time of swing peak. * $p < 0.05$, ** $p < 0.01$, ns, $p > 0.05$. Figure from preprint [31].

Thus, the tail was repositioned independently of hip alignment, similar to the lateral displacement mentioned earlier. Moreover, the oscillatory movement of the initial segment of the

tail increased notably on narrower ridges. To explore whether there was a consistent change in tail usage that could affect traversing performance, I analyzed the oscillatory movements of the tail and hips synchronized with the step cycle (1.10 B1; see Appendix A for swing phase definition). Indeed, I observed that mice tails' oscillations occurred in opposite phases on all ridges, with both hip and tail angles reaching their maximum deviations from the horizontal plane during the late phase of the contralateral limb swing. This observation, alongside the consistent lowering of the tails (1.10 B2, red) and increased amplitude of oscillation (1.10 B3, red), contrasts with the relatively stable movement of the hips observed across all ridges (1.10 B2-3, green).

When examining the cross-correlation between hip and tail oscillations on the 4mm ridge (1.10C, left; high correlation region indicated with red pixels and dark outline), I found that their movements are most strongly coupled shortly after the contralateral paw's stance onset. This coupling is most pronounced when the mouse is traversing the most challenging 4 mm ridge and diminishes on easier ridges. In contrast, the coupling between the tail and hips develops a negative correlation with broader ridges (1.10C, right; blue pixels with a dark outline), centered around the peak swing phase (cross-correlation values shown along the matrix diagonal in 1.10D). This suggests that mice may flexibly engage their tails to provide appropriate biomechanical support in diverse locomotory contexts.

1.2.3 Aim 3: Assessment of behavioral performance in the ridge with Maternal Immune activation (MIA) mice

This part of the project was done in collaboration with Yang Mi, a PhD candidate from an immunology lab at OIST. In this project we used the ridge test to assess the behavioral impairment in a mouse model of autism via mother infection during pregnancy: Maternal immune activation (MIA). Infections and various environmental factors appears to affect embryonic neurodevelopment and vulnerability to neurodevelopmental disorders. Borrell et al. ([36]) initially observed that mice offspring exposed to maternal immune activation (MIA) displayed impairments in behaviors such as prepulse inhibition (PPI), akin to those seen in patients with ASD. Bergdolt and Dunaevsky ([37]) reviewed the range of behavioral alterations in MIA offspring associated with neurodevelopmental disorders, such as social communication, as well as male-specific increases in repetitive behaviors. Such alterations are associated with cerebellar abnormal development.

We assessed the motor skills of adult offspring, both male and female, who were exposed to maternal immune activation (MIA), compared to a control group, using the ridge, as well as a battery of more classical behavioral tests (open field, grip strength, balance beam, and righting reflex). Mice were tested on the 4mm ridge. Our findings showed that both male and female MIA-exposed offspring experienced twice as many hind-limb slips as controls (male: $p < 0.01$; female: $p < 0.05$). Interestingly previous literature using the beam failed to report MIA-induced impairment in motor coordination ([38]). Additionally, male MIA-exposed offspring exhibited a notable decrease in crossing speed ($p < 0.001$), while female MIA-exposed offspring did not ($p = 0.5699$). However, motor performance in the open field test and grip strength were similar between MIA-exposed offspring and controls. Moreover, the tail position does not seem to be affected in MIA mice VS control during ridge crossing. Other parameters, such as speed and likelihood of producing swing movements, have not been currently measured. Hence more detailed analysis is needed. These results suggest that MIA impairs balance performance in

adult offspring without affecting their basic motor activity and muscle strength.

1.3 Discussion

In this chapter, I described the results from mouse locomotion on a narrow ridge while countering roll-plane perturbations. This setup reproduces some of the challenges faced by mice in natural environments, such as walking on narrow surfaces of different widths. These findings establish that mice initiate high-speed rotational tail movements that deliver substantial angular momentum, largely counteracting roll perturbations (1.6). These tail dynamics are only slightly modulated by proprioceptive context defined by the ridge width (1.7), suggesting that tail swing, triggered by tilts, is a type of all-or-nothing response.

Beyond externally-induced tail movements, I demonstrate purposeful adjustments in hind body and tail posture during unrestrained locomotion on the ridge. Mice shift their hind-bodies laterally and lower their tails towards the horizontal plane when locomoting on increasingly narrow surfaces (1.8). Furthermore, the tails engage in phase-locked oscillatory movements with respect to the contralateral hindlimb step cycle (1.10). These oscillations and their coupling with hip movements are more pronounced when traversing narrower ridges, even though hip rocking remains largely invariant across different ridge dimensions. It seems possible that the tail is recruited to provide compensatory angular momentum under conditions where the hip/body rotation is not sufficient to ascertain that the center of mass remains safely within the base of support. Constructing a more detailed model as well as high-resolution tracking of limb and body movements could potentially allow deeper understanding of the forces, torques, and context-specificity of the numerous interacting strategies that mice employ to maintain balance. Notably, even without opposable digits in their paws, it is to be expected that mice can generate some amount of stabilizing torque by opposable limb forces depending on the gait used, similarly to primates [39]. However, taking into account the considerable rear-heaviness of mice (COM is located 35.66 ± 1.87 percent closer to the tail base along the body axis), the relative contribution of the front limbs is expected to be rather limited.

1.3.1 Description of the tail response to roll perturbations

Maintaining posture and balance is a multifaceted process that involves motor strategies adapted to various context, encompassing both passive and active responses to self-motion within a dynamic environment [3]. For example, in healthy humans, "change-in-support" strategies (adjusting limb positions) are often the most effective way to regain balance. However, when constrained in paw placement, "hips-and-ankles" strategies (adjusting the body's center of mass through torque) become the primary mechanism for balancing [4]. In precarious balancing scenarios such as walking on narrow beams, humans also use upper-body strategies involving arm movements [5–7]. Similarly, in mice, while tails are typically inactive when traversing wide surfaces [40], they are engaged under challenging conditions when movement freedom is restricted.

Similar to human arms, the mouse tail serves distinct functions depending on the dynamic circumstances. When encountering sudden tilt perturbations, mice cease locomotion, and their tails respond swiftly to immediate balance threats by executing rapid rotations at high speeds, thereby generating stabilizing angular momentum. In contrast, during voluntary locomotion where the effective base of support is determined by momentary paw placement, the tail's behavior undergoes significant changes. Rather than executing large swings, the tail may function as a stabilizer, a concept proposed by previous research across different species [7].

This suggests a role for anticipatory postural adjustments, where the tail's position and movement are synchronized with the step cycle to aid in forthcoming dynamic shifts, possibly influenced by proprioceptive and descending command signals.

Based on the above results we propose that the tail operates akin to a 'fifth limb', employing distinct strategies for balancing and locomotion. Hence, a comprehensive understanding of skilled motor coordination in mouse locomotion would be incomplete without accounting for the dynamic functions of the tail. Its adaptability in assisting balance and improving locomotion highlights its importance in intricate motor activities and offers a promising area for future research in mouse motor control.

1.3.2 Assessment of locomotion performance in balancing tasks

Research into balancing strategies in animals has predominantly centered on larger species such as cats and humans, focusing on lower limb and trunk movements (see [41] for the role of the tail in cats and [42] for mentions of tail swings in large primates). A groundbreaking study by Murray and colleagues [43] has shed light on balancing strategies in mice by investigating hindlimb muscle activity during yaw plant tilts of the beam they traversed. The study utilized EMG recordings from hindlimb muscles to observe subtle movements in response to balance perturbations. I propose that the tail could represent a novel focus for studies on balancing reflexes in mice. Easily visualized and tracked using markerless methods like DeepLabCut, the tail offers a previously overlooked yet valuable metric for investigating balance in smaller rodents. Furthermore, I propose using the estimated Center of Mass (CoM) of the animal within its base of support as a direct measure of balance performance. Unlike traditional paw-slip metrics [44], which can be complex to compute and influenced by variables like substrate surface properties, tracking the CoM trajectory offers a detailed glimpse into the animal's balancing tactics. This approach provides a methodologically straightforward yet robust assessment of the animal's ability to maintain balance [45]. Integrating CoM-based balance analysis with other metrics such as traversal speed and frequency of pauses could offer further valuable insights into dissecting balancing strategies amidst specific motor challenges.

Chapter 2

Anatomical and functional characterization of circuits for tail control

2.1 Background

In the second chapter of this thesis, I will start by first introducing the neuronal candidates under investigation proposed to be involved in tail control. I will follow a bottom-up approach, similar to the framework used in the experimental plan throughout my PhD, to tackle two main questions: what are the neurons responsible for tail control in the spinal cord, and what supra-spinal inputs these neurons may receive. For this second aspect, the candidate under investigation is the vestibular system. Hence, in this background section, I will introduce the neuronal elements that make up the spinal circuitry of movement, the vestibular system, and the main tools used for the anatomical and functional dissection of such circuits.

2.1.1 Circuits responsible for movement from and to the spinal cord

The ability to execute a wide range of motor programs is a remarkable trait shared by all mammals. Each movement involves a precisely orchestrated sequence of muscle contractions, occurring at set times and with set intensity. Contraction is initiated in skeletal muscle cells, which in turn are activated by nerve terminals. During development, myoblasts fuse to form larger structures known as muscle fibers, which collectively constitute a muscle. Each muscle contributes to movement by exerting force on skeletal bones and thereby interacting with the surrounding environment.

While skeletal muscles share a common fiber structure, they vary significantly in terms of innervation, which impacts their control during movement. Muscles with smaller motor units (groups of fibers innervated by a single motor neuron) contributes to finer motor control compared to those with larger motor units (which are rather important for generating more power). This distinction is crucial when considering tasks requiring high dexterity and flexibility, such as grasping, versus more stereotyped activities like locomotion.

To execute a movement, multiple muscles must contract or relax following a complex and precise pattern. A muscle synergy can be defined as a functional unit comprising several muscle groups contracting within a similar time frame that contribute to a set movement. Notably, muscle synergies are not fixed; they can vary in composition depending on the specific task at hand.

For instance, the muscle synergies involved in locomotion are heavily utilized and reinforced throughout life, but certain muscles within these synergies may serve different functions and participate in alternative synergies.

Generation of locomotor pattern

Locomotion, in this document defined as an active shift of body in space, is a basic behaviour that is essential for the survival of any living organisms. Locomotion comes in a variety of forms such as walking, swimming, flying, crawling and so forth. In the early 20th century, Sherrington suggested that all the neurons responsible for generating movement in vertebrates reside within the spinal cord ([46], [47]). This theory, started from the observation that decerebrated animals with all peripheral sensory inputs removed were still generating locomotory patterns ([46]). More recently, electrophysiolgy recordings from the ventral roots allowed the detection of flexor and extensor motor neuron pools activity from a spinal cord preparation in vitro. This was achieved either by adding neurotransmitter agonists or by electrically stimulating the spinal cord ([48], [49]).

It has also been observed that the spinal cord can autonomously regulate locomotor speed [50], indicating its capacity not only to generate rhythmic locomotor patterns but also to modulate locomotor output independently of external influences, such as supraspinal and sensory feedback. The ability to generate rhythmic locomotor patterns is a conserved trait across evolution, evident in lower vertebrates like lamprey and Xenopus tadpole, where swimming patterns are generated through flexion and extension of trunk muscles [51], as well as in more complex mammalian locomotion, characterized by alternating flexion and extension between muscles of the right and left limbs [48, 49].

Central Pattern Generator (CPG) and rhythmic movement generation

Neuronal circuits that can generate a rhythmic pattern without external patterning input (such as sensory or supraspinal) are called central pattern generators (CPGs, [52]). CPGs are capable of initiating rhythmic activity and shaping the pattern of actvation onto alpha-motoneurons (MNs, which in turn are responsible for muscle contraction) during locomotion ([53]).

A recent study ([54]) used optogenetic to selectively stimulate neurons in an isolated preparation of spinal cord. This finding indicated that the rhythmic locomotor pattern can be independently recorded in the left and right sides of the spinal cord, as well as within different motor neuron (MN) pools within the same side. However, coordinated locomotor output relies on the communication across these modules through excitatory, inhibitory, and modulatory mechanisms ([55]). Interneurons (INs) forming the CPGs are functionally connected via chemical synapses and/or electronic coupling ([56]). While the anatomy and function of the neurons constituting the CPG have been identified in invertebrates and lower vertebrates ([57]; [58]), the specifics of the mammalian CPG remain unclear.

Indeed, much remains to be elucidated concerning the cells responsible for rhythm generation and pattern formation in the mammalian locomotor CPG. Unlike in invertebrates and lower vertebrates, where a single cell type can initiate both rhythm generation and pattern formation ([59]), the mammalian CPG involves different cells types for these functions ([**?**], [60]). As proposed by Brownstone and Wilson in 2008 ([56]), mammalian CPGs require different neuronal types for rhythm generation and pattern formation. Theoretical models have been proposed to aid

in understanding the components underlying rhythm generation and pattern formation, including the model proposed by McCrea and Rybak in 2008 ([61]), which categorizes interneurons (INs) active during locomotion into two functional levels: rhythm-generating and pattern-forming INs. Rhythm-generating cells establish the rhythm and frequency for network oscillation, while pattern-forming cells, activated downstream, regulate the duration and amplitude of motor neuron activation, essentially controlling the locomotor pattern.

Recent research by Grillner et al. in 2013 ([55]) has shown morphological differences between rhythm-generating and pattern-forming cells. The study confirmed that rhythm-generating INs are predominantly located medially compared to pattern-forming INs. It also revealed that rhythm-generating cells have shorter axons extending medially and caudally, while pattern-forming cells have longer axons projecting laterally and toward motor neuron pools. Additionally, rhythm-generating cells are primarily found in the thoracic and lumbar segments of the spinal cord, whereas this localization is not crucial for pattern-forming cells. Consequently, it is widely accepted that the mammalian CPG, unlike invertebrates or lower vertebrates, comprises distinct populations of rhythm-generating and pattern-forming interneurons.

Motoneurons organization in the spinal cord

Primary spinal alpha-motoneurons (in this text referred to as MNs) are spread throughout the spinal cord in accordance with the muscle fibers they activate. The forelimb and hindlimb motoneuron pool are located in the cervical and lumbar enlargements. Specifically, MNs responsible for controlling the muscles of the forelimbs reside in the lateral motor columns at the lower cervical segment, while those responsible for the distal forelimb and finger muscles' contraction are positioned dorsally within the same lateral columns. Similarly, MNs that control hindlimb (HL) muscles occupy the lateral columns but at lumbar levels. This arrangement of MNs into columns emerges during development under the influence of precise molecular programs both intrinsic and extrinsic in nature.

Within such motor columns, MNs maintain a topographic organization as well, with those innervating the same muscles positioned adjacently. This spatial arrangement corresponds with their shared morphology, which likely plays a crucial role in their activation by similar motor commands. Such precise organization is vital not only for establishing complex connectivity with spinal cord interneurons and receiving sensory feedback but also for receiving accurate input from supraspinal regions.

Interneurons in the spinal cord

The ventral region of the grey matter is composed by not only MNs, but is also populated by interneurons (INs) of diverse subtypes. Distinct classes of INs are generated throughout development according to a Sonic Hedgehog gradient (i.e. dorso-ventral arrangement that the Sonic Hedgehog gene (shh) is responsible for in the spinal cord) coming from the ventral plate which induces differential transcription factor expression accordingly to its levels ([62]) ([62]).

Another intriguing aspect of IN differentiation involves classifying them based on their time of birth, i.e., when neurons become postmitotic. Neurons generated at different time points exit the cell cycle at specific moments, express different transcription factors, and encounter distinct extracellular conditions. For instance, premotor neurons to hindlimb muscles, born at different embryonic stages (E10.5 and E12.5), segregate spatially along the medio-lateral axis

and connect to functionally antagonistic muscle sets ([63]). Understanding such features of spinal circuits is crucial for comprehending how brainstem neurons interact with spinal cord circuits to initiate and regulate motor execution. INs situated in the ventral spinal cord harbor the "central pattern generators" for locomotion, comprising networks of neurons essential for the rhythmic and cyclic activation patterns characteristic of quadrupedal locomotion ([64]).

Interestingly, some molecular markers characteristic of spinal cord cell types are also expressed embryonically in the reticular formation (RF). The overall structure of the RF closely resembles that of the spinal cord, maintaining a ventro-dorsal organization where motor functions predominate in the ventral part and sensory functions in the dorsal regions. In the brainstem, Hox genes serve as the predominant molecular determinants during development, contributing to the characteristic rhombomeric structure evident at the embryonic level ([65]). In adulthood, the segmental organization within the brainstem dissipates, making it more reliable to describe its structure based on nuclei ([66]). One proposed theory is that interneurons that underlie fast movements are broadly connected to each other while interneurons that govern slow precise movements have fewer connections. Ampatzis et al. (2014, [67]) has shown that connectivity among INs and MNs is organized by speed in zebrafish. V2a INs are recruited by speed of locomotion in mice as well ([68]).

Somatosensory afferents in the spinal cord

Somatosensation, comprising touch, pressure, proprioception, temperature, pain, and itch, plays a pivotal role in animal's interaction with their environment, with peripheral sensations transmitted to the spinal cord through primary afferent fibers in the dorsal horn ([69]). The dorsal horn is divided into six compartments, known as laminae, and has long been recognized as a key site for somatosensory processing. The primary sensory afferents convey somatosensory information (first transduces by receptors at the periphery) into different laminas, and they have been classically defined based on their conduction velocity and myelination into four types: A_α, A_β, A_δ, and C. C fibers convey nociceptive information, A_δ fibers transmit a mix of noxious and innocuous tactile and cold sensations, A_β fibers carry innocuous tactile information, and A_α fibers primarily relay proprioceptive signals [70],[71], ([72]). Primary afferent fibers form synapses with both excitatory and inhibitory neurons within the spinal cord, including interneurons and projection neurons ([73], [74]).

The spinal dorsal horn also receives direct descending modulation from brainstem regions such as the rostral ventromedial medulla (RVM) and locus coeruleus (LC), which regulate the excitability of spinal cord neurons ([75], [76]). Neurotransmitter signaling pathways from the brainstem, including adrenergic, opioidergic, and cannabinergic systems, directly inhibit dorsal horn neurons and reduce neurotransmitter release from primary afferents, leading to decreased pain behaviors ([77]; [78]).

Longitudinal organization of the spinal circuits

The spinal cord is organized longitudinally based on Hox genes differential expression. The Hox genes determine the structural (location in the spinal cord), and functional (connection to certain muscle groups) properties. Studies on mice show diverse distributions of neuron subclasses across different spinal segments, suggesting segmental variations in function ([79]). In contrast, zebrafish show more homogeneous distributions along the spinal axis, reflecting

perhaps different locomotor demands ([80]).

The longitudinal distribution of neuronal subpopulations also affects what type of neuronal assembly are present at different levels. For instance, interneuron classes exhibit segmental differences in connectivity, with some forming synapses with distal motor nuclei and others with axial motor neurons ([81]). Propriospinal neurons can project long axons along the spinal axis influencing postural control and interlimb coordination ([82], [83]).

Ascending projections from the spinal cord

The primary ascending spinal tracts include the gracile and cuneate fasciculi, spinothalamic tracts, and spinocerebellar tracts, with various minor tracts identified through retrograde tracing (the origins of which remains unclear, [84]). The majority of the dorsal funiculus contains the gracile and cuneate tracts, which consist of ascending axons from ipsilateral primary afferent neurons and share consistent anatomy across species [84]. Moreover, a good portion of fibers in the dorsal funiculus originates from spinal dorsal horn neurons, termed the postsynaptic dorsal column. The position of the gracile tract is indicated by Pitx2 expression, while the locations of ventral and dorsal spinocerebellar tracts are determined by previous studies showing their dorsal shift in the spinal cord. Spinothalamic fibers, traditionally categorized as lateral and ventral tracts, were found to include a dorsolateral spinothalamic tract in rats.

The dorsal and ventral spinocerebellar tracts transmit proprioceptive and cutaneous signals from Golgi tendon organs and muscle spindles to the cerebellum for the coordination of distal movements. These spinocerebellar projections exhibit distinct distribution patterns across different spinal cord segments. In cats, mossy fiber terminals originating from neurons in the cervical enlargement are observed in both the anterior and posterior vermis, while those from the thoracic segment predominantly target lobules 2b-5b in the vermis ([85], [86]). In mice, cerebellar-projecting neurons are located in various nuclei including the central cervical nucleus, dorsal nucleus, lumbar precerebellar nucleus, and sacral precerebellar nucleus, with projections primarily confined to the anterior and posterior vermis. Retrograde labeling indicates ipsilateral predominance in the dorsal nucleus, lumbar precerebellar nucleus, sacral precerebellar nucleus, and lumbar border precerebellar nucleus, whereas projections from the central cervical nucleus are predominantly contralateral.

Brainstem descending neurons for locomotion

Examining behavior as a sequence of movements helps us appreciate the intricate neural processes of selecting, tracking, adjusting, executing and learning involved. The brainstem, situated in the hindbrain and midbrain, serves as a pivotal regulator of physiological functions, particularly of movement ([69]).

Brainstem circuits are responsible for the modulation of speed and direction of locomotion. Glutamatergic neurons within the mesencephalic locomotor region (MLR), including subdivisions like the pedunculopontine nucleus (PPN) and cuneiform nucleus (CnF), play important roles in initiation and changes of locomotion, with specific subregions contributing to high-speed locomotion ([87]). Connectivity between MLR subregions and the lateral paragigantocellular nucleus (LPGi) in the medulla forms a circuit essential for high-speed locomotion. Optogenetic stimulation of MLR or LPGi neurons induces forward locomotion, indicating symmetrical distribution of unilateral locomotion signals, possibly modulated by downstream circuits ([88]).

Glutamatergic brainstem neurons expressing the transcription factor CHX10 in the gigantocellular nucleus (Gi) are implicated in interrupting locomotion and ipsilateral turning behavior, with distinct populations targeting cervical and lumbar spinal regions. Synaptic input to CHX10-expressing Gi neurons originates from contralateral superior colliculus neurons, suggesting influences on orientation-regulating brainstem neurons ([89]).

Besides the reticular formation, the vestibular complex may play a role in locomotion given its considerable projection to the spinal cord ([90]). A. Murray (2018, [34]) has shown that vestibulospinal activation identify two distinct cell types in the lateral vestibular nucleus are required for fast responses to postural perturbation during locomotion. Given the importance of this system in the presented thesis, I will dedicate the next section to introduce the vestibular system, from transduction of head movement signal to its motor output via the vestibulospinal pathway.

2.1.2 The vestibular system

The vestibular system stabilizes gaze and maintains posture, supporting our sense of movement and orientation ([91]). The vestibular organs are located in the temporal bone, and they consists of otolith organs sensing linear acceleration and semicircular canals sensing angular acceleration. Receptor cells transduce head movement into signal transmitted through the vestibular nerve (VIII cranial nerve) to control eye movements, posture, and balance ([69]). Unlike other sensory systems, understanding the significance of vestibular function in our daily lives is not as straightforward. When the vestibular system functions normally, we usually do not perceive a distinct sensation from its activity because it is integrated with visual, proprioceptive, and other sensory inputs, resulting in a sense of motion. Moreover, the vestibular system's crucial roles in gaze stabilization and postural control are challenging to grasp ([69]). Clinical studies have shed light on vestibular function, with one notable case being JC, who experienced complete vestibular loss after streptomycin treatment. He described feeling as if he was inside a flexible tube while walking and used strategies to minimize symptoms, highlighting the difficulties faced by individuals with abnormal vestibular function in everyday activities, where even small head movements can cause gaze instability and postural imbalance ([91]).

Studies in the past few decades have deepened our understanding of the neuronal circuits in the vestibular system responsible for gaze stabilization, balance, and posture ([92], [1], [93], [94]). The vestibulo-ocular reflex (VOR), ensuring clear vision during movement, adapts impressively to behavioral requirements, offering a model system for understanding neural circuits and behavior ([91]). Furthermore, the vestibular complex maintains postural equilibrium, adjusting during self-generated movements and external disturbances mainly through the vestibulospinal system.

Structure of the vestibular labyrinth

The otolith organs, the utricle and the saccule, detect linear acceleration. They contain hair cells in a gelatinous matrix with solid $CaCO_3$ crystals (otoconia) covering them. During linear acceleration, the inertia of otoconia causes them to lag, bending the cilia of hair cells and either exciting or inhibiting them (depending on the direction of motion of the otoconia wrt the cilia). This mechanism enables the otolith organs to perceive gravity, as well as transient linear accelerations. The semicircular canals, arranged orthogonally, detect angular acceleration. Each canal contains a cupula, an elastic membrane, which deflects according to rotational movement. Neural output from sensory cells in the canals represents rotational velocity, owing to mathematical integration of input signals. By integrating information from all three canals, the brain constructs a 3D representation of head rotation in space.

The vestibular complex

The vestibular complex (in the present document referred also interchangeably with vestibular nuclei) represents the first central stage of vestibular processing, and it is where vestibular information is integrated with proprioceptive information from muscles and joints, with the goal to maintain balance in most mammals [95]. The vestibular complex of mice can be subdivided into four major nuclei: Lateral vestibular nucleus (LAV), Medial vestibular nucleus (MV), Superior vestibular nucleus (SV), Spinal (inferior, or descending) vestibular nucleus (SPIV); as well as some other more or less prominent subgroups such as the x and y nuclei. The last 2 are

considered "accessory nuclei of the vestibular complex", as they do not receive direct projection from the VIII cranial nerve, but maintain a close location and connectivity with the major nuclei of the vestibular complex.

The axons of the majority of bipolar vestibular nerve afferents extensively branch out and connect with all subnuclei. Consequently, vestibular nerve (VN) neurons receive inputs from both regular and irregular afferents (defined based on the regularity of their firing rate, where the first one is considered to rely on rate coding, and the second one on temporal coding [92]), as well as from various semicircular canal and otolith organs. Electrophysiological recordings in adult rats suggest that approximately 80 percent of VN neurons integrate inputs from both otolith and semicircular canal stimuli ([96]). This convergence pattern is also observed across different species such as frogs, mice, cats, and monkeys ([97]). Predominantly, the convergence of afferent inputs from semicircular canals and otolith organs occurs in the lateral and dorsal vestibular nuclei, with lesser involvement in the medial vestibular nucleus. Sparse inputs from otolith organs are received by the superior vestibular nucleus. Inputs from the utricle mainly target the dorsal vestibular nucleus, while those from the saccule primarily terminate in the lateral and dorsal vestibular nuclei. Horizontal and vertical semicircular canals are the primary sources of inputs to the medial and superior vestibular nuclei, respectively. Neurons in the vestibular nuclei are functionally classified based on their sensitivity to movement direction and type, which also reflects their predominant anatomical connections and functional roles.

Medrea and Cullen [98] recorded from Vestibular-Only (VO) neurons in the vestibular nuclei in mice (while being exposed to head rotation in a turntable), showing that indeed proprioceptive and vestibular information is integrated by single VN neurons. Importantly, while during external applied perturbations neuronal responses are well predicted by summation of neck and vestibular sensitivities, during self-generated movements neuronal responses are suppressed. Taking into account that VO neurons send descending projections to the spinal cord, this result suggests that vestibular modulation of spinal activity is reduced during active motion. This has important functional implications for the current proposal, and it might indicate that the vestibular nuclei play an important role in response of external perturbation (platform tilt), as opposed to self-generated condition (locomotion), where modulation from the vestibular system to spinal motoneurons and interneurons might be attenuated.

Importantly, however, Medrea and Cullen [98] showed also that bimodal neurons (that is, neurons that respond to vestibular and proprioceptive stimuli) encode static neck position during active as well as passive conditions. This result is relevant for studies on the mouse, but interestingly does not extend to primates (VO neurons do not encode static neck position, [98]). This difference may depend on the fact that primates often use head-on-body movements, and they can move their head quite independently from the rest of the body to ensure clear binocular vision by precise alignment of the axis of gaze. In contrast, mouse head and body motions are more strongly correlated, and the sensitivity of vestibular neurons to static neck may enhance spinal reflexes that maintain the head in a stable position with respect to the body. In the next section I will focus on one of the vestibular nuclei (the lateral one), given that the main hypothesis of the presented thesis is around its involvement in tail control in balancing.

The lateral vestibular nucleus

The lateral vestibular nucleus (LVN), also referred to as Deiters' nucleus, is a brainstem structure essential for processing vestibular information. It receives input from the inner ear's semicircular

canals and is pivotal in coordinating balance, posture, and eye movement. Although primarily serving as an output nucleus, the LVN projects to various regions within the central nervous system ([91]). Notable targets of LVN output include:

1. **Spinal Cord:** The LVN directly projects to the spinal cord, specifically targeting motor neurons in the ventral horn. These projections contribute to muscle tone regulation and control of limb and trunk movements.

2. **Medial Vestibulospinal Tract:** LVN projections extend to the medial vestibulospinal tract, which descends bilaterally in the spinal cord. This tract influences motor neurons responsible for postural adjustments, such as the extensor muscles of the trunk and proximal limb muscles.

3. **Reticular Formation:** LVN projections also reach the reticular formation, a complex neuronal network in the brainstem involved in regulating arousal, attention, and various autonomic functions. The reticular formation integrates vestibular information to modulate these functions.

4. **Cerebellum:** The LVN provides input to the cerebellum, particularly the flocculonodular lobe and vermis. These cerebellar regions are crucial for coordinating eye movements, maintaining balance, and adjusting postural control based on vestibular input.

5. **Thalamus:** Some LVN projections target the thalamus, specifically the ventral posterior nuclei. The thalamus serves as a relay station, transmitting vestibular information to other brain regions involved in perception and sensorimotor integration.

6. **Cranial Nerve Nuclei:** The LVN establishes connections with various cranial nerve nuclei, including the oculomotor nucleus (controlling eye movements), the abducens nucleus (involved in lateral eye movements), and the spinal trigeminal nucleus (contributing to head and neck reflexes).

The lateral vestibular nucleus (LVN) consists of a diverse population of neurons, including Deiters' neurons and interneurons. Deiters' neurons, located exclusively within LVN, are part of the vestibulospinal reflexes, innervating extensor motoneurons responsible for antigravity muscles and receiving inhibitory inputs from the cerebellum. Studies indicate that LVN neurons exhibit lower input resistance and larger cell size, rendering them less sensitive to sinusoidal current injections. Additionally, robust inhibitory innervation from the cerebellum to LVN has been shown, as well as excitatory inputs from utricular, saccular, and posterior canal primary afferents to Deiters' neurons ([99]).

Anatomical studies have revealed a topographical organization of neurons within the LVN [100]. Specifically, rostroventral Deiters' neurons mostly project to the cervical spinal cord, while dorsocaudal Deiters' neurons project to the lumbar spinal cord [100]. The tonic discharge and temporal response properties of Deiters' neurons to inhibitory and excitatory current injections (electrophysiolgy experiments performed in [99]) suggest a requirement for significant synaptic input to modulate their baseline activity. Contrasting with other neuron types whose axons descend in the spinal cord, such as reticulospinal neurons and cortical pyramidal neurons (i.e. they are quiescent at rest, and they fire during locomotion[101]), Deiters' neurons exhibit tonic firing rate at rest. This tonic activity may be due to their involvement in postural stability,

in contrast to neurons involved in voluntary motor pathways ([101], [102], [103]). In other words, Deiters' neurons exhibit low sensitivity or gain, necessitating substantial input to significantly modify their discharge rate. This aligns with their role in tonically activating antigravity extensor muscles, where minor signals regarding head and body movement do not appreciably alter Deiters' neuron activity.

Importantly, Deiter neurons axons constitutes the major component of the lateral vestibulospinal tract (LVST). This is one of the two most important tracts (together with the medial vestibulospinal tract) for postural reflexes, and it was a main subject of investigation in this thesis, hence I will dedicate the sections below to introduce its function, as well as its connectivity with downstream output.

The vestibulospinal system

In the last century most of the research on the vestibulospinal system has focused on reflexes and reduced preparations [104]. Thanks to these studies we now know much of the neuronal substrates involved in neck adjustments following head displacement (VCR), and postural adjustments (VSR). The lateral vestibulospinal tract descends from the vestibular nuclei to the lumbosacral spinal cord [105]. Stimulation of LVN can elicits EPSP in ankle and knee extensor motoneurons with a short latency, suggesting the presence of monosynaptic pathways [106].

Wilson and Maeda [107] showed that there are short-latency, disynaptic pathways between the VIII cranial nerve and neck motoneurons as well. In their experiments stimulation of the anterior and horizontal canals evoked EPSPs in the neck motoneurons, while stimulation of the posterior canal nerve resulted in IPSPs in the same neurons. These potentials were abolished by ablation of the medial longitudinal fasciculus (MLF), where most of the disynaptic connections from the ampulla goes through [107]. Despite the presence of these short-latency pathways between VN and neck motoneurons, three observations indicate that the indirect pathways may play a more important role in VCR.

- Transection of MLF has little effect on phase/gain of neck activity in response to horizontal rotation.
- Intravenous infusion of sodium pentobarbital, which has a stronger effect on multisynaptic connections then disynaptic one, shows great decrease in reflex gain.
- VCR shows a great phase lag with respect to discharge in the vestibular nerve and VN firing. Moreover this lag is higher for lower frequency (strongest at 0.1 Hz), implying that central pathways perform a partial integration of the signal coming from the labyrinth.

These results suggest that for VCR the functionally more important pathways are multisynaptic. These pathways possibly involve the reticular formation [108].

Vestibulospinal reflexes

In this section I will review some of the studies that describe reflexes involved with the maintenance of postural equilibrium. This is relevant for the current thesis, given that the circuit I aim to describe for tail control may resemble the neuronal circuits that control limbs.

Most of the early studies on vestibulospinal reflexes have been done in decerebrate preparations [108, 109]. These studies were conducted by eliminating the vestibular input (labyrinthectomy), or the proprioceptive input (dorsal roots ablation).
After eliminating the proprioceptive input, neck rotations have particular effects on limb tone. Pitching the head up decreases hindlimb tone and increases extensor forelimb tone. Roll causes an increase in extensor tone on the controlateral side to the rotation. Yaw rotations induce increase in ipsilateral limbs tone [110]. This suggests that vestibulospinal reflexes may have an effect on limb motor control as well.

How are limb muscles affected by head movement? The cervical and lumbar enlargements, which contains motoneurons controlling limb muscles, receive projections from the lateral vestibular spinal tract (LVST), and reticular spinal tract (RST). LVST activation induces excitation of ipsilateral extensor motoneurons and inhibition of flexors. LVN stimulation shows monosynaptic excitatory connections with ipsilateral hindlimb motoneurons [106], but also in this case polysynaptic pathways may play a bigger role. When applying trains of stimulation on LVN neurons rather than single shocks, the multisynaptic action will have significant impact on the targeted motoneurons. The involvement of polysynaptic pathways mediated by interneurons leads to the facilitation observed in [106] and also allows integration of descending vestibular inputs with supraspinal or non-vestibular segments of the spinal cord.

There are several types of interneurons that may be involved in the integration of different inputs. C3-C5 propriospinal neurons receive converging inputs from LVST, neck afferents and reticulospinal neurons, and project to lumbar spinal cord [111]. Some interneurons located in the lumbar segment of the spinal cord also receive converging vestibulospinal and reticulospinal inputs and send their output to motoneurons in the lumbar segment [112]. Ia interneurons inhibit some types of flexor motoneurons by activation of Ia afferents (originating in muscle spindles of extensor muscles). Grillner [106] describe that Ia interneurons receive a high convergence of other inputs, such as controlateral cutaneous and high threshold muscle afferents (coFRA).

Some of the interneurons within L4-L5 are excitatory or inhibitory premotor neurons. Their activity elicits monosynaptic EPSPs or IPSPs in lumbar motoneurons [113]. Stimulation of LVN neurons has effects on controlateral motoneurons as well, despite the fact that LVST descends ipsilaterally [114]. A candidate pathway for this entails flexor reflex afferents (FRA), composed of muscle afferents that elicit ipsilateral flexion and controlateral extension (mediated by commisural interneurons). [115].

So far I have listed examples of LVST action on alpha motoneurons. However most descending tracts modulate activity of gamma motoneurons, that is motoneurons innervating intrafusal fibers of muscle spindles. Grillner [116] has shown that LVN stimulation excited monosynaptically extensor gamma motoneurons. At the same time, flexor gamma motoneurons where inhibited by LVN. This suggests that LVN can modulate gamma and alpha motoneurons acting on the same muscle in parallel. Activation of gamma motoneurons can act as a positive feedback, increasing alpha motoneurons discharge. This effect (so called alpha-gamma linkage) and the presence of several pathways for vestibular spinal reflexes (VSR) suggests that there are overlapping motor strategies (i.e. redundancy), which is a fundamental principle in a system so important for animal survival such a the one meant at maintaining posture. In summary, in addition to direct vestibulospinal pathways, input from the vestibular nuclei is relayed to motoneurons via spinal interneurons ([117], [118]), and the reticulospinal system [119]. Such polysynaptic pathways likely integrate vestibular and proprioceptive signals [95]. This relation is expanded on in the following section.

The vestibulospinal and the reticulospinal system

The relation between the vestibulospinal and reticulospinal system has been proposed to play an important role in postural stability during locomotion [120]. The vestibulospinal system, together with the reticulospinal system, ensures an appropriate level of muscle tone in the extensor muscles and modifies this muscle tone in response to changes in the orientation of the head and/or the body [120].

Neurons of the reticulospinal tract are situated in the pons and the medulla, and project to the spinal cord via the medial reticulospinal tract, which originates from the nucleus pontis oralis, the pontis reticularis, and the nucleus reticularis gigantocellularis [121]. Most of these projections are ipsilateral, and run through the MLF [122]. The lateral reticulospinal tract comes from the nucleus gigantocellularis and magnocellularis, and projects controlaterally and ipsilaterally [123]. The reticulospinal tract projects to all segments of the spinal cord making it a good candidate for playing a role in postural control. Ladpli and Brodal [124] showed that nuclei in the vestibular complex project to the medial pontomedullary reticular formation, supporting the idea of a vestibulo-reticulospinal connection. From a functional perspective, Peterson [125] showed that neurons in the medial pontomedullary reticular formation could be activated by electrical stimulation of the vestibular nerve, with latencies suggesting polysynaptic and disynaptic connections.

The lateral and medial reticulospinal tract have connections with spinal neurons, especially alpha and gamma motoneurons. Inputs to reticulospinal neurons come from many regions, including the vestibular system, somatosensory system, and cerebellum. Somatosensory inputs, originating in high-threshold receptors are also indirect, involving relays in spinal cord and in the brain stem. Moreover, the ispilateral dentate nucleus and controlateral fastigial nucelus project to reticulospinal neurons [126].

The role of motor signals and proprioception in vestibular processing

Integrating sensory information, such as proprioception, with motor commands is essential to construct accurate representations of our environment. These sensory information can be generated either by external sensory stimuli (exafference), or by self-generated movements (reafference). In order to make correct interpretation of our environment and select the appropriate motor response it is fundamental to distinguish between these two sources of information. One of the first model was proposed in the 19th century by Von Holst [127]. According to this model, an efference copy is sent to sensory areas to cancel sensory information caused by self-generated movements. This framework has been adopted across many different fields in neuroscience to explain visual, somatosensory, auditory, vestibular processing [95].

In the vestibular system sensory reafference is cancelled at the first central stage of processing. In fact, while vestibular afferents do not distinguish between self-generated versus passive movements, VO neurons in the vestibular nuclei preferentially respond to passive vestibular stimulation. Vestibular reafference cancellation has been shown to occur across species, mice, cats, and non-human primates [128–130]. This cancellation depends on there being a perfect match between the actual and expected proprioceptive feedback [131]. VO neurons mediate vestibulospinal reflexes, hence vestibular reafference leads to vestibulospinal reflexes (VSR) suppression during self-generated movements.

Somatosensory inputs from hindlimbs is very relevant to understand the balance strategies implemented in terrestrial animals. Studies have shown that VN neuronal activity is modulated

during passive limb movements, or fictive locomotion [132, 133]. However most of those studies were done in decerebrated animals, which can significantly alter physiological properties of VN neurons. Importantly, McCall [129] showed that VN firing rate is affected by passive hindlimb movements also in the awake cat. Interestingly, the encoding of hindlimb movement direction by VN neurons was more frequent in intercollicular decerebrate animals (81.4 per cent vs 41.5 per cent neurons). Also, sustained firing rate in response to limb flexion or extension was more frequent in decerebrate animals. The same study also reported modulation in the activity of VN neurons during voluntary limb contractions. This might be due to an efference copy signal relayed to the vestibular nucleus and/or a sensory feedback from the limbs. In fact voluntary muscle contraction provides a stronger proprioceptive feedback than passive hindlimb movement, especially due to gamma motoneurons activity ([134]).

The vestibulocerebellum and the deep cerebellar nuclei (DCN)

Although it was introduced in passing earlier, I would like to dedicate a section to introduce the vestibulocerebellum, given its role in sensory integration of proprioception and vestibular information, and its intimate structural and functional relation with the vestibular system. Despite the cerebellum not being a focus of study of this thesis, I believe understanding its function has helped me keep in mind the bigger picture of motor learning when examining the tail response to balance perturbation.

The vermis and intermediate cerebellum are characterized by two somatotopic maps, one in the anterior and one in the posterior lobe. The head and trunk are represented by the vermis (which integrates vestibular, visual and auditory inputs), while the limbs by the intermediate parts of the cerebellar cortex. The cortex receives inputs from spinal afferents which conveys information related to step cycle of locomotion (ventral pathway) and sensory feedback during movement (dorsal pathway) [135].

The vermis receives vestibular inputs (either primary or secondary). Specifically the I to V lobules (anterior vermis) integrates vestibular and neck-related proprioceptive related signals, while lobules VI and VII of the posterior lobe is related to visual-vestibular processing (information regarding visual movement is conveyed by the nucleus prepositus, and the dorsolateral pontine nucleus (DLPN). DLPN also gets input from the deep layers of the superior colliculus. Stimulation studies have shown that the oculomotor vermis is implicated in the generation of saccadic movements. Lesions of oculomotor vermis or the caudal fastigial nucleus (its target area), impair saccadic movements and smooth pursuit eye movements.

The deep cerebellar nuclei (DCN) consist of 3 nuclei: the dentate nucleus (receiving projections from the lateral portion of the cerebellum), the interpositus (with inputs from the intermediate portion of the cerebellar cortex), and the fastigial nucleus (receiving projections from the cerebellum). This last nucleus is the more tightly linked to the vestibular system, as it receives direct projetions from the vestibular nerve. There seems to be a topographical organization of these nuclei, such that the dentate nucleus controls activity of limb extremities for manipulation of objects, the interpositus control of limbs and the medial (or fastigial) is related to postural control of axial muscles.

The fastigial nucleus can be functionally divided into anterior and posterior parts, with the anterior part more sensitive to head velocity in darkness, while the posterior part responds to pursuit and saccadic eye movements. The rostral fastigial nucleus is involved in posture and head movement control, projecting to the spinal cord or vestibulospinal neurons and receiving input

from vestibular organs and neck proprioceptors [136]. Approximately half of rostral fastigial nucleus neurons are unimodal (responding exclusively to head movement), while the other half are bimodal (responding to body motion). The caudal fastigial nucleus receives afferents from the oculomotor vermis and is involved in voluntary and saccadic eye movements, but not in the vestibulo-ocular reflex or head movement [137].

The anterior and posterior interpositus nuclei contribute to locomotion and reaching, with lesion studies showing deficits in obstacle avoidance and limb flexion control during locomotion [138]. These nuclei are also implicated in eye blink conditioning based on single-unit recordings and lesion studies. The dentate nucleus is involved in voluntary movements, as its stimulation induces upward eye movements and lesion studies reveal impairments in visuomotor sequence learning [139].

2.1.3 Viral strategies to target neurons and reveal connectivity/function

Since the last century, researchers have sought to understand the connectivity between neurons in the spinal cord and brainstem ([69]). Traditional tracers and toxins, such as Cholera Toxins B-Subunit (CTB), have been instrumental in identifying the location and molecular characteristics of MNs innervating specific muscle groups. By utilizing tracers that are transported retrogradely to cell bodies, researchers have made significant contributions to modern neuroanatomy [140]. Despite their utility, these techniques possess several limitations, notably the inability to infect synaptic terminals, specific cell types or spread transsynaptically. Additionally, some methods necessitate lesioning at the injection site to facilitate tracer penetration, potentially leading to false positive results. A notable advancement has been the use of viruses engineered to spread transsynaptically, particularly when combined with mouse genetics, marking a substantial leap forward in neuroanatomical research [141, 142].

Viruses have developed very efficient and flexible mechanisms for infecting specific cell types, making them versatile tools for neuroscience research. They can serve as transsynaptic tracers, retrograde tracers, or anterograde tracers [143]. For instance, rabies virus has evolved to initially infect MNs at the neuromuscular junction and subsequently spread across synapses throughout the nervous system [144]. Pseudorabies virus has been employed to trace the network of neurons connected to a specific pool of motoneurons. However, a challenge with this approach is the potential for multi-synaptic transfer, which is governed only by the duration of the infection period (where sometimes a few hours can make a significant difference in the resulted network of neurons trasfected). Despite this limitation, rabies tracing has proven invaluable for anatomical studies, and there have been intriguing attempts to leverage it for in vivo physiological investigations [145]. Nonetheless, researchers have encountered issues with rabies virus cytotoxicity, which can alter the vitality and physiological properties of infected neurons. To address this concern, a modified version of rabies virus has been developed and tested, downregulating its replication machinery post-infection, thereby offering a revolutionary approach for studying functionally connected neuron populations [146]. In contrast, adeno-associated viruses (AAVs) are widely used for targeting and infecting neurons at the cellular level. AAVs offer advantages over rabies viruses, as they do not compromise neuronal vitality and can be utilized as conditionally expressing tools in conjunction with mouse transgenic lines expressing Cre or other recombinases in defined neuronal populations. AAVs have been employed to express various reporter proteins, receptors, and surface channels, catering to the needs of researchers. The elucidation of AAV molecular biology in recent years has facilitated

the modification and mutation of viral surface protein expression, enabling the creation of AAVs with highly efficient retrograde properties [147].

2.2 Methodology and Results

2.2.1 Aim1: Characterization of tail motoneurons in spinal cord

In this section I will present the methods and results from the anatomical tracing of tail-MNs in the sacral spinal cord. I will start by describing the virus injection protocol used, and the tissue processing, as well as image acquisition and the analysis pipeline. Finally in the results I will describe the localization and morphological properties of the tail-MNs innervating the extrinsic lateral muscle.

Procedure for virus injection

Viruses carrying fluorescence marker genes (GFP and tdTomato) were used for anatomical tracing, while viruses carrying genes for optogenetic actuators (ChR2) were delivered for stimulation. All viral constructs were introduced to the desired area by means of stereotactic injection. For this, the animal was deeply anesthetized by placing it in an anesthesia induction chamber with 3-4 percent isoflurane, and after the anesthetic state was confirmed, it was fixed in a stereotactic frame with a pair of obtuse ear bars and mouth/nose clamp under constant 1.5 - 2.5 percent isoflurane anesthesia. The eyes of the animal were covered with eye ointment (Mycochlorin) to prevent eye drying and damage. A thermal pad was used to control the animal's temperature. Using sterile tools, the skin and muscle were penetrated by a glass pipette used to inject the virus. The skin and soft tissue covering the skull were opened using sterile tools, and a small (< 1mm) craniotomy was created using a surgical drill at the selected location. For spinal cord injection, the skin and fascia above the sacral spine were opened, and laminectomy was carefully performed to expose the S1-S4 spinal cord. For tail injection, hair was removed using a shaving cream and a blade, and the tail was fixed using a spinal cord holder. For brain, spinal cord, and tail injections, a thin quartz capillary pipette was inserted into the desired stereotactic location, and a total volume of < 1 ul of solution was injected slowly (<30 nl / min) using a Nanoinjector (Neurostar, Germany). After injection, the pipette was slowly withdrawn, and the skin covering the skull or spinal cord was closed with sutures or superglue. Fascia was also sutured in spinal cord injection. Topical anesthetic was applied to the site of surgery, and systemic analgesic (carprofen, 7.5 mg/kg, or buprenorphine, 0.05 mg/kg) was administered subcutaneously, and carprofen-medicated food was provided ad libitum. The animal was closely observed until recovery from the isoflurane anesthesia. Further deliveries of the analgesic were administered every 12 hours for 3 days or more.

The virus constructs used were adeno-associated virus (AAV), with capsid AAV8, AAV9, or AAV retrograde, and promoters were either hsyn or CAG (as specified in our virus transfection protocol RDE-2022-041-2, with titer $\geq 7 \times 10^{12}$ vg/mL). Four to six weeks of labeling/transfection time were needed after the injection of viral constructs. During this postoperative phase, the animals were regularly monitored to detect any possible problems in recovery.

Tissue preparation and image acquisition

Perfusion and slicing

The brain and spinal cord of C57BL/6 (CLEA Japan, Shizuoka, Japan), was collected after per-

fusion for perfusion-fixing, the animal was deeply anesthetized with MMB overdose (containing Medetomidine HCL, 1 mg/ml; Midazolam, 5 mg/ml; and Butorphanol tartrate, 5 mg/ml; dosage 0.05 ml/g) and after they were unconscious (verified with an absence of the toe pinch reflex), the heart was exposed and the animal was transcardially perfused, first with phosphate-buffered saline (PBS; pH 7.4) to clear the blood and then with fixative solution (4 percent paraformaldehyde, PFA), and finally the tissue was extracted and left in 4 percent PFA overnight. After fixation, the tissue was immersed in 10 percent sucrose in PBS until it sank (6-12 hours), followed by immersion in 20 percent sucrose for another 6 hours, and in 30 percent sucrose in PBS overnight. The tissue was gently rocked every 2-3 hours, ensuring it did not come into contact with bubbles or the air surface interface. Coronal brainstem sections, 50 to 100 µm thick, were cut using a vibratome (5100MZ-plus; Campden Instruments, Loughborough, UK) with ceramic blades (38 x 7 x 0.5 mm, model 7550-1-C, Campden Instruments, Loughborough, UK) or a Cryostat (Leica CM1950, Wetzlar, Germany). The sections were then mounted on slides with Vectashield (H-1200, VectorLabs, CA) mounting medium and covered with 1.5 coverslip glass (Harvard Apparatus, MA)

Image acquisition
Confocal image stacks were obtained from sections labeled using viral methods with a Zeiss LSM 880 confocal system (Zeiss, Germany). Low-magnification imaging utilized a 5x objective (Plan-Apochromat 5x M27; NA 0.16; Zeiss, Germany) with z-steps of less than 10 um. High-magnification imaging was performed with a 40x objective (Plan-Apochromat 40x Oil DIC M27; NA 1.4; using Zeiss Immersion oil; Zeiss, Germany) with z-steps between 0.1 to 1 µm for tissue sections between 50 to 100 µm thick. For multi-channel images acquired in line-scan mode, the following excitation/emission wavelengths were used: eGFP (and AF 488) at 488 nm / 490–535 nm, and tdTomato at 561 nm / 470–655 nm.

Pre-processing overview

Image pre-processing involved applying a gentle Gaussian blur (radius of 1 pixel), before optimizing brightness levels to enhance the visibility of neuronal soma outlines. Then we traced neurons with the Freehand selections tool in ImageJ. Vaa3D or Imaris was occasionally used for examining three-dimensional neuronal morphology. Traced neurons silhouettes somas are saved in the ROI manager, and a Z projection is performed for comparison of mean gray values. Overlapping neurons are separated for clarity by dividing the stacks, so that one neuron will be visible in most of one substack. Measurements are then analyzed, and results are saved in an Excel sheet. For further processing and analyses, I used custom-scripts in python (via Jupyter Notebook).

Spinal cord registration onto the atlas

I have adopted a standardized approach to determine the spinal cord segment of interest. This standardization is based on the length of the line that grossly divides the dorsal horn from the rest of the spinal cord. The measurements were obtained using the Allen Spinal Cord Atlas. The following table provides the information to determine the spinal cord segment based on line length measurements (unit is micrometer).

Spinal Segment	Line Length Threshold (µm)
S1	< 1600
S2	< 1300
S3	< 1150
S4	< 950
Co1	< 800
Co2	< 700
Co3	< 650

Table 1: Line length thresholds for different spinal segments.

After deciding the spinal segment identity, to complete the registration procedure, the following steps were followed: first, the unique region of interest (ROI) from the atlas was added to the ROI manager. Then, the same ROI was located on the image to be registered. Finally, the 'Align Image by Line ROI' function was used for the linear registration. After quality check (QC), if the image registration resulted distorted on the dorso-ventral axis, the procedure was repeated by drawing a second ROI that passes vertically by the central canal (CC). These steps were repeated manually for each stacks obtained, and a mask containing the area of interest (either segmented axons or soma location) was extracted and data for the same mouse and same segment were overlaid with z-projection.

Tail-MNs distribution within the spinal cord

The injection strategy, depicted in panel A 2.1, involved the administration of either a toxin (CTB-488) or virus (AAVrg.CAG.eGFP) into the lateral extrinsic muscle, as illustrated in the microCT scan muscle reconstruction (more details on the reconstruction in Chapter 1). Panel B shows a representative spinal cord section from levels S3-S4, where the z-projection of several sections containing labeled tail-MNs is displayed. Notably, the labeled tail-MNs, will be considered here as putative alpha motoneurons (based on their location in lamina IX and soma size, as per [148]), which are the motoneurons responsible for the contraction of the lateral tail muscle. The labeled MNs are shown exclusively on the right side of the ventral horn (given that they project ipsilaterally to the right lateral muscle). Panels C and D depict density maps illustrating the distribution of lateral tail-MNs across S3 and S4 in three mice. These maps are superimposed on the respective atlas hemisections from the Allen Spinal Cord Atlas (registration process described above). Additionally, the normalized mean for the distribution of tail-MNs (N=3) is provided alongside the distribution map. The density map highlights that the tail-MNs of the lateral extrinsic muscle form a tight cluster in the ventro-medial portion of lamina IX in S3-S4 spinal cord sections.

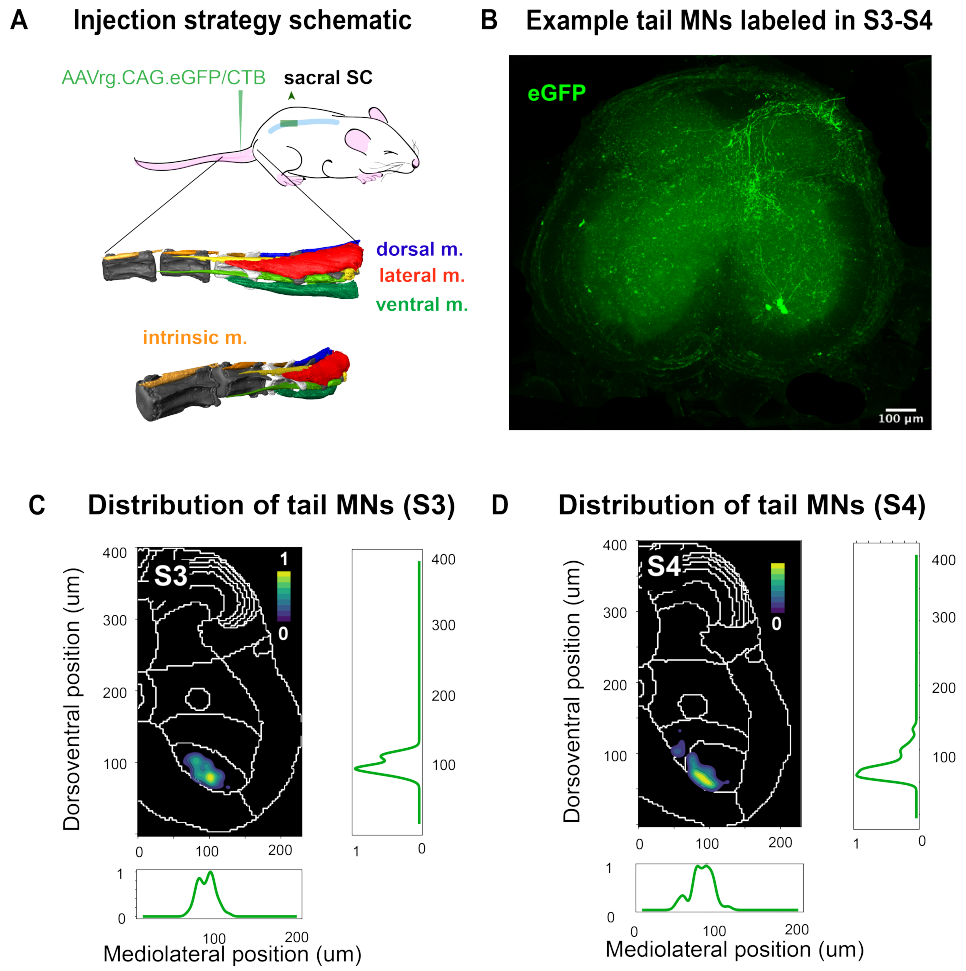

Figure 2.1: Distribution of tail MNs in sacral spinal cord. Panel A shows the injection strategy schematic of the toxin (CTB-488), or virus (AAVrg.CAG.eGFP). The injection was performed in the lateral extrinsic muscle (red, shown in the microCT scan muscle reconstruction). Vertebra in white is Co4 for reference. Panel B displays an example of spinal cord sections from level S3-S4 where several sections containing labeled tail-MNs were overlapped in a z-projection. The labeled tail-MNs (innervating lateral tail muscle) are shown in the right side of the ventral horn. Panel C and D show the density map of distribution of lateral tail-MNs for 3 mice in S3 (C), and S4 (D), overlaid with the respective atlas hemisection (Allen Spinal Cord Atlas). On the side of the overlaid distribution map, the normalized mean for the distribution of tail-MNs (N=3).

Morphological analysis of the tail-MNs data revealed a possible labeling bias of cholera toxin subunit B (CTB) and adeno-associated viruses (AAVs) injections. Representative examples of putative gamma-motoneurons labeled with AAVs and putative alpha motoneurons labeled with CTB, both situated in lamina IX of a spinal cord section at the S3 level (50 µm thick), are depicted in Panel A 2.2. Panel B illustrates the distribution of soma area sizes, manually drawn from stacks spanning from S3 to S4, across four mice. Notably, AAV-labeled neurons (dark green, n = 348) and CTB-labeled neurons (light green, n = 120) exhibit significantly differences in distribution, with soma sizes of AAV-labeled MNs being smaller (AAV = 186.2±10.29 um2; CTB = 670.9±17.54 um2; ($t(149) = 3.314$, $p < 0.01$)). This result may be important to consider when using viruses or other tracers for motoneurons labeling in general.

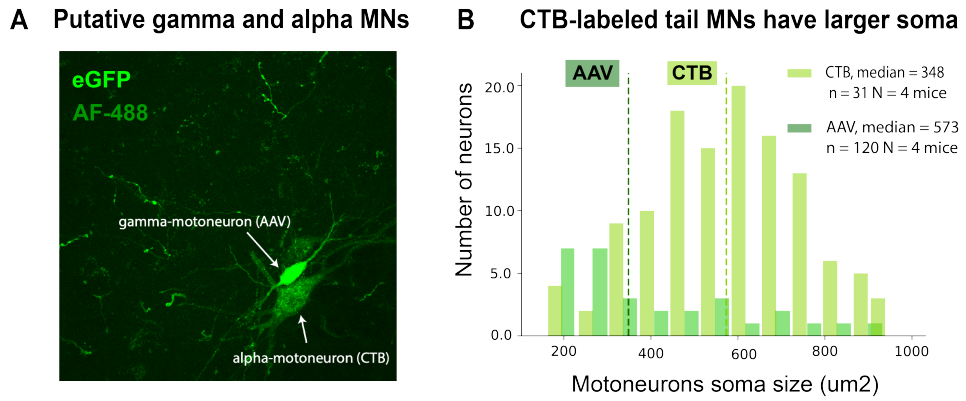

Figure 2.2: Selective bias of labeling from CTB Vs AAVs injections. Panel A shows an example of putative gamma-motoneurons (labeled with AAV), and putative alpha motoneuron (labeled with CTB), located in lamina IX of an S3 section (50um thick). Panel B shows the distribution of soma area size manually drawn from stacks from S3-S4 (N = 4 mice) for AAV (dark green, n = 348), and CTB (light green, n = 120). Confocal acquisition were obtained with a 20x objective (Plan-Apochromat 20x M27; NA 0.8; Zeiss, Germany).

2.2.2 Aim2: Characterization of vestibulospinal neurons

In this section I will present the results from the anatomical tracing of vestibulospinal neurons that project to the sacral spinal cord. This anatomical characterization was an important milestone of the project, as it reveals a structural link between the vestibular system and the spinal circuits responsible for tail movement. I will present the results into two section, firstly the vestibulospinal axons projection pattern in the spinal cord (with emphasis on the direct projection onto tail-MNs), and the location of sacral-vestibulospinal neuron in the vestibular complex.

Vestibulospinal axons distribution in the spinal cord

In this section I will present the density map of tail axon projections onto the sacral spinal cord. Panels A and B in 2.3 depict the sacVS axons distribution density observed across laminas in spinal cord segments S3 and S4, respectively (N=3). The mediolateral and dorsoventral position histograms highlights the widespread projection of these axons in the ventral horn, with a peak distribution between lamina VIII and IX (where tail MNs are distributed). Panels C and D in 2.3 display the same data, with overlaid tail motoneuron soma density maps for segments S3 and S4, respectively (n = 3). Despite the clear overlap, the density map shows that VeS axons do not project exclusively to tail MNs.

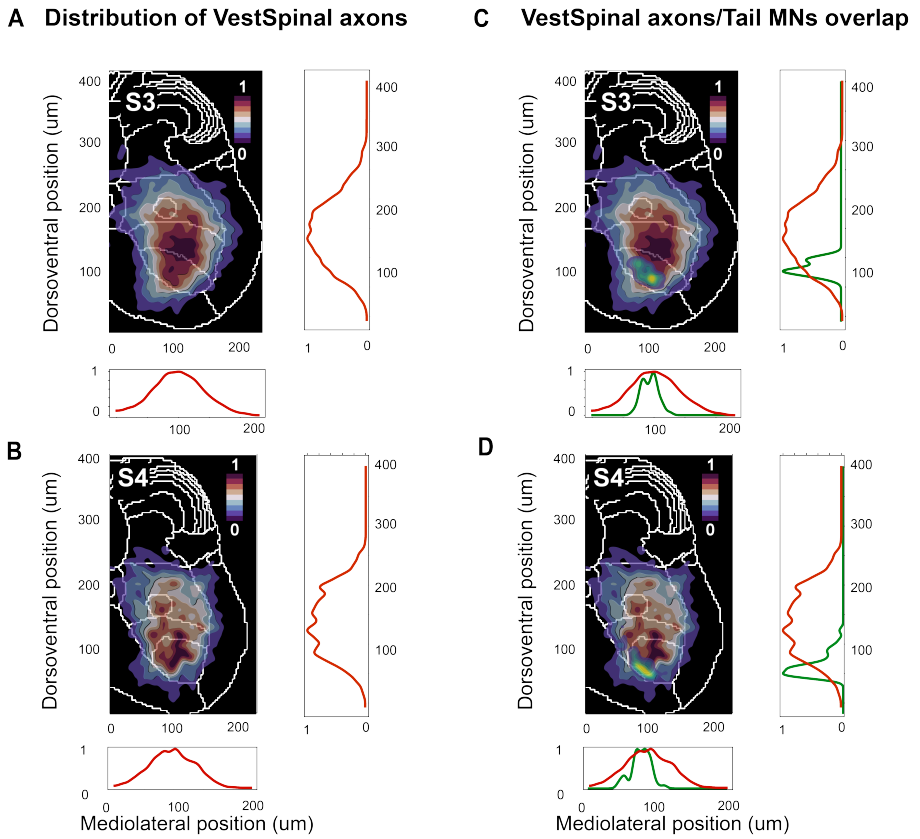

Figure 2.3: Density map of tail axons projection onto sacral spinal cord. Panel A-B sacVS axons in S3 and S4 respectively. Heatmap is normalized to peak intensity and shows the average across 3 mice. Mediolateral and Dorsoventral position histogram highlights the broad projection of these axons in the ventral horn. Panel C-D show the same data with overlaid tail-MNs soma density maps for S3 and S4 respectively (n=3).

Interestingly, the highest absolute density of axons is in lamina VII, VIII and IX, where interneurons, premotor and motor neurons are respectively located, as show in panels A and B of figure 2.4 for S3 and S4 respectively. To make sure that the results were not biased by the bigger area of certain laminas I show the normalization by area of the region of interest (panels C and D from figure 2.4. The normalized distribution interestingly reveals a high axonal density in the preCerebellar nuclei, that is nuclei in the sacral spinal cord that project mostly to the vermis of the cerebellum ([85]).

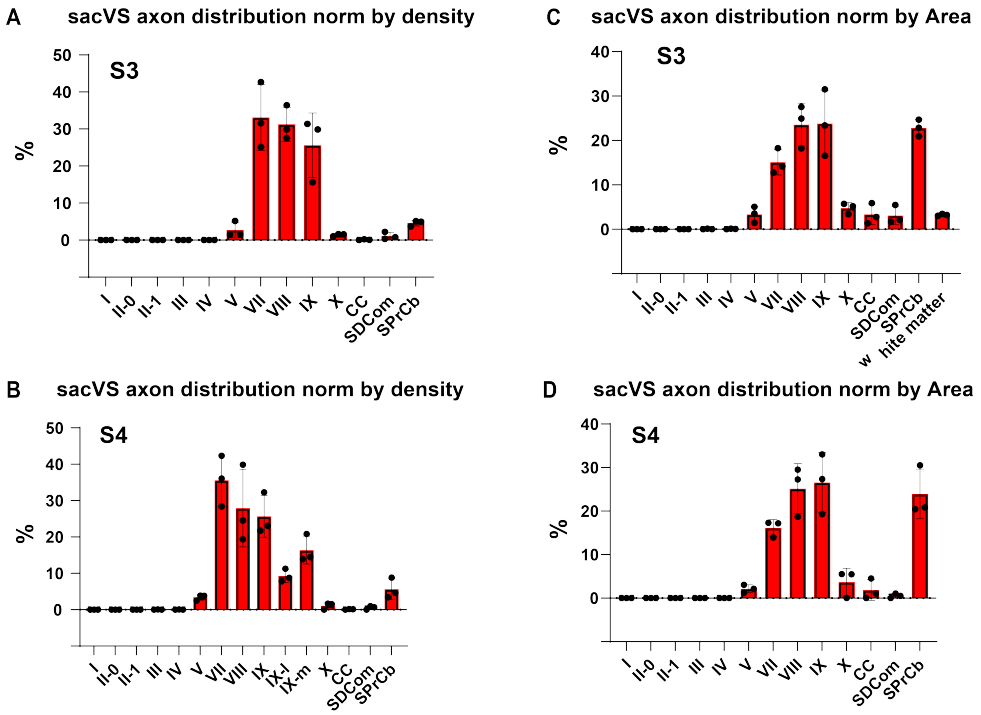

Figure 2.4: Distribution of sacVS axon across laminas. Panels A and B show the sacVS axonal distribution in S3 and S4, revealing highest axonal density in laminae VII, VIII, and IX. To account for laminar size variations, panels C and D present the normalized distribution, highlighting a prominent axonal density in the preCerebellar nuclei as well. Data is shown as mean ± SEM and each dot is the value per one mouse (N=3).

A conditional approach for viral injection was employed to selectively target sacVS neurons (by injecting CRE-expressing virus in the sacral ventral spinal cord, and CRE-dependent tdTomato-expressing virus in the vestibular complex). The same mouse was also injected intramuscularly in the lateral tail muscle for labeling of tail-MNs (injection strategy shown in 2.5 panel A). A representative example of a tail-MN labeled with virus (GFP in green) in an S3 spinal cord section is depicted in Panel B, obtained with a 20x objective. Higher magnification (40x objective) reveals putative synaptic contacts on the primary dendrite and soma. Finally, the number of tail MNs receiving putative synaptic contacts was estimated manually by counting how many tail MNs received at least 3 putative synaptic at $< 1\mu$m distance from the soma surface (panel C). This shows that $67 \pm 4.51\%$ of tail-MNs labeled with CTB-AF488 also received putative synaptic contacts from sacVS neurons ($n = 74, N = 3$). This result is in line with previous literature in mouse hindlimbs ([34]).

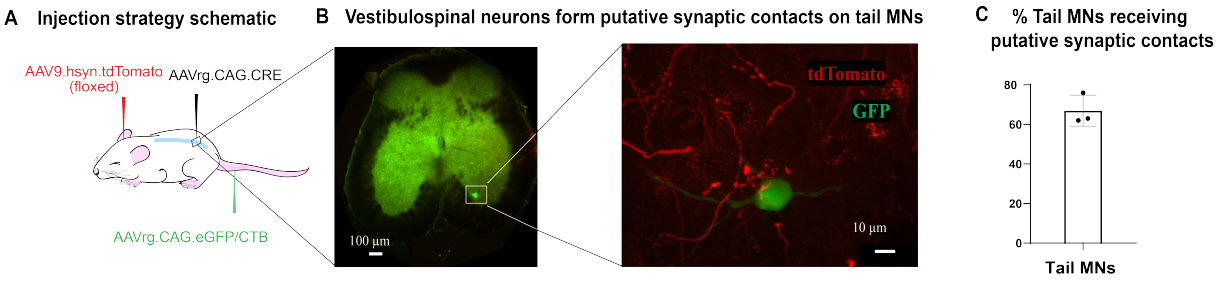

Figure 2.5: Vestibulospinal axons form putative synaptic contacts with tail MNs. Panel A shows the injection strategy used to target selectively sacVS neurons and label in the same mouse tail-MNs. B shows example of tail-MN labeled with virus (GFP in green) in an S3 spinal cord section acquired in LSM880 confocal with a 20x objective (Plan-Apochromat 20x M27; NA 0.8; Zeiss, Germany). High magnification is shown on the right (Objective "Plan-Apochromat" 40x Oil DIC M27; NA 1.4; using Zeiss Immersoil oil; Zeiss, Germany), highlighting putative synaptic contacts on the primary dendrite and the soma. In C the quantification of tail-MNs percentage receiving putative synaptic contacts from the vestibulospinal axons. Each dot is the value per one mouse (n=74, N=3). Shown is mean ± SEM.

Morphological characterization and distribution of sacVS neurons

Figure 2.6 panel A illustrates the injection schematic, which was consistent with the method described in Figure 2.5, enabling the selective labeling of SacVN soma. In Figure 2.6 panel B, a high-magnification image (Plan-Apochromat 20x M27; NA 0.8; Zeiss, Germany) of the vestibular complex shows the distribution of sacVN soma (labeled with tdTomato) within the complex. Furthermore, Figure 2.6 panel C shows a histogram of the distribution of somata area size of labeled sacVN compared to labeled nucleus X (nuX) neurons. The somata area size of labeled sacVN (purple, n=171, N=3) is significantly larger than the labeled nuX neurons (red, n=47, N=3) (sacVN=670.9±17.24 um2; CTB=186.2±10.29 um2; ($t(216) = 14.29$, $p < 0.001$)). Key anatomical landmarks, including the 4th ventricle (4V), Vestibular Nuclei (VN), inferior cerebellar peduncle (icp), trigeminal spinal tract (sp5), and nucleus X (nuX), are annotated for reference.

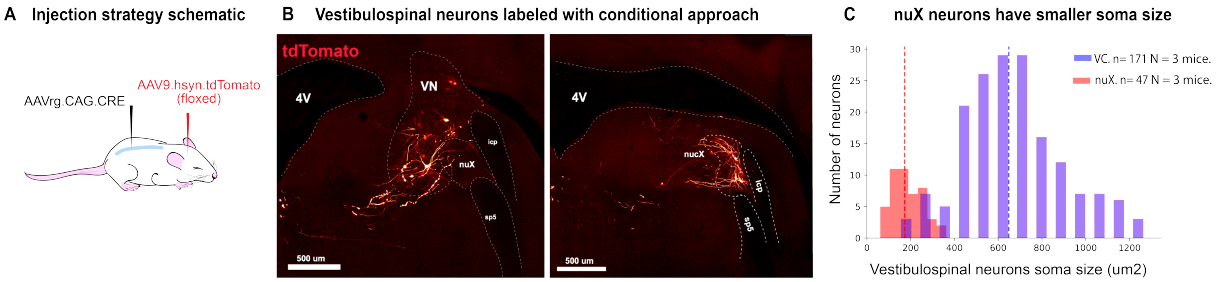

Figure 2.6: sacVN location within the vestibular complex. Panel A shows the injection schematic (same as Figure 2.5) to selectively label the sacVN soma. Panel B shows a high magnification (Plan-Apochromat 20x M27; NA 0.8; Zeiss, Germany) acquisition of the vestibular complex with labeled sacVN soma (labeled with tdTomato). In C, histogram showing the distribution of somata area size of labeled sacVN (purple, n=171, N=3) versus labeled nuX neurons (red, n=47, N=3). 4V=4th ventricle, VN=Vestibular Nuclei, icp=inferior cerebellar peduncle, sp5=trigeminal spinal tract, nuX=nucleus X.

Figure 2.7A displays the distribution of labeled sacVS neurons visualized using *napari-brainrender*. The highlighted 3D mesh of the vestibular complex is shown in rose-pink, overlaid with the atlas in gray. Panel B provides different views of the vestibular complex along with labeled regions of interest (ROIs) for three mice. The percentage distribution of sacVS neurons across the vestibular complex shows that most neurons are located in the most rostral position of the spinal vestibular nucleus (SPIV) (2.7C). In contrast, lumbar-projecting vestibulospinal neurons (lumbVS) are dispersed throughout the rostro-caudal and dorso-ventral aspects of LVN according to prior studies in mice ([84], [34]). In summary, by reconstructing the position of sacVS neurons following the conditional approach illustrated in 2.6 panel A, we found that these neurons form a distinct cluster in the rostral region of SPIV. This supports the notion that sacVS neurons represent a distinct subpopulation.

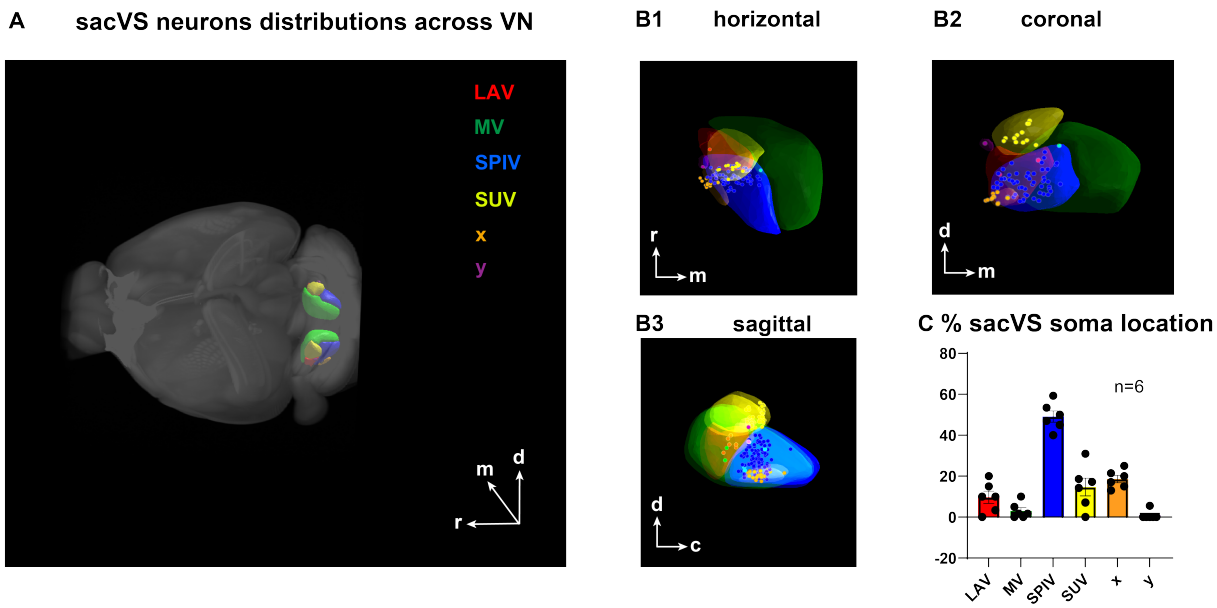

Figure 2.7: Distribution of sacVS neurons across the vestibular complex. Panel A shows the distribution of the labeled sacVS neurons in napari-brainrender. In rose-pink, the highlighted 3D-mesh of the vestibular complex overlaid with the atlas (gray). In panel B, different views of the vestibular complex and labeled ROIs for 3 mice as top, posterior, and side view (B1, B2, B3 respectively). Panel C shows the percentage distribution of sacVS neurons across the vestibular complex. LAV=Lateral vestibular nucleus, MV=Medial vestibular nucleus, SPIV=Spinal vestibular nucleus, SUV=Superior vestibular nucleus, x=nucleus X, y=nucleus Y.

2.2.3 Aim3: Optogenetic activation of the vestibular complex

In this section I will describe the methods and results of the functional (optogenetic) manipulation experiments. I will first describe the optogenetic implantation protocol used, and then move to the results from the stimulation of the vestibular nucleus unilaterally.

Procedure for optogenetic implantation

At the beginning of the fiber implantation surgery, the mouse was induced with 5 percent Isoflurane and then maintained at 1.8 percent Isoflurane throughout the procedure using a stereotaxic apparatus. The head was secured using sharp mouse ear bars, and pre-operative measures included the application of eye ointment, scalp shaving, and Lidocaine ointment application. An incision was made from between the ears to between the eyes, and the skull was cleaned of periosteum before being dried. A black enameled 0.4mm needle was installed in the stereotaxic apparatus, ensuring consistency by marking the groove used in the needle holder. Bregma and Lambda were marked, and DV was checked not to exceed 50um. The needle was moved to the midpoint, and pitch was examined, avoiding values larger than 50um. Coordinates (AP 5.9, ML +-1.55, DV 4.35) were reached, using markers on the skull for reference, and caution was taken for bleeding over the cerebellum with the use of gelfoam. Drilling was performed at the marked points, with periodic rechecks of coordinates. Post-drilling, Lambda and Bregma were rechecked, and the edges of craniotomies were blackened using a sharpie. The needle was moved to coordinates again, slightly entering the hole, and the ink was scratched to

create crosshairs. This process was repeated with specific movements to note DV coordinates. Depth total from the skull was calculated, and the right implant was installed. After returning to DV 0, the needle was replaced with the fiber implant, moved to the skull surface, and the depth total from the skull was lowered. A small drop of super glue was applied at the insertion point, left to cure for 5 minutes, and the implant was released. The second implant was installed on the left side following the same procedure. While waiting for the glue to cure, a porcelain dish was stored at -80C. Once cured, dental cement was mixed in the dish and applied to the skull and implants. The skin was pulled over the cement, stitches were placed in front and behind the implant, and the mouse number was written on the dental cement. Analgesia was administered, and the mouse was returned to the cage on a heat pad.

Optogenetic stimulation of VN

In this section I will present the results from the optogenetic activation of vestibular complex. To achieve this, we used a mixture (50:50) of silk fibroin and virus for expressing ChR receptor (as shown in [149]) and applied it on the cannula tip (approach diagram shown in 2.8 A). The cannula was implanted bilaterally on top of the vestibular complex (2.8 B). This technique allowed precise and controlled delivery of the viral vectors to the target site within the vestibular complex.

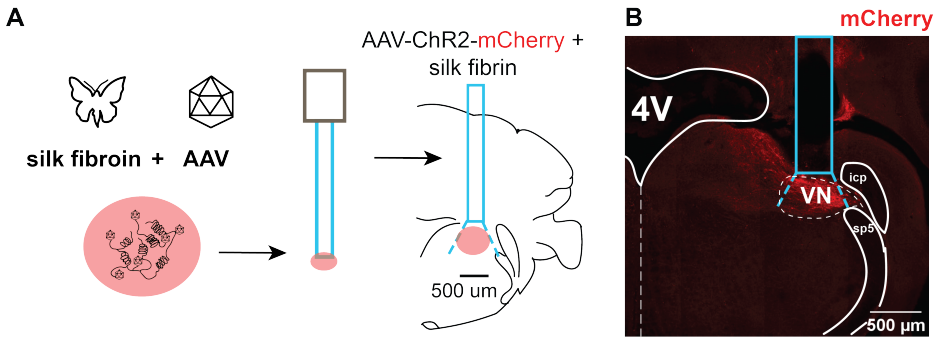

Figure 2.8: Approach for optogenetic stimulation of vestibular complex. In panel A, approach for delivery of virus using silk fibroin applied on the cannula tip. Optic cannulas were implanted bilaterally on the vestibular nucleus. In panel B, an example of cannula placement in a brainstem section, with region labeled in mcherry due to virus delivery. The tissue was imaged using confocal microscope (Zeiss LSM880). 4V=4th ventricle, VN=Vestibular Nuclei, icp=inferior cerebellar peduncle, sp5=trigeminal spinal tract, nuX=nucleus X.

Two weeks after surgery, mice were handled (4 days) and trained on the ridge (1 week), and I started experimental recordings 5 weeks after injection (appropriate transfection time based on the anatomical tracing study presented above). When light stimulation was delivered unilaterally (500 ms constinous pulse at 2-3mW measured at the tip of optic cannnula) on mice during locomotion, the most striking response occured in the ridge (4mm) with a robust rotation of the tail in the roll axis (2.9, bottom panel). These movements were not consistently evoked on a flat surface (2.9, top panel and 2.10, panel b), highlighting the different effect that the activation yielded in different conditions.

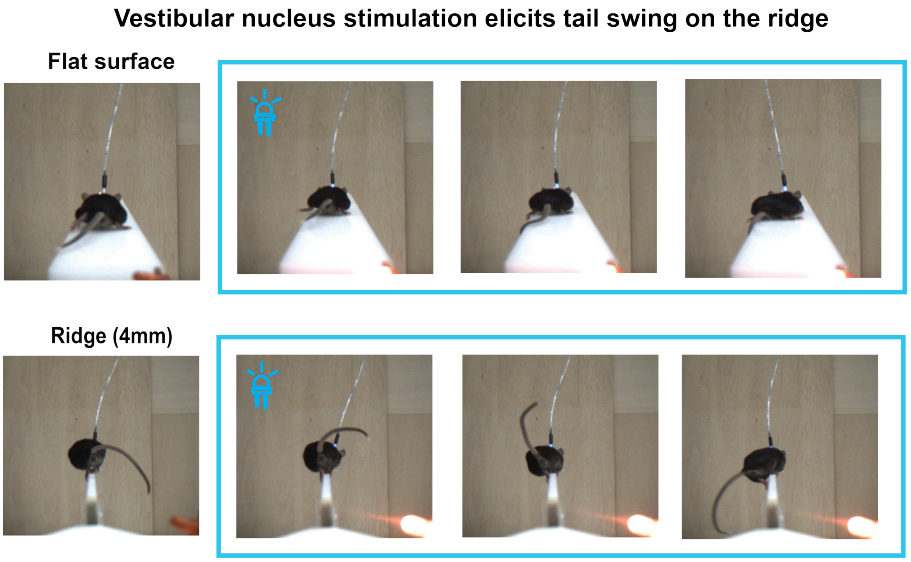

Figure 2.9: Unilateral photo-activation of the vestibular complex effect on tail movement during ridge VS flat surface crossing. One example snapshots from the same mouse, showing the typical tail movement in response to the photo-activation of the vestibular complex (continuous 500 ms pulse for a duration of 500 ms, in blue) while crossing a flat surface (top), and ridge (bottom). Colored rectangle indicates frames capturing the response during the optogenetic stimulation.

In figure 2.10 I show the time series average (single line, light shaded), as well as the mean across mice (N=6 mice, mean plus minus sem) for unilateral photo-activation on the left side (top panel 2.10 A and B, ridge and flat surface respectively), and on the right side (top panel 2.10 C and D, ridge and flat surface respectively). As shown the optogenetic stimulation leads to tail movement that is directional dependent on the ridge (left activation elicits a CW tail movement, while right activation a CCW response), but not on the flat surface.

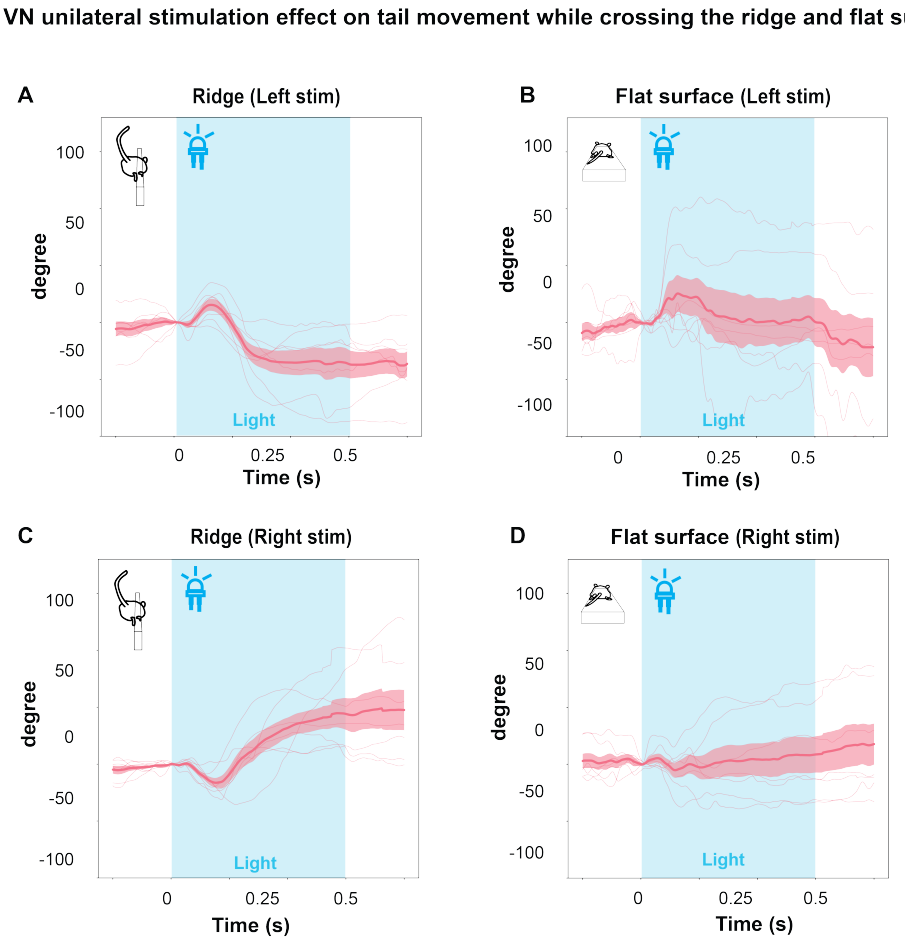

Figure 2.10: Light-evoked changes in tail roll rotation. Top Left: Mean ± SEM light-evoked changes in tail roll rotation for each animal (n = 5 mice) and across animals (darker red trace). The shaded blue area represents the time of photo-activation (continuous 500 ms pulse for a duration of 500 ms, in blue). Insets show what condition is displayed in the plot (ridge or flat surface). Top panels show tail rotations while mice were crossing the ridge (A), or the flat surface (B). Bottom panels show tail movement in response to right activation of the vestibular complex in the ridge (C) or flat surface crossing (D). Downwards traces represent clockwise rotation and upwards traces counterclockwise rotation.

Next I examined the effect of activation on the base of support. As extending the base of support has been shown to be an effective strategy in response to a balance perturbation [150], we wanted to show whether such effect can be consistently elicited by unilateral stimulation of the vestibular complex. Indeed we showed a stark increase in the base of support in response to the photo-activation on a flat surface regardless of the direction of the stimulation (2.11, panels A, D, E), but not in the ridge (2.11, panels B, C). This is to be expected given that during locomotion on the ridge the base of support cannot be increased by widening the position of the limbs, contrary to a flat surface.

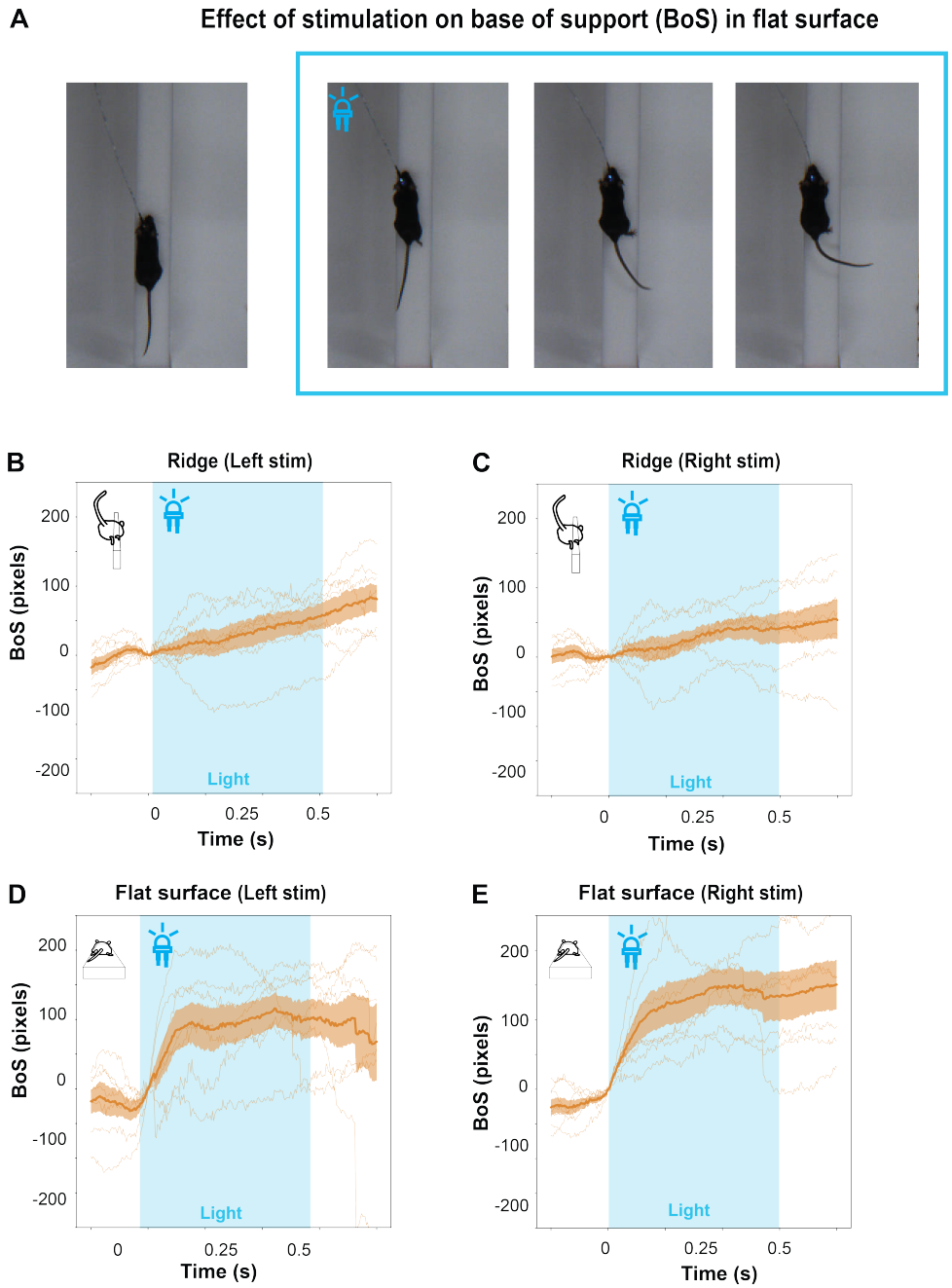

Figure 2.11: Effect of stimulation on base of support (BoS) in flat surface and ridge test. Panel A show example snapshots from one trial, showing the typical effect on the base of support to the photo-activation of the vestibular complex (continuous 500 ms pulse for a duration of 500 ms, in blue) while crossing a flat surface (top). Colored rectangle indicates frames capturing the response during the optogenetic stimulation. Panels B and C show the averaged change of BoS area for each mouse (light single line), and the average across mice (darker shade, N = 6 mice, mean ± SEM) while crossing the ridge after photoactivation on the left and right implant respectively. Panels D and E show the same for trials where mice were crossing the flat surface.

Finally, I analyzed the effect of the stimulation on the mouse forward speed. As shown in (2.12) the optogenetic stimulation decreases speed to the point of stopping the mouse in most cases (red dotted line), and in some cases the mouse was walking backwards of a few steps (as

indicated by mean traces below the red line). As mice walk faster on a flat surface as compare to the ridge ([31]), we observed a stronger decrease in speed on a flat surface, indicating that the stimulation has in both condition the effect of bringing the mouse to a stop, rather than just decelerating.

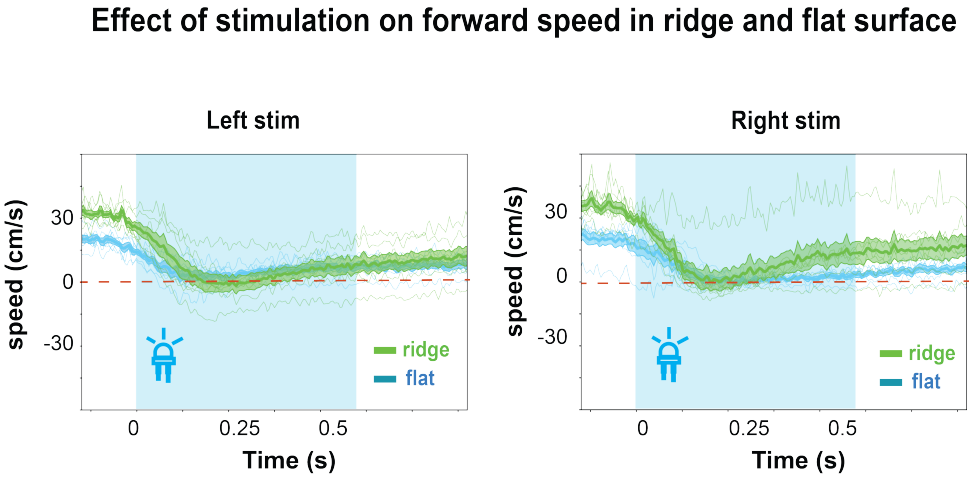

Figure 2.12: Effect of stimulation on mouse forward speed. Left panel represents the change in forward speed during the photo-activation of the left vestibular complex (continuous 500 ms pulse for a duration of 500 ms, in blue) while crossing a flat surface (blue), or ridge (green). Right panel shows the response during stimulation of the right VN. Colored rectangle indicates frames capturing the response during the optogenetic stimulation.

2.2.4 Aim4: Selective activation of the sacral vestibulospinal neurons

The experimental approach designed for the selective targeting of sacral vestibulospinal neurons is shown in (2.13), which consists on the injection of a virus leading to the retrograde expression of ChR (AAVrg.CAG.ChR-tdTomato) into the sacral spinal cord and the bilateral implantation of optic cannula in the left and right vestibular nuclei. Two weeks after surgical procedures mice were handled for four consecutive days, and trained on the ridge for another five consecutive days. Following training the experimental recording started at 5 weeks after the retrograde injection, to allow appropriate transfection time. As shown in (2.13A and B) the implants are connected to the optic fiber via a ceramic sleeve, and the cable is supported by a commutator attached to a rail with a movable piece, allowing for flexible movement. The cannula was implanted bilaterally on top of the vestibular nuclei (AP:-5.9, ML:1.55, DV:4.5). Figure (2.13)B1 and B2 shows the anatomical location of the implant in two sections representing the rostral (top) and caudal (bottom) sections respectively of the right vestibular nucleus (identified by the anatomical landmark of the 4th ventricle and icp and sp5 tracts, [91]).

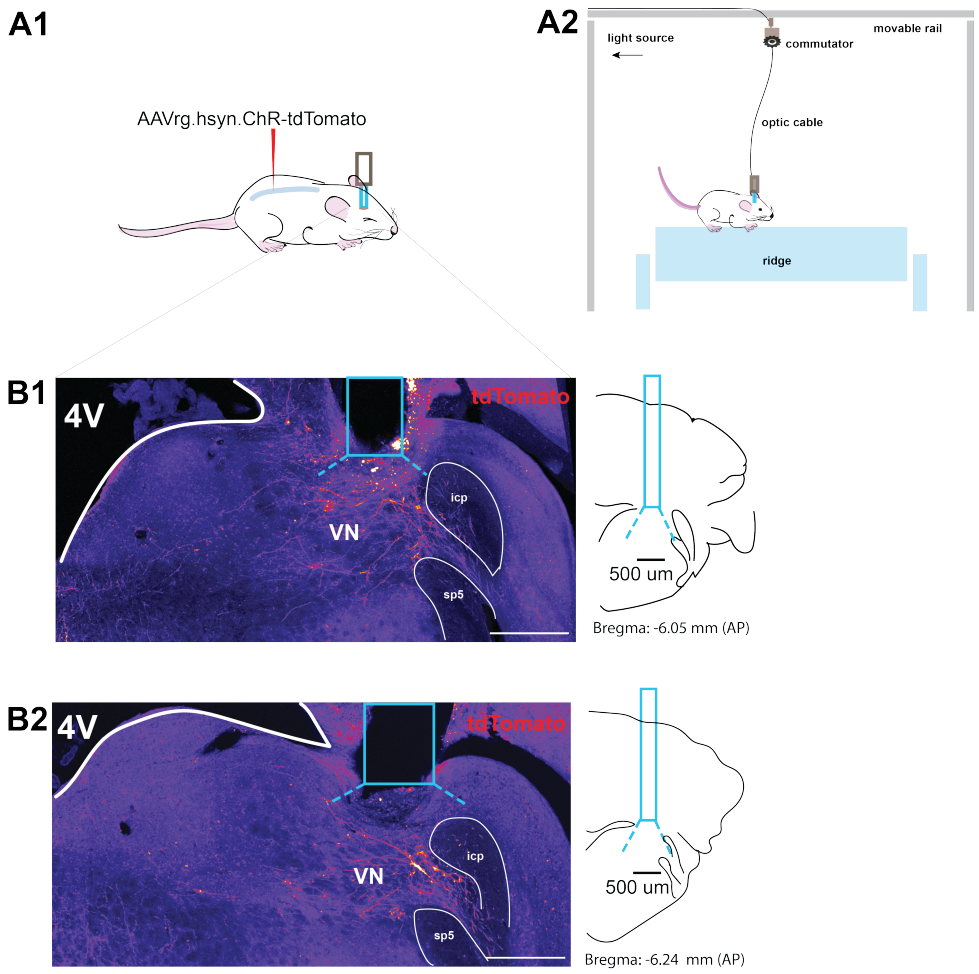

Figure 2.13: Experimental approach for selective targeting of sacral vestibulospinal neurons. Panel A1 shows diagram of surgery procedure for selective photoactivation, that is injection of retrograde ChR in the sacral spinal cord, and bilateral implantation of the optic cannula in the left and right vestibular nuclei. Panel A2 shows a diagram of the behavioral set-up. The implants are attached to the optic fiber through a ceramic sleeve, and the cable is held through a commutator onto a rail with a movable piece to allow flexible movement. In panel B the image shown the location of the implant for one example mouse and vestibular neurons labeled via the retrograde spinal cord injection with td-Tomato at level -6 Bregma (AP), and -6.20 Bregma (AP) in B1 and B2 respectively. 4V: 4th ventricle, icp: inferior cerebellar peduncle, sp5: facial nerve. Blue rectangle shows the implant placement.

The effect of sacVS photoactivation on tail movement was assessed while mice crossed the ridge. Tail movement was initially assessed by plotting the single trials time locked to photoactivation. As shown in (2.14)A the photoactivation does not have a coherent effect on tail movement (compared to the effect of the entire vestibular nucleus stimulation, as shown on the plot on the top left). However I noticed that in some instances the activation led to a tail swing during optogenetic stimulation more than during mocked trials (2.14B1-B2). This observation led me to hypothesize that the effect of the activation of this pathway is the increase in likelihood of tail swinging motion. Indeed as shown in (2.14)C1 the tail significantly produces more swing movements. Next, I was interested in testing if this activation was directional dependent (i.e. the side of the stimulation will affect the direction of the tail swing). This was tested by dividing the trials in ipsilateral (C2, tail is on the same lower quadrant as the stimulation, e.g. tail on the left and stimulation on the left vestibular nucleus) and contralateral (C3, tail on the opposite side of

the stimulation). As shown in (2.14)C2 and C3, the effect of the photoactivation on tail motion depends on whether the tail was placed in the same side of the implant where the stimulation was delivered (n=7 implants, N=4 mice, mean ± SEM).

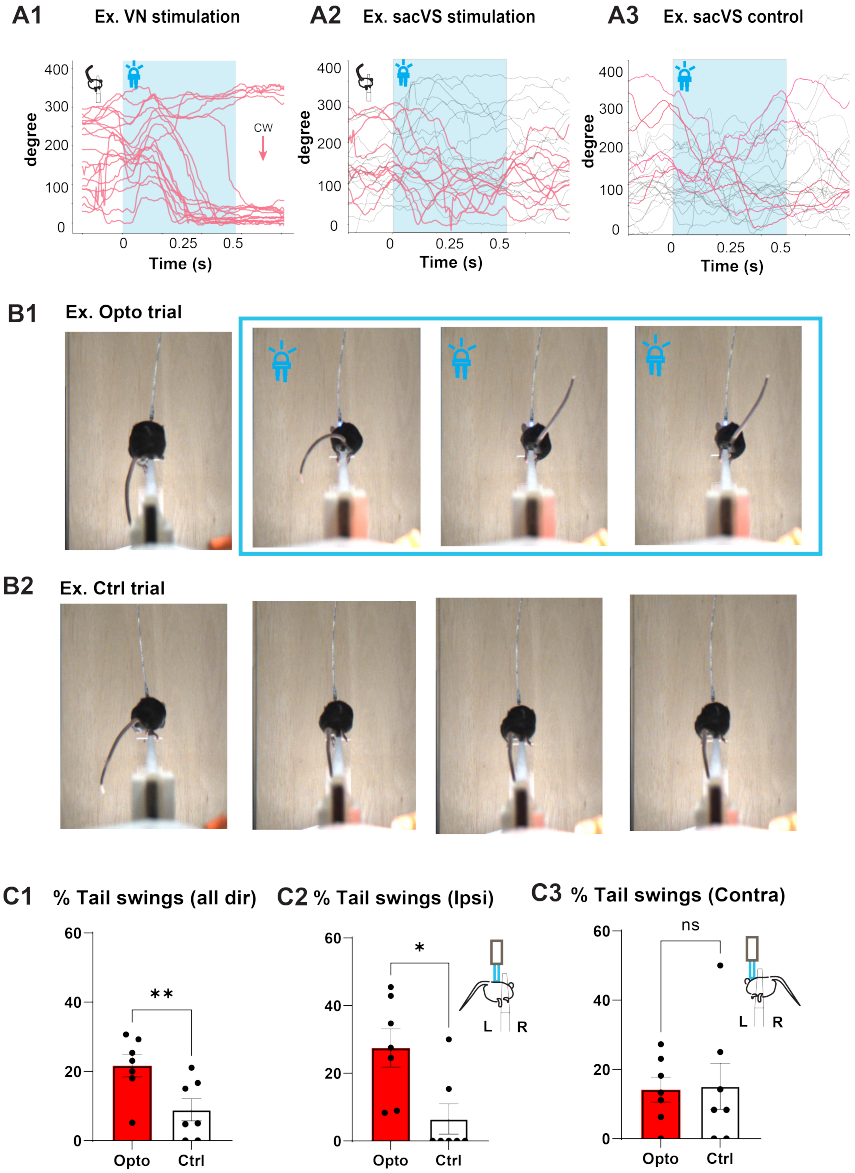

Figure 2.14: Effect of sacVS stimulation on tail swinging movement in the ridge. Comparison between time series example for one mouse showing changes in tail angle in response to photoactivation in the vestibular complex (A1), sacVS neurons (A2), and mocked trials (A3) while crossing the ridge. Panel B shows screenshots response during stimulation of the left sacVS neurons (B1) and mocked activation in the same mouse (B2). Colored rectangle indicates frames capturing the response during the optogenetic stimulation. Panel C1 shows the percentage of trials where a tail swing (regardless of the direction) occurred during the stimulation (n=7 implants, N=4 mice. Mean plus minus SEM). Panels C2-C3 show the percentage of trials where a tail swing occurred in ipsilateral trials (C2, tail on the same side of the implant being stimulated), or contra (C3, tail on the opposite side) during the stimulation (n=7 implants, N=4 mice. Mean plus minus SEM).

The effect of sacral vestibulospinal (sacVS) stimulation on the base of support (BoS) was evaluated while mice crossed the ridge and the flat surface. The averaged changes in BoS area

for each stimulation are shown with light single lines, and the overall average across all sessions is presented as a bold single line (n=7 implants, N=4 mice, mean ± SEM). Shown in figure (2.15) are the changes in the BoS while crossing the ridge during mocked trials and photoactivation (2.15A and B respectively). No effect of the activation on the BoS area is shown in either the ridge (blue) or the flat surface (orange) conditions.

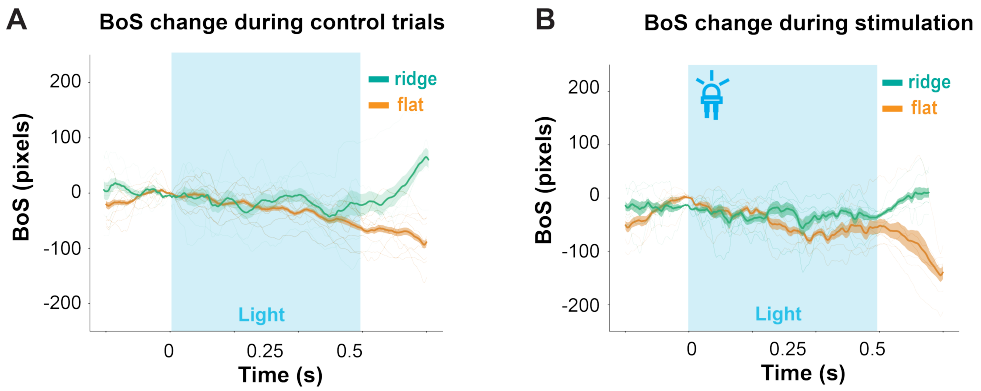

Figure 2.15: Effect of sacVS stimulation on the base of support on ridge and flat surface. Shown are the averaged changes of base of support (BoS) area for each stimulation side (light single line), and the average across all sessions (n=7 implants, N=4 mice. Mean plus minus SEM) while crossing the ridge (blue) and flat surface (orange) during mocked trials and photoactivation (A and B respectively).

2.3 Discussion

In this second chapter I described the results from the investigation of the neuro-anatomical substrate for tail control. I showed that the tail-MNs innervating the lateral extrinsic muscle form a cluster in the ventro-medial region of the S3-S4 spinal cord. Further, following the core-hypothesis of this thesis, I investigated what is the relation (if any) between the vestibular system and the spinal circuits for tail control. Indeed I showed that there is a cluster of vestibulospinal neurons located mainly in the rostral portion of SPIV. These sacVS neurons' axons branch out broadly in the ventral horn of the spinal cord (S3-S4), with the highest density of axons being located in lamina 8 and 9, where pre-motor and motor neurons are located.

Moreover in the second chapter I described the distinct and context-dependent effects of vestibular activation on tail movement, highlighting the functional specificity and adaptability of the vestibulospinal pathways. These findings demonstrate that optogenetic stimulation of the vestibular complex results in pronounced tail movements, especially during locomotion on a narrow ridge, whereas the same stimulation induces an increase in the base of support (BoS) when mice are on a flat surface. This differential response underscores the importance of the vestibular system in modulating motor outputs tailored to environmental demands and postural challenges.

2.3.1 Differential vestibular activation effect on ridge and flat surface

The results presented in this chapter show that unilateral optogenetic stimulation of the vestibular complex elicits robust, directional tail rotations during ridge locomotion. The induced movements are consistent with the hypothesis that vestibulospinal pathways play a crucial role in maintaining balance and stability by controlling tail position and movement. The observed clockwise (CW) and counterclockwise (CCW) tail rotations, dependent on the side of vestibular stimulation, suggest a finely tuned mechanism where the vestibular system communicates with tail motoneurons to counteract perturbations and maintain equilibrium on narrow surfaces. Interestingly, the absence of consistent tail movement on a flat surface suggests that the vestibular system's influence on tail dynamics is context-sensitive. The lack of directional tail responses on the flat surface implies that the vestibular-induced tail adjustments are primarily engaged during conditions requiring enhanced stability and balance, such as ridge walking. This finding aligns with previous studies indicating that tail movements are integral to postural control and stabilization during complex locomotor tasks ([34]).

In contrast to the tail's specific and directional responses, vestibular activation on a flat surface predominantly affects the hindlimbs (leading to an increase in the BoS). This response is characterized by a widening of the limb positions, which serves as a strategy to enhance stability and counterbalance the effects of vestibular perturbation. The increase in BoS area observed during flat surface locomotion is in line with the role of the vestibular system in modulating hindlimb positioning to maintain postural stability. The distinct lack of BoS alteration on the ridge further emphasizes the context-dependent nature of vestibular influences. On the ridge, where lateral space is restricted, widening the BoS is not feasible, necessitating alternative stability mechanisms, such as the observed tail movements. These differential effects underscore the versatility of vestibulospinal pathways in employing varied motor strategies based on environmental constraints.

2.3.2 Tail movement as a primer for balance control?

The differential responses of tail and whole-body to vestibular activation underscore the complexity and adaptability of vestibulospinal control mechanisms. Tail movements provide rapid and efficient postural corrections during precarious locomotion, while adjustments in hindlimb positioning offer a robust means to enhance stability on more stable surfaces. This dual strategy highlights the evolutionary advantage of having multiple, context-specific responses to vestibular signals, ensuring optimal balance and stability. The selective activation of sacVS neurons did not produce consistent directional tail movements, but it did increase the likelihood of tail swings, suggesting that these neurons provide the "vestibular context" to downstream effectors in the spinal cord. The observation that tail swings were more frequent when the tail was on the same side as the stimulation highlights the role of sacVS neurons in fine-tuning postural adjustments in specific contexts.

The lack of significant changes in BoS during sacVS stimulation on the ridge suggests that tail movements primarily serve to enhance balance in conditions where widening the BoS is not feasible. On a flat surface, however, the increased BoS area during vestibular complex stimulation indicates that tail movements complement hindlimb adjustments to maintain stability. In summary, this study demonstrates that tail movements, driven by a specialized group of tail MNs and modulated by sacVS neurons, play a crucial role in balance control. These movements act as a primer for maintaining postural stability, particularly in challenging terrains. Understanding the neural mechanisms underlying tail-mediated balance control can provide broader insights into the general principles of motor coordination and postural regulation. Ultimately, as discussed in the first chapter, defining balance as a complex skill necessitates recognizing it as an integration of multisensory responses, where the vestibular system, proprioception, and motor pathways cohesively interact to achieve stability and adapt to diverse environmental demands.

Conclusion

The presented body of research addressed the questions of how mice use their tails to maintain balance and what is the neuronal substrate of this motor program. By demonstrating the role of the tail in counteracting roll-plane perturbations and maintaining stability on a narrow surface, these findings complement the traditional focus on limb movements in balance research. Measuring tail movement could introduce a novel metric for dissecting the function of vestibular circuits in mice, potentially making the study of balance-related reflexes in rodents more accessible (as tail kinematics is possible to track using a camera). This shift in focus towards the tail's dynamic contributions not only could enhance our understanding of rodent motor control but also highlights the tail's functional versatility as both a reactive stabilizer (in response to external perturbations) and an integral part of locomotion (self-generated movements). Consequently, these insights can influence broader research into the neural and biomechanical strategies employed by other species, especially other rodents, where similar principles may apply to upper-body and limb movements during complex motor tasks.

2.3.3 Limitations

As discussed in chapter 1, the movement of the front of the body (front paws or head) was not measured extensively, so that poses some limits to the ability to capture possible whole body effect of the tail in balancing. However, using video recording of small head displacements would be challenging using cameras, and it should rather be done by using a gyroscope implant attached to their head (which might affect the overall mouse balance). Moreover, I observed that the back of the mouse shows greater changes to more challenging environments, while the front remains relatively stable. Therefore I think that the measurements focusing on the back of the body are sufficient to capture the main role of the tail in maintaining balance during the task.

The lack of an in-depth biomechanical model of the mouse limits the understanding of the interplay between passive and active components of the tail movement observed. Although the tail reflex shown here is likely attributed to active tail control, it would be possible there to be an intrinsic advantage for mice in having a tail (e.g. by lowering their COM). Based on the relative low weight of the tail compared to its massive relative length, I think that the active control of the tail could play a bigger role in affecting balance and posture.
This study only shows subtle changes in the tail swing response, despite quite large changes in the perturbation angle or ridge widths. The tail swing seems to be an all or nothing response that is triggered when the rest of the body has limitations (in terms of rotational range or maximum velocity that it can reach). This seems to suggests that the tail serves an auxiliary role in the complex balancing machinery that allows mice to stay upright.

In the result section of Chapter 2 I showed the directional effect of unilateral stimulation

of sacVS neurons on tail control in different context. These results, however, cannot rule out possible effects of collateral projections of the vestibulospinal pathway to target areas in the spinal cord other than the tail-MNs in the sacral spinal cord. In fact as shown from the anatomical results in Chapter 2 of this thesis descending pathways have several targets (including different subclasses of interneurons), hence it is unlikely that the effects observed on tail excitability originates exclusively from the direct projections to tail-MNs, also given the need to control motoneurons pools spread across several segments of the spinal cord in order to generate the tail response shown here. Characterizing all the possible downstream targets of the vestibulospinal pathway goes beyond the scope of this thesis, however it will provide useful insights to understanding how supraspinal information regarding the vestibular context is integrated by different neuronal populations in the spinal cord to produce appropriate motor responses. One possible way to understand the selective effect of vestibulospinal axons projection to tail MNs would rely on a complex experiment involving transynaptic rabies and implantation of optic cannula on the ventral horn of the spinal cord. This last surgical procedure is only recently becoming viable by the introduction of microLED probes adapted to mice spinal cord ([151]). However it has been tested only on the thoracic spinal cord (and more recently on the cervical) which are significantly larger than the sacro-coccygeal spinal cord where tail-MNs are located.

Another limitation of this research has been the lack of transynaptic experiments, due to restriction of the facilities at OIST. Such experiment would have allowed to show the projections from sacVS neurons formed active synaptic contacts to tail motoneurons (instead I was limited in referring to the observed synaptic contacts as "putative"). Moreover, by using AAV transfection for targeting vestibulospinal neurons projecting to the sacral spinal cord (both for optogenetic and anatomical studies), I could not rely on selective stimulation of tail vestibulospinal neurons (which is likely a subgroup of the population targeted in the presented optogenetic approach). However as noticed above, the number and location of the sacVS neurons seem to outline a selective clustered population of vestibular neurons.

2.3.4 Future directions

Future research should aim to build on these foundational findings by developing high-resolution models and tracking systems for mouse tail and body movements, allowing for a more detailed analysis of the forces and torques involved in balance maintenance.
In the last few decades, a lot of effort has been put into building biomechanical-accurate models of mouse hindlimbs ([152], [153]), and more recently forelimbs and digits (Eiman Azim's lab, unpublished). The most comprehensive up-to-date biomechanical model of whole-body mouse ([154]) focused indeed on modeling hindlimbs and forelimbs given the lack of availability of anatomical and functional data on other parts of the mouse body. In the present study, I reported anatomical and functional data for the tail usage, providing an ethologically relevant task in which the tail is used to maintain balance. The ridge set-up can be easily adapted to allow EMG recordings, which would help to dissect the contribution of different muscles to the generation of the tail reflex here described; similarly it would be possible to integrate piezo-electric sensor sheets on the ridge surface, which could be distributed along the platform to measure the contribution of changes in the proprioceptive environments to the different balancing strategies observed in the ridge task.
Further, hereby I presented the analogy of the tail reflex to VOR or VCR. It would be interesting in the future to study if the tail reflex can be "conditioned", that is if association to conditioning

stimuli (such as LED, or air-puff) can be used to elicit the tail reflex without the unconditioned stimulus (i.e. platform tilt), and consequently study the cerebellar contribution to such mode of learning. Most cerebellar learning studies have used the classical eye-blink conditioning, which has provided a rich set of insights on the mechanisms involved in learning. However, I think that using a more naturalistic paradigm could build on the existing knowledge and provide additional insights on how cerebellar and spinal circuitry interact during locomotion.

Moreover, in the present study I have not used any method for direct or indirect measures of neuronal activity (such as electrophisiology or calcium imaging respectively). An ingenious set-up has been recently described for zebrafish ([155]) to allow recording of calcium imaging and tail behavioral data in response to roll-perturbations. A similar idea could be adapted to the existing swing set-up described in chapter 1, and it would allow for an interesting comparison of balancing strategies and their neuronal substrates between land-based and water-based vertebrates.

Finally, investigating the potential similarities between the tail reflex described in this thesis and other vestibular-driven reflexes like the Vestibulo-Ocular and Vestibulo-Collic Reflexes could further elucidate the tail's role in balance and stability. Expanding the scope to include comparative studies across different rodent species and even other small mammals may reveal evolutionary adaptations and commonalities in balance control mechanisms. Ultimately, integrating these findings with broader research on motor coordination and postural regulation could lead to new therapeutic approaches for balance disorders in humans, leveraging the principles of compensatory angular momentum and context-specific motor strategies observed in mice.

Bibliography

[1] B Horak F. Postural orientation and equilibrium : what do we need to know about neural control of balance to prevent falls ? *Age Aging*, pages 7–11, 2006.

[2] Jong Hyun Park, Youn Joo Kang, and Fay B Horak. What is wrong with balance in parkinson's disease? *J Mov Disord*, 8(3):109–114, Sep 2015.

[3] Kathleen E Cullen and Omid A Zobeiri. Proprioception and the predictive sensing of active self-motion. *Current opinion in physiology*, 20:29–38, 2021.

[4] Brian E Maki and William E McIlroy. The role of limb movements in maintaining upright stance: the "change-in-support" strategy. *Physical therapy*, 77(5):488–507, 1997.

[5] Kim J Boström, Tim Dirksen, Karen Zentgraf, and Heiko Wagner. The contribution of upper body movements to dynamic balance regulation during challenged locomotion. *Frontiers in human neuroscience*, 12:8, 2018.

[6] Keli Shen, Ahmed Chemori, and Mitsuhiro Hayashibe. Reproducing human arm strategy and its contribution to balance recovery through model predictive control. *Frontiers in neurorobotics*, 15:679570, 2021.

[7] Stacey Shield, Ricardo Jericevich, Amir Patel, and Ardian Jusufi. Tails, flails, and sails: How appendages improve terrestrial maneuverability by improving stability. *Integrative and comparative biology*, 61(2):506–520, 2021.

[8] Anne Shumway-Cook and Marjorie H Woollacott. *Motor control: translating research into clinical practice*. Lippincott Williams Wilkins, 2007.

[9] J. L. McKay, T. J. Burkholder, and L. H. Ting. Biomechanical capabilities influence postural control strategies in the cat hindlimb. *Journal of biomechanics*, 40(10):2254–2260, 2007.

[10] M. Moriyama, M. Kouzaki, and S. Hagio. Anticipatory postural control in adaptation of goal-directed lower extremity movements. *Sci Rep*, 14(1):4142, Feb 2024.

[11] N. K. Zhang, S. K. Zhang, L. I. Zhang, H. W. Tao, and G. W. Zhang. Sensory processing deficits and related cortical pathological changes in alzheimer's disease. *Front Aging Neurosci*, 15:1213379, Aug 2023.

[12] J. Lackner and P. DiZio. Human orientation and movement control in weightless and artificial gravity environments. *Exp Brain Res*, 130:2–26, 2000.

[13] L. Borel, C. Redon-Zouiteni, P. Cauvin, M. Dumitrescu, A. Devèze, J. Magnan, and P. Péruch. Unilateral vestibular loss impairs external space representation. *PLoS One*, 9(2):e88576, 2014.

[14] L. Valizadeh, R. Mofateh, S. Zahednejad, R. Salehi, M. Karimi, and M. Mehravar. Walking performance during concurrent cognitive and motor tasks in individuals with nonspecific chronic low back pain: A case-control study. *Med J Islam Repub Iran*, 37:81, Jul 2023.

[15] H. Fujita, K. Kasubuchi, S. Wakata, M. Hiyamizu, and S. Morioka. Role of the frontal cortex in standing postural sway tasks while dual-tasking: A functional near-infrared spectroscopy study examining working memory capacity. *Biomed Res Int*, 2016:7053867, 2016.

[16] M. J. Schwaner, S. T. Hsieh, I. Braasch, S. Bradley, C. B. Campos, C. E. Collins, C. M. Donatelli, F. E. Fish, O. E. Fitch, B. E. Flammang, B. E. Jackson, A. Jusufi, P. J. Mekdara, A. Patel, B. J. Swalla, M. Vickaryous, and C. P. McGowan. Future tail tales: A forward-looking, integrative perspective on tail research. *Integrative and Comparative Biology*, 61:521–537, August 2021.

[17] Lauren Sallan. Fish 'tails' result from outgrowth and reduction of two separate ancestral tails. *Current Biology*, 26:R1224–R1225, 2016.

[18] G. C. Hickman. The mammalian tail: a review of functions. *Mammal Review*, 9(4):143–157, 1979.

[19] E.P. Kingsley, E.R. Hager, J.M. Lassance, et al. Adaptive tail-length evolution in deer mice is associated with differential hoxd13 expression in early development. *Nature Ecology & Evolution*, 8:791–805, 2024.

[20] B. Xia, W. Zhang, G. Zhao, X. Zhang, J. Bai, R. Brosh, A. Wudzinska, E. Huang, H. Ashe, G. Ellis, M. Pour, Y. Zhao, C. Coelho, Y. Zhu, A. Miller, J. S. Dasen, M. T. Maurano, S. Y. Kim, J. D. Boeke, and I. Yanai. On the genetic basis of tail-loss evolution in humans and apes. *Nature*, 626(8001):1042–1048, 2024.

[21] Sarah T. Mincer and Gabrielle A. Russo. Substrate use drives the macroevolution of mammalian tail length diversity. *Proceedings of the Royal Society B: Biological Sciences*, 287, February 05 2020.

[22] George A Bartholomew and Herbert H Caswell. American society of mammalogists locomotion in kangaroo rats and its adaptive significance published by : American society of mammalogists. 32(2):155–169, 2019.

[23] M.J. Schwaner, G.A. Freymiller, R.W. Clark, and C.P. McGowan. How to stick the landing: Kangaroo rats use their tails to reorient during evasive jumps away from predators. *Integrative and Comparative Biology*, 61(2):442–454, Sep 2021.

[24] B. E. Horner. *Arboreal adaptations of Peromyscus, with special reference to the use of the tail*. PhD thesis, University of Michigan, 1948.

[25] Emily R Hager and Hopi E Hoekstra. Tail length evolution in deer mice: linking morphology, behavior, and function. *Integrative and Comparative Biology*, 61(2):385–397, 2021.

[26] H Shinohara. The Musculature of the Mouse Tail is Characterized by Metameric Arrarmements of Bicipital Muscles. *Okajimas Folia Anat. Jpn.*, 76(0167):157–169, 1999.

[27] Vojtěch Škop, Naili Liu, Juen Guo, Oksana Gavrilova, and Marc L Reitman. The contribution of the mouse tail to thermoregulation is modest. *American Journal of Physiology-Endocrinology and Metabolism*, 319(2):E438–E446, 2020.

[28] R. John. Genetic analysis of tail rattling in the mouse. *Nature*, 241:549–551, 1973.

[29] C W Buck, N Tolman, and W Tolman. The tail as a balancing organ in mice. *American Society of Mammalogists*, 6, 1925.

[30] Ana S Machado, Dana M Darmohray, João Fayad, Hugo G Marques, and Megan R Carey. A quantitative framework for whole-body coordination reveals specific deficits in freely walking ataxic mice. *eLife*, 4:e07892, oct 2015.

[31] Salvatore Andrea Lacava, Necmettin Isilak, and Marylka Yoe Uusisaari. Mice tails function in response to external and self-generated balance perturbation on the roll plane. *bioRxiv*, April 2024. Preprint. Available at: `https://doi.org/10.1101/2024.04.18.589832`.

[32] Yoonsun Yang, Joonyeol Lee, and Gunsoo Kim. Integration of locomotion and auditory signals in the mouse inferior colliculus. *Elife*, 9:e52228, 2020.

[33] Jesse V Jacobs and FB4382099 Horak. Cortical control of postural responses. *Journal of neural transmission*, 114:1339–1348, 2007.

[34] Andrew J Murray, Katherine Croce, Timothy Belton, Turgay Akay, and Thomas M Jessell. Balance control mediated by vestibular circuits directing limb extension or antagonist muscle co-activation. *Cell reports*, 22(5):1325–1338, 2018.

[35] Andrew A. Biewener and Sheila N. Patek. *Animal Locomotion*. Oxford University Press, illustrated edition, 2018.

[36] J. Borrell, J. M. Vela, A. Arévalo-Martin, E. Molina-Holgado, and C. Guaza. Prenatal immune challenge disrupts sensorimotor gating in adult rats: implications for the etiopathogenesis of schizophrenia. *Neuropsychopharmacology*, 26(2):204–215, 2002.

[37] Lindsay Bergdolt and Anna Dunaevsky. Brain changes in a maternal immune activation model of neurodevelopmental brain disorders. *Progress in Neurobiology*, 175:1–19, 2019.

[38] A. Cougnoux, M. Fellmeth, T. Gu, C. D. Davidson, A. L. Gibson, W. J. Pavan, and F. D. Porter. Maternal immune activation modifies the course of niemann-pick disease, type c1 in a gender specific manner. *Molecular Genetics and Metabolism*, 129(2):165–170, Feb 2020. Epub 2019 Oct 17.

[39] Andrew R. Lammers and Timothy Gauntner. Mechanics of torque generation during quadrupedal arboreal locomotion. *Journal of Biomechanics*, 41(11):2388–2395, 2008.

[40] Ana S Machado, Dana M Darmohray, Joao Fayad, Hugo G Marques, and Megan R Carey. A quantitative framework for whole-body coordination reveals specific deficits in freely walking ataxic mice. *elife*, 4:e07892, 2015.

[41] Curt Walker, Charles J Vierck Jr, and Louis A Ritz. Balance in the cat: role of the tail and effects of sacrocaudal transection. *Behavioural brain research*, 91(1-2):41–47, 1998.

[42] C. Walker, C. J. Vierck, and L. A. Ritz. Balance in the cat: role of the tail and effects of sacrocaudal transection. *Behavioural Brain Research*, 91(1-2):41–47, 1998.

[43] Andrew J Murray, Katherine Croce, Timothy Belton, Turgay Akay, and Thomas M Jessell. Balance control mediated by vestibular circuits directing limb extension or antagonist muscle co-activation. *Cell reports*, 22(5):1325–1338, 2018.

[44] Lucas Wahl, Fabian MP Kaiser, Mieke F Bentvelzen, Joshua J White, Martijn Schonewille, and Aleksandra Badura. Detecting ataxia using automated analysis of motor coordination and balance of mice on the balance beam. *bioRxiv*, pages 2023–07, 2023.

[45] EM Latash, WH Barnett, H Park, JM Rider, AN Klishko, BI Prilutsky, and YI Molkov. Frontal plane dynamics of the centre of mass during quadrupedal locomotion on a split-belt treadmill. *Journal of the Royal Society Interface*, 17(170):20200547, 2020.

[46] C.S. Sherrington. *Integrative Actions of the Nervous System*. Yale University Press, New Haven, CT, 1906.

[47] T. Graham-Brown. The intrinsic factors in the act of progression in the mammal. *Proceedings of the Royal Society of London*, 84:308–319, 1912.

[48] AC Kwan, SB Dietz, WW Webb, and RM Harris-Warrick. Activity of hb9 interneurons during fictive locomotion in mouse spinal cord. *Journal of Neuroscience*, 29(37):11601–11613, Sep 16 2009.

[49] TM Anderson, MD Abbinanti, JH Peck, M Gilmour, RM Brownstone, and MA Masino. Low-threshold calcium currents contribute to locomotor-like activity in neonatal mice. *Journal of Neurophysiology*, 107(1):103–113, Jan 2012. Epub 2011 Oct 12.

[50] J.-R. Cazalets, S. Bertrand, Y. Sqalli-Houssaini, and F. Clarac. Gabaergic control of spinal locomotor networks in the neonatal rat. *Annals of the New York Academy of Sciences*, 860:168–180, 1998.

[51] Keith T. Sillar. The development of central pattern generators for vertebrate locomotion. In María A. Pastor and Julio Artieda, editors, *Advances in Psychology*, volume 115, pages 205–221. North-Holland, 1996.

[52] C.A.G. Wiersma and K. Ikeda. Interneurons commanding swimmeret movements in the crayfish, *Procambarus clarki* (girard). *Comparative Biochemistry and Physiology*, 12(4):509–525, 1964.

[53] Ole Kiehn and Simon J.B. Butt. Physiological, anatomical and genetic identification of cpg neurons in the developing mammalian spinal cord. *Progress in Neurobiology*, 70(4):347–361, Jul 2003.

[54] Martin Hägglund, Kimberly J. Dougherty, Lotta Borgius, and Ole Kiehn. Optogenetic dissection reveals multiple rhythmogenic modules underlying locomotion. *Proceedings of the National Academy of Sciences*, 110(28):11589–11594, June 24 2013. Edited* by Sten Grillner, Karolinska Institutet, Stockholm, Sweden, and approved May 21, 2013 (received for review March 8, 2013).

[55] Sten Grillner and Thomas M. Jessell. Measured motion: searching for simplicity in spinal locomotor networks. *Current Opinion in Neurobiology*, 19(6):572–586, Dec 2009. Epub 2009 Nov 10.

[56] Robert M. Brownstone and J. Michael Wilson. Strategies for delineating spinal locomotor rhythm-generating networks and the possible role of hb9 interneurones in rhythmogenesis. *Brain Research Reviews*, 57(1):64–76, Jan 2008. Epub 2007 Aug 14.

[57] Sten Grillner, Tatiana Deliagina, Örjan Ekeberg, Abdeljabbar el Manira, Ronald H. Hill, Anders Lansner, Grigori N. Orlovsky, and Peter Wallén. Neural networks that co-ordinate locomotion and body orientation in lamprey. *Trends in Neurosciences*, 18(6):270–279, Jun 1995.

[58] Anders Lansner, Jeanette H. Kotaleski, and Sten Grillner. Modeling of the spinal neuronal circuitry underlying locomotion in a lower vertebrate. *Annals of the New York Academy of Sciences*, 860:239–249, 1998.

[59] Eve Marder and Dirk Bucher. Central pattern generators and the control of rhythmic movements. *Current Biology*, 11(23):R986–R996, 2001.

[60] I. A. Rybak, K. J. Dougherty, and N. A. Shevtsova. Organization of the mammalian locomotor cpg: Review of computational model and circuit architectures based on genetically identified spinal interneurons. *eNeuro*, 2(5):ENEURO.0069–15.2015, 2015.

[61] David A. McCrea and Ilya A. Rybak. Modeling the mammalian locomotor cpg: insights from mistakes and perturbations. *Progress in Brain Research*, 165:235–253, 2007.

[62] Thomas M. Jessell. Neuronal specification in the spinal cord: inductive signals and transcriptional codes. *Nature Reviews Genetics*, 1(1):20–29, Oct 2000.

[63] Marco Tripodi, Anna E. Stepien, and Silvia Arber. Motor antagonism exposed by spatial segregation and timing of neurogenesis. *Nature*, 479(7371):61–66, Oct 19 2011.

[64] Martyn Goulding and Samuel L. Pfaff. Development of circuits that generate simple rhythmic behaviors in vertebrates. *Current Opinion in Neurobiology*, 15(1):14–20, Feb 2005.

[65] Nicholas P. Pringle, Wai-Ping Yu, Sarah Guthrie, Henk Roelink, Andrew Lumsden, Alan C. Peterson, and William D. Richardson. Determination of neuroepithelial cell fate: induction of the oligodendrocyte lineage by ventral midline cells and sonic hedgehog. *Developmental Biology*, 177(1):30–42, Jul 10 1996.

[66] Joseph Altman and Shirley A. Bayer. Development of the brain stem in the rat. iii. thymidine-radiographic study of the time of origin of neurons of the vestibular and auditory nuclei of the upper medulla. *Journal of Comparative Neurology*, 194(4):877–904, Dec 15 1980.

[67] Konstantinos Ampatzis, Jie Song, Jessica Ausborn, and Abdeljabbar El Manira. Separate microcircuit modules of distinct v2a interneurons and motoneurons control the speed of locomotion. *Neuron*, 83(4):934–943, Aug 20 2014.

[68] Kimberly J. Dougherty and Ole Kiehn. Functional organization of v2a-related locomotor circuits in the rodent spinal cord. *Annals of the New York Academy of Sciences*, 1198:85–93, Jun 2010.

[69] Eric R. Kandel, James H. Schwartz, Thomas M. Jessell, Steven A. Siegelbaum, and A. James Hudspeth. *Principles of Neural Science*. McGraw-Hill, Health Professions Division, 4th edition, 2000.

[70] Håkan Olausson, Yves Lamarre, Hans Backlund, and et al. Unmyelinated tactile afferents signal touch and project to insular cortex. *Nat Neurosci*, 5:900–904, 2002.

[71] Akihiko Ikoma, Martin Steinhoff, Sonja Ständer, Gil Yosipovitch, and Martin Schmelz. The neurobiology of itch. *Nature reviews. Neuroscience*, 7(7):535–547, 2006.

[72] Allan I Basbaum, Diana M Bautista, Gregory Scherrer, and David Julius. Cellular and molecular mechanisms of pain. *Cell*, 139(2):267–284, 2009.

[73] Y. Lu and E. R. Perl. A specific inhibitory pathway between substantia gelatinosa neurons receiving direct c-fiber input. *The Journal of neuroscience : the official journal of the Society for Neuroscience*, 23(25):8752–8758, 2003.

[74] Tomonori Takazawa and Amy B MacDermott. Synaptic pathways and inhibitory gates in the spinal cord dorsal horn. *Annals of the New York Academy of Sciences*, 1198:153–158, 2010.

[75] G. F. Gebhart. Descending modulation of pain. *Neuroscience and biobehavioral reviews*, 27(8):729–737, 2004.

[76] Ke Ren and Ronald Dubner. Interactions between the immune and nervous systems in pain. *Nature medicine*, 16(11):1267–1276, 2010.

[77] Michael H Ossipov and G. F. Gebhart. Opioid, cholinergic and alpha-adrenergic influences on the modulation of nociception from the lateral reticular nucleus of the rat. *Brain research*, 384(2):282–293, 1986.

[78] Frank Porreca, Michael H Ossipov, and G. F. Gebhart. Chronic pain and medullary descending facilitation. *Trends in neurosciences*, 25(6):319–325, 2002.

[79] Angela Sweeney, Brett Filson, Angela Kennedy, Lara Collinson, and Steven Gillard. A paradigm shift: relationships in trauma-informed mental health services. *BJPsych Advances*, 24(5):319–333, 2018.

[80] E Rebecka Björnfors and Abdeljabbar El Manira. Functional diversity of excitatory commissural interneurons in adult zebrafish. *eLife*, 5:e18579, 2016.

[81] Meng-Yang Wu, Martin Carbo-Tano, Oriane Mirat, François-Xavier Lejeune, Jérémie Roussel, Fang-Bao Quan, Kevin Fidelin, and Claire Wyart. Spinal sensory neurons project onto the hindbrain to stabilize posture and enhance locomotor speed. *Current Biology*, 31(15):3315–3329.e5, 2021.

[82] Ludwig Ruder, Aya Takeoka, and Silvia Arber. Long-distance descending spinal neurons ensure quadrupedal locomotor stability. *Neuron*, 92(5):1063–1078, 2016.

[83] Andrew M Pocratsky, Catherine T Shepard, Justin R Morehouse, David A Burke, Amanda S Riegler, Jared T Hardin, Joseph E Beare, Crystal Hainline, Gregory J States, Bradley L Brown, Scott R Whittemore, and David S Magnuson. Long ascending propriospinal neurons provide flexible, context-specific control of interlimb coordination. *eLife*, 9:e53565, 2020.

[84] Charles Watson and Mark Harrison. The location of the major ascending and descending spinal cord tracts in all spinal cord segments in the mouse: actual and extrapolated. *Anat Rec (Hoboken)*, 295(10):1692–1697, 2012.

[85] Masahiro Matsushita and Hiroshi Yaginuma. Spinocerebellar projections from spinal border cells in the cat as studied by anterograde transport of wheat germ agglutinin-horseradish peroxidase. *Journal of Comparative Neurology*, 288(1):19–38, 1989.

[86] Gulgun Sengul and Charles Watson. Chapter 8 - ascending and descending pathways in the spinal cord. pages 115–130, 2015.

[87] Dario Masini and Ole Kiehn. Targeted activation of midbrain neurons restores locomotor function in mouse models of parkinsonism. *Nature Communications*, 13:504, 2022.

[88] Clara I van der Zouwen, Justine Boutin, Maxime Fougère, Anthony Flaive, Miguel Vivancos, Alessandro Santuz, Turgay Akay, Philippe Sarret, and Dmitri Ryczko. Freely behaving mice can brake and turn during optogenetic stimulation of the mesencephalic locomotor region. *Frontiers in Neural Circuits*, 15:639900, 2021.

[89] Jacob M Cregg, Sundeep K Sidhu, Roberto Leiras, et al. Basal ganglia–spinal cord pathway that commands locomotor gait asymmetries in mice. *Nature Neuroscience*, 27:716–727, 2024.

[90] Emily C Witts and Andrew J Murray. Vestibulospinal contributions to mammalian locomotion. *Current Opinion in Physiology*, 8:56–62, 2019.

[91] Jay M Goldberg, Victor J Wilson, Kathleen E Cullen, Dora E Angelaki, Darrin M Broussard, Jean Buttner-Ennever, Kikuro Fukushima, and Lloyd B Minor. *The Vestibular System: A Sixth Sense*. Oxford University Press, 2012.

[92] Kathleen E Cullen and J M Goldberg. Vestibular control of the head: possible functions of the vestibulocollic reflex. *Exp Brain Res*, 210(0):331–345, 2011.

[93] J Maurer, T Frommeld, and W Mann. Vestibular function after acoustic neuroma removal with preservation of one branch of the vestibular nerve. *Otology & neurotology : official publication of the American Otological Society, American Neurotology Society [and] European Academy of Otology and Neurotology*, 23(5):749–754, 2002.

[94] Robert J Peterka, Kevin D Statler, Diane M Wrisley, and Fay B Horak. Postural compensation for unilateral vestibular loss. *Front Neurol*, 2:57, 2011.

[95] Jessica X. Brooks and Kathleen E. Cullen. Predictive sensing: The role of motor signals in sensory processing. *Biological Psychiatry: Cognitive Neuroscience and Neuroimaging*, 4(9):842 – 850, 2019. Corollary Discharge: Circuits to Psychosis.

[96] Hans Straka, Andreas Zwergal, and Kathleen E Cullen. Vestibular animal models: contributions to understanding physiology and disease. *Journal of neurology*, 263(Suppl 1):S10–23, Apr 2016.

[97] Albert Erives, Dan Eber, Ebenezer Yamoah, and Bernd Fritzsch. The senses: A comprehensive reference. 01 2021.

[98] Ioana Medrea and Kathleen E. Cullen. Multisensory integration in early vestibular processing in mice: the encoding of passive vs. active motion. *Journal of Neurophysiology*, 110(12):2704–2717, 2013. PMID: 24089394.

[99] I. M. Stitt, T. P. Wellings, H. R. Drury, P. Jobling, R. J. Callister, A. M. Brichta, and R. Lim. Properties of deiters' neurons and inhibitory synaptic transmission in the mouse lateral vestibular nucleus. *Journal of Neurophysiology*, 128(1):131–147, 2022.

[100] Neil H Barmack. Central vestibular system: vestibular nuclei and posterior cerebellum. *Brain research bulletin*, 60(5-6):511–541, 2003.

[101] Tatiana G Deliagina, Pavel V Zelenin, Patrik Fagerstedt, Sten Grillner, and Grigori N Orlovsky. Activity of reticulospinal neurons during locomotion in the freely behaving lamprey. *Journal of neurophysiology*, 83(2):853–863, 2000.

[102] Mark M Walton, Bettina Bechara, and Neeraj J Gandhi. Role of the primate superior colliculus in the control of head movements. *Journal of neurophysiology*, 98(4):2022–2037, 2007.

[103] Stephen Thankachan, Patrick M Fuller, and Jun Lu. Movement- and behavioral state-dependent activity of pontine reticulospinal neurons. *Neuroscience*, 221:125–139, 2012.

[104] Jay Goldberg, V.J. Wilson, K.E. Cullen, D.E. Angelaki, D.M. Broussard, J. Buttner-Ennever, K. Fukushima, and L.B. Minor. The vestibular system: A sixth sense. *Oxford University Press.*, pages 1–560, 01 2012.

[105] R. Nyberg-Hansen and T.A. Mascitti. Sites and mode of termination of fibers of the vestibulospinal tract in the cat. An experimental study with silver impregnation methods. *The journal of comparative neurology*, 1964.

[106] S. Grillner and T. Hongo. Vestibulospinal effects on motoneurones and interneurones in the lumbosacral cord. *Progress in Brain Research*, 37:243 – 262, 1972.

[107] V J Wilson and M Maeda. Connections between semicircular canals and neck motorneurons in the cat. *Journal of Neurophysiology*, 37(2):346–357, 1974. PMID: 4815209.

[108] G. Bilotto, J. Goldberg, B.W. Peterson, and V.J. Wilson. Dynamic properties of vestibular reflexes in the decerebrate cat. *Exp Brain Research*, 37:243 – 262, 1982.

[109] V.J. Wilson, K. Ezure, and S.G.B. Timerick. Tonic neck reflex of the decerebrate cat: response of spinal interneurons to natural stimulation of neck and vestibular receptors. *J. Neurophysiology*, 1984.

[110] KW. Lindsay, TDM. Roberts, and JR. Rosenberg. Asymmetrical tonic labyrinth reflexes and their interactionwith neck reflexes in the decerebrate cat. *J. Physiology*, 37:243 – 262, 1976.

[111] B. Alstermark, A. Lundberg, U. Norrsell, and E. Sybirska. Integration in descending motor pathways controlling the forelimb in the cat. 9. differential behavioural defects after spinal cord lesions interrupting defined pathways from higher centres to motoneurones. *Exp. Brain Research*, 37:243 – 262, 1981.

[112] Fausto Baldissera, Hans Hultborn, and Michael Illert. Integration in spinal neuronal systems. *The Nervous System*, 1, 01 2011.

[113] P Cavallari, S A Edgley, and E Jankowska. Post-synaptic actions of midlumbar interneurones on motoneurones of hind-limb muscles in the cat. *The Journal of Physiology*, 389(1):675–689, 1987.

[114] T. Hongo, N. Kuda, and R. Tanaka. The vestibulospinal tract: crossed and uncrossed effects on hindlimb motoneurons in the cat. *Exp Brain Research*, 37:243 – 262, 1975.

[115] Piotr Krutki, Elzbieta Jankowska, and Stephen A. Edgley. Are crossed actions of reticulospinal and vestibulospinal neurons on feline motoneurons mediated by the same or separate commissural neurons? *Journal of Neuroscience*, 23(22):8041–8050, 2003.

[116] S. Grillner. Supraspinal and segmental control of static and dynamic gamma-motoneurones in the cat. *Acta Physiol Scand Suppl.*, 37:243 – 262, 1969.

[117] O. Pompeiano, P.Wand, and UC. Srivastava UC. Responses of renshaw cells coupled with hindlimb extensor motoneurons to sinusoidal stimulation of labyrinth receptors in the decerebrate cat. *Pflügers Arch*, 37:243 – 262, 1985.

[118] Ross HG and M. Thewissen. Inhibitory connections of ipsilateral semicircular canal afferents onto renshaw cells in the lumbar spinal cord of the cat. *J physiology*, 37:243 – 262, 1987.

[119] P. S. Bolton, T. Goto, R. H. Schor, V. J. Wilson, Y. Yamagata, and B. J. Yates. Response of pontomedullary reticulospinal neurons to vestibular stimuli in vertical planes. role in vertical vestibulospinal reflexes of the decerebrate cat. *Journal of Neurophysiology*, 67(3):639–647, 1992. PMID: 1578249.

[120] Kiyoji Matsuyama and Trevor Drew. Vestibulospinal and reticulospinal neuronal activity during locomotion in the intact cat. i. walking on a level surface. *Journal of Neurophysiology*, 84(5):2237–2256, 2000. PMID: 11067969.

[121] R. Nyberg-Hansen and T.A. Mascitti. Functional organization of descending supraspinal fibre systems to the spinal cord. Anatomical observations and physiological correlations. *Ergeb Anat Entwicklungsgesch*, 1964.

[122] B W Peterson, K Fukushima, N Hirai, R H Schor, and V J Wilson. Responses of vestibulospinal and reticulospinal neurons to sinusoidal vestibular stimulation. *Journal of Neurophysiology*, 43(5):1236–1250, 1980. PMID: 7373364.

[123] Kiyoji Matsuyama, Futoshi Mori, Katsumi Nakajima, Trevor Drew, Mamoru Aoki, and Shigemi Mori. Locomotor role of the corticoreticular–reticulospinal–spinal interneuronal system. *Brain Mechanisms for the Integration of Posture and Movement*, 143:239 – 249, 2004.

[124] Roongtam Ladpli and Alf Brodal. Experimental studies of commissural and reticular formation projections from the vestibular nuclei in the cat. *Brain Research*, 8(1):65 – 96, 1968.

[125] B.W. Peterson, R.A. Maunz, N.G. Pitts, and R.G. Mackel. Patterns of projection and branching of reticulospinal neurons. *Exp. Brain Res.*, 143:239 – 249, 1981.

[126] Victor J. Wilson and Barry W. Peterson. Vestibulospinal and reticulospinal systems. *Comprehensive Physiology*, pages 667–702, 2011.

[127] H. Von Holst. Relations between the central nervous system and the peripheral organs. *Br J Anim Behav*, 22(11):RC226–RC226, 1954.

[128] T. Hongo, N. Kudo, and R. Tanaka. Effects from the vestibulospinal tract on the contralateral hindlimb motoneurones in the cat. *Brain Research*, 37:243 – 262, 1971.

[129] Andrew A. McCall, Derek M. Miller, William M. DeMayo, George H. Bourdages, and Bill J. Yates. Vestibular nucleus neurons respond to hindlimb movement in the conscious cat. *Journal of Neurophysiology*, 116(4):1785–1794, 2016. PMID: 27440244.

[130] G.T. Gdowski, R. Boyle, and R.A. McCrea. Vestibular nucleus neurons respond to hindlimb movement in the conscious cat. *Arch Ital Biol*, 116(4):1785–1794, 2000. PMID: 27440244.

[131] Jefferson E. Roy and Kathleen E. Cullen. Selective processing of vestibular reafference during self-generated head motion. *Journal of Neuroscience*, 21(6):2131–2142, 2001.

[132] Milad S. Arshian, Candace E. Hobson, Michael F. Catanzaro, Daniel J. Miller, Sonya R. Puterbaugh, Lucy A. Cotter, Bill J. Yates, and Andrew A. McCall. Vestibular nucleus neurons respond to hindlimb movement in the decerebrate cat. *Journal of Neurophysiology*, 111(12):2423–2432, 2014. PMID: 24671527.

[133] B. J. Jian, T. Shintani, B. A. Emanuel, and B. J. Yates. Convergence of limb, visceral, and vertical semicircular canal or otolith inputs onto vestibular nucleus neurons. *Experimental Brain Research*, 144(2):247–257, May 2002.

[134] Stephanie Muise, Chris Lam, and Leah Bent. Reduced input from foot sole skin through cooling differentially modulates the short latency and medium latency vestibular reflex responses to galvanic vestibular stimulation. *Experimental brain research. Experimentelle Hirnforschung. Expérimentation cérébrale*, 218:63–71, 01 2012.

[135] Yu I Arshavsky, I M Gelfand, G N Orlovsky, and G A Pavlova. Messages conveyed by descending tracts during scratching in the cat. i. activity of vestibulospinal neurons. *Brain Research*, 159(1):99–110, 1978.

[136] Aasef G Shaikh, Hui Meng, and Dora E Angelaki. Multiple reference frames for motion in the primate cerebellum. *J Neurosci*, 24(19):4491–4497, 2004.

[137] Richard Mackel and Emi Miyashita. Dorsal column input to thalamic vl neurons: an intracellular study in the cat. *Exp Brain Res*, 88:551–559, 1992.

[138] Vlastislav Bracha, Frederick P Kolb, Keith B Irwin, and James R Bloedel. Inactivation of interposed nuclei in the cat: classically conditioned withdrawal reflexes, voluntary limb movements and the action primitive hypothesis. *Experimental brain research*, 126(1):77–92, 1999.

[139] Michael C Chubb and Albert F Fuchs. Contribution of y group of vestibular nuclei and dentate nucleus of cerebellum to generation of vertical smooth eye movements. *Journal of neurophysiology*, 48(1):75–99, 1982.

[140] JL Lanciego and FG Wouterlood. A half century of experimental neuroanatomical tracing. *Journal of chemical neuroanatomy*, 42(3):157–183, 2011.

[141] Jonathan J. Nassi, Constance L. Cepko, Richard T. Born, and Kevin T. Beier. Neuroanatomy goes viral! *Frontiers in Neuroanatomy*, 9, 2015.

[142] Floris G Wouterlood, Bart Bloem, Huibert D Mansvelder, Antonio Luchicchi, and Karl Deisseroth. A fourth generation of neuroanatomical tracing techniques: exploiting the offspring of genetic engineering. *Journal of neuroscience methods*, 235:331–348, 2014.

[143] Jing Li, Tong Liu, Yuhui Dong, Kunio Kondoh, and Zhongming Lu. Trans-synaptic neural circuit-tracing with neurotropic viruses. *Neurosci Bull*, 35(5):909–920, 2019. Epub 2019 Apr 19.

[144] Giorgio Ugolini. Rabies virus as a transneuronal tracer of neuronal connections. *Advances in virus research*, 79:165–202, 2011.

[145] Cheng Xu, Sabrina Krabbe, Jan Gründemann, Paolo Botta, Jacob P Fadok, Fumitaka Osakada, Dorothee Saur, Benjamin F Grewe, Mark J Schnitzer, Edward M Callaway, and Andreas Lüthi. Distinct hippocampal pathways mediate dissociable roles of context in memory retrieval. *Cell*, 167(4):961–972.e16, 2016.

[146] Elena Ciabatti, Ana González-Rueda, Letizia Mariotti, Francesca Morgese, and Marco Tripodi. Life-long genetic and functional access to neural circuits using self-inactivating rabies virus. *Cell*, 170(2):382–392.e14, 2017.

[147] Daniel G Tervo, Betty Y Hwang, Shivakumar Viswanathan, Thomas Gaj, Mikhail Lavzin, Kimmo D Ritola, Santiago Lindo, Sally Michael, Elena Kuleshova, Dana Ojala, Chinfei C Huang, Charles R Gerfen, Jennifer Schiller, Joshua T Dudman, Adam W Hantman, Loren L Looger, David V Schaffer, and Anna Y Karpova. A designer aav variant permits efficient retrograde access to projection neurons. *Neuron*, 92(2):372–382, 2016.

[148] Silvia Arber. Motor circuits in action: specification, connectivity, and function. *Neuron*, 74(6):975–989, Jun 21 2012.

[149] Skyler L Jackman, Christopher H Chen, Selmaan N Chettih, Shay Q Neufeld, Iain R Drew, Chimuanya K Agba, Isabella Flaquer, Alexis N Stefano, Thomas J Kennedy, Justine E Belinsky, Keiramarie Roberston, Celia C Beron, Bernardo L Sabatini, Christopher D Harvey, and Wade G Regehr. Silk fibroin films facilitate single-step targeted expression of optogenetic proteins. *Cell Reports*, 22(12):3351–3361, 2018.

[150] J. Bosquée, J. Werth, G. Epro, et al. The ability to increase the base of support and recover stability is limited in its generalisation for different balance perturbation tasks. *European Review of Aging and Physical Activity*, 18(20), 2021.

[151] Clemens Kathe, Francois Michoud, Philipp Schönle, et al. Wireless closed-loop optogenetics across the entire dorsoventral spinal cord in mice. *Nature Biotechnology*, 40(2):198–208, 2022.

[152] William L. Johnson, Devin L. Jindrich, Roland R. Roy, and V. Reggie Edgerton. A three-dimensional model of the rat hindlimb: musculoskeletal geometry and muscle moment arms. *Journal of Biomechanics*, 41(3):610–619, 2008. Epub 2007 Dec 3.

[153] John P. Charles, Omar Cappellari, Andrew J. Spence, Dominic J. Wells, and John R. Hutchinson. Muscle moment arms and sensitivity analysis of a mouse hindlimb musculoskeletal model. *Journal of Anatomy*, 229(4):514–535, October 2016. Epub 2016 May 12.

[154] S. T. Ramalingasetty, S. M. Danner, J. Arreguit, S. N. Markin, D. Rodarie, C. Kathe, G. Courtine, I. A. Rybak, and A. J. Ijspeert. A whole-body musculoskeletal model of the mouse. *IEEE Access*, 9:163861–163881, 2021. Epub 2021 Dec 6.

[155] T. Sugioka, M. Tanimoto, and Si. Higashijima. Biomechanics and neural circuits for vestibular-induced fine postural control in larval zebrafish. *Nature Communications*, 14(1):1217, 2023.

[156] Alexander Mathis, Pranav Mamidanna, Kevin M. Cury, Taiga Abe, Venkatesh N. Murthy, Mackenzie W. Mathis, and Matthias Bethge. Deeplabcut: markerless pose estimation of user-defined body parts with deep learning. *Nature Neuroscience*, 2018.

Appendix A

COM measurement using the reaction board

In this study, measurements of body and tail mass and length were obtained from six mice carcasses. These mice were of the same sex, strain, and age (10-12 weeks) as those used in the experimental recording. The weight of these mice and the experimental group was compared to ensure the anatomical measurements extracted from the carcasses can be generalized to the experimental group, and no significant difference is shown (t(19)=0.27, p=0.7922). The center of mass (CoM) was determined from these carcasses utilizing the reaction board method. The reaction board consists of a rigid board supported at each end by an edge. Under one end is a scale, the other end is elevated such that the board is level. The initial scale reading (R1) as well as the length of the board between the knife-edges (d) are noted before the measurement. After placing the carcass, the scale reading increases to a new value (R2). The placement of the added weight (x) relative to the end (A) determines how much of the carcass weight (W) is reflected as an increase in the scale reading. If the CoM of the carcass falls exactly half way between the knife edges, then the increase in thescale reading (R2 – R1) will be exactly half of the carcass weight. The CoM estimation was used to compute distances between the CoM and the tail base, as well as the snout. After estmation of the CoM, the tail was dissected at its base from the body and the weight and length of the tail and the body was measured.

After estmation of the CoM, the tail was dissected at its base from the body and the weight and length of the tail and the body was measured. See Table 2.2.

Table 2.2: Anatomical measurements.

Parameter	**mean±SEM**	n	**Test**
Body weight (carcass) (g)	20.27±0.58	$n = 6$	
Body radius (carcass) (cm)	2.08±0.15	$n = 6$	
Tail weight (carcass) (g)	0.5±0.03	$n = 6$	
Tail length (carcass) (cm)	7.05±0.19	$n = 6$	
Whole body weight (carcass) (g)	20.77±0.47	$n = 6$	
Whole body weight (experiment) (g)	20.40±0.25	$n = 15$	Whole body weight (carcass VS experiment) p=0.79, t-test(19)
CoM dist to tail base (norm) (carcass)	35.66±1.87	$n = 6$	

Statistical analysis was performed using unpaired t-test. n refers to the number of mice

Anatomical measurements

In this study, measurements of body and tail mass and length were obtained from six mice carcasses. These mice were of the same sex, strain, and age (10-12 weeks) as those used in the experimental recording. The weight of these mice and the experimental group was compared to ensure the anatomical measurements extracted from the carcasses can be generalized to the experimental group, and no significant difference is shown (t(19)=0.27, p=0.7922). The center of mass (CoM) was determined from these carcasses utilizing the reaction board method.

Tilting ridge traverse (TRT) task

The tilting ridge set-up consists of a thin acrylic ridge (4 to 10 mm wide, 50 cm long) attached on one end to a motor (S3003 Servo Motor, Futaba, Japan) controlled by a Bonsai script that

can tilt the ridge left and right direction with varying amplitudes. A small platform was placed at both ends of the ridge for the mouse to comfortably reside before and after the trial. Mouse movement was recorded at 300 FPS with two high-speed cameras (Blackfly S USB3, Teledyne FLIR, Wilsonville, OR, USA), one placed 50 cm above the ridge and another at the rear end of the ridge. Video recordings were saved in mpg format.

Animal training

After 2-week handling and habituation period, mice were trained to cross the platform using the 5-mm (days 1, 3, 5 of training) and 8-mm (days 2 and 4) ridges. The mice were gently encouraged to traverse the ridge, using a plastic tube from their home cages placed in front of them as an incentive if necessary. No food or other rewards were used, and the animals were not incentivised artificially (e.g. with food deprivation or stressors). Each training session lasted until the mouse could cross the platform without stops for 10 times in a row. Each training session lasted for approximately 2 hours. Each mouse underwent such training for three consecutive days. On the fourth and fifth day random-direction tilt was introduced in 2 out of 5 crossing trials. All 15 mice used in this study successfully acquired the task and traversed the ridge at the end of the 5th training day.

Tracking tail and body movements

Videos were recorded with the top and rear cameras as described above. The nose, tail, hips and hind paw trajectories were extracted using DeepLabCut (version 2.1.7; `https://github.com/DeepLabCut/DeepLabCut` [156]). A total of 200 image frames (10 videos selected from perturbation/non-perturbation trials, as well as different widths, 20 frames/video) were used to label and train models from both camera views. 90 % of the labeled frames were used for training, and the remaining 10 % for testing. We used a ResNet-50-based neural network for 1,000,000 training iterations, where the cross-entropy loss plateaued to 0.001. We then used a p-cutoff of 0.9 to condition the X,Y coordinates for future analysis. This network was then used to analyze videos.

In addition to the hind body kinematics, position of the body centroid was estimated using the top camera view as the average position of the mouse body silhouette using a custom-made script in Bonsai. Silhouette was extracted by first applying a filter to binarize the image (to separate the region of interest (ROI) from the background), and then extract the ROI centroid. The point in time were the ROI centroid became visible under the top camera were used to extract the time-aligned traces captured by both cameras. Out of this trace the 500 points (centered in time) of the time series were used to compute angles displacement during a trial. Tails and hips angles time-series were either extracted for the trial, or for a step cycle. A step cycle was identified based on the peak of the x projection time-series of the contralteral (with respect to the position of the tail) hind paw marker. This time-point is used to separate the trials based on steps events and project the time-series of hips and tail angles centered in time around this event.

Kinematics analysis

Custom Python scripts (Python 3.7.4; Windows 10) were used to compute angles and instantenous velocities for all DeepLabCut-extracted markers, as well as the speed of the Bonsai-

extracted centroid trajectories. All time series were applied a smooth filter (Hanning smoothing) of 10 frames (33 ms) before further processing.

Following parameters were computed from the extracted trajectories:

- **Roll-plane tail angle**: the angle of the initial segment of the tail with respect to vertical as seen from the posterior camera. 180 degrees corresponts to tail pointing up.
- **Yaw-plane tail angle**: the angle of the initial segment of the tail with respect to the ridge, as seen from the top camera. 0 degrees corresponds to tail pointing straight back.
- **Hip angle**: alignment of a line connecting the two hip markers with respect to vertical, as seen from the posterior camera. 90 degrees corresponds to horizontal alignment.
- **Instantenous angular velocity** is the frame by frame gradient of the tail angle.
- **Back angle** is the angle between the tail base, the centroid, and the line parallel to the ridge passing through the tail base. It is used to estimate the mouse back posture while crossing the ridge. 0 degrees corresponds to the hind body being aligned straight back along the ridge.
- **Front angle** is the angle between the centroid, the nose, and the line passing through the nose and parallel to the ridge. 0 degrees corresponds to the head being aligned straight ahead along the ridge.
- **Tail-on-body angle** is obtained by subtracting the back angle from tail angle (determined by tail 2nd marker, tail base and the line parallel to the ridge passing through the tail base). 0 degrees corresponds to the tail being aligned straight back along the ridge.

Cross-correlation analysis of tail and hip momemta

The cross-correlation was calculated between hips and tail momentum time bins for trials with a certain width. "Hotspots" and "coldspots" were defined by collecting cells with values in positive and negative 5 percentile for the total distribution of correlation and highlighting region with the highest number of contigous cells.

Appendix B

Table 2.3: Tail kinematic measurements.

Parameter	**mean±SEM**	n	**Statistical Test**
Time to Peak (IL tail) (s)	$\mathbf{0.16 \pm 0.0014}$	$\mathbf{n = 168}$	
Time to Peak (CL tail) (s)	$\mathbf{0.14 \pm 0.0017}$	$\mathbf{n = 167}$	**IL VS CL** $p < 0.0001$**,** t**-test (333)**
Time to Peak (IL body) (s)	$\mathbf{0.12 \pm 0.0016}$	$\mathbf{n = 187}$	
Time to Peak (CL body) (s)	$\mathbf{0.11 \pm 0.0017}$	$\mathbf{n = 176}$	**IL VS CL** $p < 0.0001$**,** t**-test (361)**
Reaction Time (IL tail) (s)	0.062 ± 0.00011	$n = 168$	
Reaction Time (CL tail) (s)	0.062 ± 0.00012	$n = 167$	IL VS CL $p = 0.96$, t-test (333)
Slope (IL tail) (rotations/s)	2.20 ± 0.037	$n = 168$	
Slope (CL tail) (rotations/s)	2.12 ± 0.038	$n = 167$	IL VS CL $p = 0.15$, t-test (333)

Statistical analysis was performed using unpaired t-test. n refers to the number of trials. CL, contralateral trials; IL, ipsilateral trials.

Table 2.4: Angular momentum attenuation with respect to tilt (IL trials)

Parameter	**mean ± SEM**	n	**p-value (ANOVA)**
Attenuation			$\mathbf{p < 0.0001}$**, ANOVA**
Tail	$\mathbf{0.51 \pm 0.008}$	$n = 269$	
Hips	$\mathbf{0.33 \pm 0.010}$	$n = 269$	**Tail vs. Hips** $\mathbf{p < 0.0001}$ **(post-hoc)**
Total	$\mathbf{0.84 \pm 0.014}$	$n = 269$	**Hips vs. Total** $\mathbf{p < 0.0001}$ **(post-hoc)**

Statistical analysis was performed using ANOVA followed by Bonferroni's post-test. n refers to the number of trials. IL, ipsilateral.

Table 2.5: Effect of varying tilt amplitude.

Parameter	**mean±SEM**	**n**	**p-value (ANOVA)**
Max slowing			**p=0.0010, ANOVA**
S	0.94 ± 0.0096	$n = 56$	
M	0.91 ± 0.016	$n = 57$	S vs. M p=0.18 (post-hoc)
L	$\mathbf{0.97 \pm 0.0072}$	$n = 60$	**M vs. L** $p = 0.0004$ **(post-hoc)**
Traveled distance (mm)			**p=0.0004, ANOVA**
S (mm)	65.12 ± 2.83	$n = 56$	
M (mm)	74.05 ± 3.80	$n = 57$	S vs. M p=0.75 (post-hoc)
L (mm)	$\mathbf{56.92 \pm 2.20}$	$n = 60$	**M vs. L** $p = 0.0001$ **(post-hoc)**
Angular momentum (Tail) ((kg*cm)/s)			**p<0.0001, ANOVA**
S ((kg*cm)/s)	1.02 ± 0.049	$n = 56$	
M ((kg*cm)/s)	$\mathbf{1.58 \pm 0.069}$	$n = 57$	**S vs. M** $p < 0.0001$ **(post-hoc)**
L ((kg*cm)/s)	1.63 ± 0.053	$n = 60$	M vs. L p=0.97 (post-hoc)
Angular momentum (Hips) ((kg*cm)/s)			p=0.17, ANOVA
S ((kg*cm)/s)	1.00 ± 0.070	$n = 56$	
M ((kg*cm)/s)	1.10 ± 0.078	$n = 57$	S vs. M p=0.71 (post-hoc)
L ((kg*cm)/s)	1.03 ± 0.073	$n = 60$	M vs. L p=0.90 (post-hoc)
Tilt compensation (Tail)			**p<0.0001, ANOVA**
S	0.63 ± 0.031	$n = 56$	
M	0.53 ± 0.023	$n = 57$	S vs. M p=0.14 (post-hoc)
L	$\mathbf{0.38 \pm 0.012}$	$n = 60$	**M vs. L** $p = 0.0014$ **(post-hoc)**
Tilt compensation (Hips)			**p<0.0001, ANOVA**
S	0.62 ± 0.044	$n = 56$	
M	$\mathbf{0.37 \pm 0.026}$	$n = 57$	**S vs. M <0.0001 (post-hoc)**
L	$\mathbf{0.24 \pm 0.017}$	$n = 60$	**M vs. L** $p = 0.0092$ **(post-hoc)**
Tilt compensation (Tail+Body)			**p<0.0001, ANOVA**
S	1.26 ± 0.049	$n = 56$	
M	$\mathbf{0.91 \pm 0.036}$	$n = 57$	**S vs. M p<0.0001 (post-hoc)**
L	$\mathbf{0.61 \pm 0.020}$	$n = 60$	**M vs. L p<0.0001 (post-hoc)**

Statistical analysis was performed using ANOVA followed by Bonferroni's post-test, with results indicated with brackets where applicable. S, small tilt, 10 degrees; M, medium tilt, 20 degrees; L, large tilt, 30 degrees. n refers to the number of trials. vs, versus.

Table 2.6: Effects of varying ridge width during tilted trials

Parameter	**mean±SEM**	**n**	**p-value (ANOVA)**
Early phase ang mom (Tail) ((kg*cm)/s)			**p=0.0175, ANOVA**
4mm ((kg*cm)/s)	0.66 ± 0.050	$n = 57$	
5mm ((kg*cm)/s)	0.65 ± 0.032	$n = 78$	4 vs. 5 p=0.98 (post-hoc)
8mm ((kg*cm)/s)	0.59 ± 0.029	$n = 78$	5 vs. 8 p=0.57 (post-hoc)
10mm ((kg*cm)/s)	0.51 ± 0.032	$n = 59$	8 vs. 10 p=0.27 (post-hoc)
Early phase ang mom (Body) ((kg*cm)/s)			p=0.28, ANOVA
4mm ((kg*cm)/s)	0.70 ± 0.077	$n = 57$	
5mm ((kg*cm)/s)	0.82 ± 0.050	$n = 78$	4 vs. 5 p=0.35 (post-hoc)
8mm ((kg*cm)/s)	0.73 ± 0.051	$n = 78$	5 vs. 8 p=0.46 (post-hoc)
10mm ((kg*cm)/s)	0.69 ± 0.047	$n = 59$	8 vs. 10 p=0.94 (post-hoc)
Late phase ang mom (Tail) ((kg*cm)/s)			p=0.077, ANOVA
4mm ((kg*cm)/s)	0.68 ± 0.037	$n = 57$	
5mm ((kg*cm)/s)	0.78 ± 0.026	$n = 78$	4 vs. 5 p=0.051 (post-hoc)
8mm ((kg*cm)/s)	0.71 ± 0.024	$n = 78$	5 vs. 8 p=0.22 (post-hoc)
10mm ((kg*cm)/s)	0.76 ± 0.030	$n = 59$	8 vs. 10 p=0.63 (post-hoc)
Late phase ang mom (Body) ((kg*cm)/s)			p=0.78, ANOVA
4mm ((kg*cm)/s)	0.41 ± 0.066	$n = 57$	
5mm ((kg*cm)/s)	0.26 ± 0.062	$n = 78$	4 vs. 5 p=0.15 (post-hoc)
8mm ((kg*cm)/s)	0.22 ± 0.040	$n = 78$	5 vs. 8 p=0.94 (post-hoc)
10mm ((kg*cm)/s)	0.23 ± 0.050	$n = 59$	8 vs. 10 p=0.99 (post-hoc)

Statistical analysis was performed using ANOVA followed by Bonferroni's post-test. n refers to the number of trials. vs., versus.

Table 2.7: Locomotory performance on ridges with different widths

Parameter	**mean±SEM**	**n**	**p-value (ANOVA)**
Paw slips			**p<0.0001, ANOVA**
4mm	0.86 ± 0.11	$n = 14$	
5mm	$\mathbf{0.47 \pm 0.10}$	$n = 14$	**4 VS 5 p=0.037 (post-hoc)**
8mm	$\mathbf{0.076 \pm 0.02}$	$n = 14$	**5 VS 8 p=0.0011 (post-hoc)**
10mm	$\mathbf{0.024 \pm 0.016}$	$n = 14$	**8 VS 10 p=0.024 (post-hoc)**
Traversing speed (cm/s)			**p<0.0001, ANOVA**
4mm (cm/s)	19.05 ± 0.51	$n = 14$	
5mm (cm/s)	$\mathbf{20.78 \pm 0.65}$	$n = 14$	**4 VS 5 p=0.0017 (post-hoc)**
8mm (cm/s)	$\mathbf{23.37 \pm 0.60}$	$n = 14$	**5 VS 8 p=0.0067 (post-hoc)**
10mm (cm/s)	$\mathbf{26.81 \pm 0.69}$	$n = 14$	**8 VS 10 p=0.0003 (post-hoc)**
45mm (cm/s)	$\mathbf{36.87 \pm 0.81}$	$n = 14$	**8 VS 10 p<0.0001 (post-hoc)**
CoM within BoS			**p<0.0001, ANOVA**
4mm	0.89 ± 0.016	$n = 14$	
5mm	$\mathbf{0.97 \pm 0.0057}$	$n = 14$	**4 vs. 5 p=0.0066 (post-hoc)**
8mm	$\mathbf{0.99 \pm 0.00049}$	$n = 14$	**5 vs. 8 p=0.0021 (post-hoc)**
10mm	1.00 ± 0.00	$n = 14$	8 vs. 10 p=0.15 (post-hoc)
45mm	1.00 ± 0.00	$n = 14$	8 vs. 10 N/A
CoM lateral movement (mm)			**p<0.0001, ANOVA**
4mm (mm)	1.04 ± 0.063	$n = 14$	
5mm (mm)	0.85 ± 0.025	$n = 14$	4 vs. 5 p=0.12 (post-hoc)
8mm (mm)	0.95 ± 0.061	$n = 14$	5 vs. 8 p=0.62 (post-hoc)
10mm (mm)	$\mathbf{1.18 \pm 0.097}$	$n = 14$	**8 vs. 10 p=0.013 (post-hoc)**
CoM centrality			**p<0.0001, ANOVA**
4mm	0.48 ± 0.031	$n = 14$	
5mm	$\mathbf{0.66 \pm 0.0099}$	$n = 14$	**4 vs. 5 p=0.0014 (post-hoc)**
8mm	$\mathbf{0.76 \pm 0.015}$	$n = 14$	**5 vs. 8 p=0.0012 (post-hoc)**
10mm	0.76 ± 0.019	$n = 14$	8 vs. 10 p=0.99 (post-hoc)
Slip count/speed (4-5mm)	**r=-0.55**	$n = 14$	**p=0.0020, linear regression**
Slip count/Centrality (4-5mm)	r=-0.35	$n = 14$	p=0.066, linear regression

Statistical analysis was performed using ANOVA followed by Bonferroni's post-test. n refers to the number of mice. vs., versus.

Table 2.8: Posture on ridges with different widths.

Parameter	**mean±SEM**	**n**	**p-value (ANOVA)**
Front mean (°)			p=0.14, ANOVA
4mm (°)	1.99 ± 0.10	$n = 14$	
5mm (°)	1.80 ± 0.0075	$n = 14$	4 vs. 5 p=0.24 (post-hoc)
8mm (°)	1.75 ± 0.090	$n = 14$	5 vs. 8 p=0.95 (post-hoc)
10mm (°)	1.78 ± 0.088	$n = 14$	8 vs. 10 p=0.94 (post-hoc)
Back mean (°)			**p=0.013, ANOVA**
4mm (°)	8.85 ± 0.94	$n = 14$	
5mm (°)	8.36 ± 0.58	$n = 14$	4 vs. 5 p=0.79 (post-hoc)
8mm (°)	$\mathbf{6.80 \pm 0.43}$	$n = 14$	**5 vs. 8 p=0.022 (post-hoc)**
10mm (°)	6.38 ± 0.37	$n = 14$	8 vs. 10 p=0.28 (post-hoc)
Tail-on-body mean (°)			**p=0.0070, ANOVA**
4mm (°)	30.24 ± 1.76	$n = 14$	
5mm (°)	28.86 ± 1.37	$n = 14$	4 vs. 5 p=0.64 (post-hoc)
8mm (°)	$\mathbf{24.45 \pm 1.76}$	$n = 14$	**5 vs. 8 p=0.077 (post-hoc)**
10mm (°)	22.67 ± 1.55	$n = 14$	8 vs. 10 p=0.19 (post-hoc)
Front mean/speed	r=0.300	$n = 14$	p=0.141, linear regression
Back mean/speed	r=0.0498	$n = 14$	p=0.715, linear regression
Tail-on-body mean/speed	**r=0.291**	$n = 14$	**p=0.0291, linear regression**
Front mean/Centrality	r=-0.147	$n = 14$	p=0.279, linear regression
Back mean/Centrality	r=-0.192	$n = 14$	p=0.155, linear regression
Tail-on-body mean/Centrality	r=-0.061	$n = 14$	p=0.655, linear regression

Statistical analysis was performed using ANOVA followed by Bonferroni's post-test. n refers to the number of mice. vs., versus.

Table 2.9: Tail and hips position and rotational range during a step cycle while locomoting on ridges with different width.

Parameter	**mean±SEM**	**n**	**p-value (ANOVA)**
Mean position (tail) (°)			**p<0.0001, ANOVA**
4mm (°)	100.7 ± 6.59	$n = 14$	
5mm (°)	112.1 ± 5.37	$n = 14$	4 vs. 5 p=0.18 (post-hoc)
8mm (°)	$\mathbf{129.8 \pm 3.91}$	$n = 14$	**5 vs. 8 p=0.0019 (post-hoc)**
10mm (°)	$\mathbf{135.8 \pm 4.15}$	$n = 14$	**8 vs. 10 p=0.049 (post-hoc)**
Mean position (hips) (°)			**p=0.0033, ANOVA**
4mm (°)	82.03 ± 0.60	$n = 14$	
5mm (°)	82.60 ± 0.58	$n = 14$	4 vs. 5 p=0.69 (post-hoc)
8mm (°)	$\mathbf{84.51 \pm 0.55}$	$n = 14$	**5 vs. 8 p=0.035 (post-hoc)**
10mm (°)	84.32 ± 0.61	$n = 14$	8 vs. 10 p=0.97 (post-hoc)
Rotation range (tail) (°)			**p=0.0002, ANOVA**
4mm (°)	75.94 ± 6.82	$n = 14$	
5mm (°)	67.71 ± 5.50	$n = 14$	4 vs. 5 p=0.12 (post-hoc)
8mm (°)	$\mathbf{52.62 \pm 3.20}$	$n = 14$	**5 vs. 8 p=0.020 (post-hoc)**
10mm (°)	$\mathbf{46.08 \pm 2.95}$	$n = 14$	**8 vs. 10 p=0.042 (post-hoc)**
Rotation range (hips) (°)			p=0.39, ANOVA
4mm (°)	26.00 ± 0.89	$n = 14$	
5mm (°)	25.23 ± 0.94	$n = 14$	4 vs. 5 p=0.84 (post-hoc)
8mm (°)	24.58 ± 1.16	$n = 14$	5 vs. 8 p=0.67 (post-hoc)
10mm (°)	24.71 ± 1.01	$n = 14$	8 vs. 10 p=0.99 (post-hoc)

Statistical analysis was performed using ANOVA followed by Bonferroni's post-test. n refers to the number of mice. vs., versus.

Appendix C

Pipeline for Registration of Brainstem Slice onto Atlas

The location of sacral vestibular neurons (sacVN) within the vestibular complex is described in this section. Such distribution is obtained after registration of the confocal images onto the Allen atlas using a custom-adapted pipeline described below: **Segmentation and Annotation in QuPath:**

1. **Step 1:** Use QuPath software to segment and annotate the regions of interest (ROIs) in both the source brain images (the images to be registered) and the target brain images (the reference atlas).

2. **Step 2:** Export the annotated images and corresponding ROIs from QuPath. These files will serve as inputs for the ABBA pipeline.

Initial Alignment in ABBA:

1. **Step 3:** Import the exported images and annotations into the ABBA (Automated Brain Alignment) pipeline.

2. **Step 4:** Utilize the interactive transformation tool within ABBA to perform a rough manual alignment of the source and target brain images. This step involves adjusting the positioning to ensure an approximate match between the two sets of images.

Refinement with Spline Transformation:

1. **Step 5:** Apply the spline transformation in ABBA to correct for local deformations and anatomical variations between the source and target brains. The spline transformation works by optimizing a smooth deformation field defined by control points placed across the brain images.

Global Alignment with BigWarp:

1. **Step 6:** Use the bigwarp transformation within ABBA to address larger-scale deformations and achieve alignment of the global brain structures. BigWarp employs a hierarchical, multi-resolution approach, allowing for the efficient registration of high-dimensional data, accommodating significant anatomical differences between the source and target.

Import and Review in QuPath:

1. **Step 7:** After completing the registration process in ABBA, import the aligned source and target images back into QuPath.

2. **Step 8:** Perform further analysis, visualization, and quantification of the registered brain regions within QuPath. This step ensures that the alignment is satisfactory and allows for detailed examination of the results.

Refinement and Iteration:

1. **Step 9:** If any registrations are found to be unsatisfactory, refine the alignment by re-exporting the data from QuPath and passing it back into the ABBA pipeline. Repeat the alignment steps as necessary to achieve optimal registration.

This pipeline provides a systematic approach for accurately registering brainstem slices onto an atlas, combining the strengths of both QuPath and ABBA for precise anatomical alignment and analysis.